



The analog of cGAMP, c-di-AMP, activates STING mediated cell death pathway in estrogen-receptor negative breast cancer cells

Hitesh Vasiyani¹ · Anjali Shinde¹ · Milton Roy¹ · Minal Mane¹ · Kritarth Singh² · Jyoti Singh¹ · Dhruv Gohel¹ · Fatema Currim¹ · Khushali Vaidya³ · Mahesh Chhabria³ · Rajesh Singh¹

Accepted: 30 March 2021 / Published online: 10 April 2021
© The Author(s), under exclusive licence to Springer Science+Business Media, LLC, part of Springer Nature 2021

Abstract

Immune adaptor protein like STING/MITA regulate innate immune response and plays a critical role in inflammation in the tumor microenvironment and regulation of metastasis including breast cancer. Chromosomal instability in highly metastatic cells releases fragmented chromosomal parts in the cytoplasm, hence the activation of STING via an increased level of cyclic dinucleotides (cDNs) synthesized by cGMP-AMP synthase (cGAS). Cyclic dinucleotides 2' 3'-cGAMP and its analog can potentially activate STING mediated pathways leading to nuclear translocation of p65 and IRF-3 and transcription of inflammatory genes. The differential modulation of STING pathway via 2' 3'-cGAMP and its analog and its implication in breast tumorigenesis is still not well explored. In the current study, we demonstrated that c-di-AMP can activate type-1 IFN response in ER negative breast cancer cell lines which correlate with STING expression. c-di-AMP binds to STING and activates downstream IFN pathways in STING positive metastatic MDA-MB-231/MX-1 cells. Prolonged treatment of c-di-AMP induces cell death in STING positive metastatic MDA-MB-231/MX-1 cells mediated by IRF-3. c-di-AMP induces IRF-3 translocation to mitochondria and initiates Caspase-9 mediated cell death and inhibits clonogenicity of triple-negative breast cancer cells. This study suggests that c-di-AMP can activate and modulates STING pathway to induce mitochondrial mediated apoptosis in estrogen-receptor negative breast cancer cells.

Keywords Stimulator of interferon gene (STING) · Cyclic GMP AMP synthase (cGAS) · Interferon regulatory factor3 (IRF-3) · Apoptosis · Cyclic dinucleotides (cDNs)

Introduction

The crosstalk between tumor cells, infiltrating immune cells and stroma in breast cancer tumor microenvironment (TME) provides an optimal niche for the growth and proliferation of cancer cells [1]. Hypoxic TME of solid tumors promotes the clonal evolution of the cancer cells which leads to the progression of the tumor [2]. Hypoxic TME can also induce necrotic cell death leading to the release of intrinsic danger-associated molecular patterns (DAMPs), which can activate

innate immune response [3]. The activation of the innate immune system and its regulation during tumorigenesis is emerging [4] however, its role in the acquisition of tumorigenic phenotype, its physiological and chemical modifiers are not well understood.

Our previous reports demonstrated that innate immune regulators are uniquely positioned at mitochondria which in turn links the inflammatory pathways and metabolism, hence playing an important role in the metabolic adaption of tumor cells [5]. STING (Stimulator of interferon gene) is also known as MITA, MPYS, TMEM 173 is localized at the ER/mitochondria contact site and is a major regulator of the type I immune response. Interestingly, STING is differentially expressed in ER/PR positive and negative breast cancer patients, therefore can differentially regulate inflammatory cell death [6]. The implication of increased level of STING in triple-negative breast cancer cells and association with metastasis and resistance to cell death is not well understood.

✉ Rajesh Singh
singhraj1975@gmail.com

¹ Department of Biochemistry, The M.S. University of Baroda, Vadodara, Gujarat 390002, India

² Department of Cell and Developmental Biology, University College London, Gower Street, London WC1E 6BT, UK

³ L. M. College of Pharmacy, Navrangpura, Ahmedabad, Gujarat 380 009, India

The release of nuclear DNA in cytoplasm, either in highly proliferating cells or stressed solid TME is sensed by cyclic GMP-AMP synthase (cGAS) which adds phosphate bond between the 2 and 3 carbons of GMP and AMP nucleotide [7], hence synthesis of 2' 3'-cGAMP, a ligand for the innate immune receptor STING. The binding of 2' 3'-cGAMP to STING activates downstream signalling and recruits TBK-1 which phosphorylates the inflammatory transcription factors IRF-3 and p65 [8], leading to increased level of type-I IFN, and other chemokines [9]. Type-I IFNs are pleiotropic cytokines and are known for their anti-tumor effects [10]. In the tumor microenvironment (TME), type-I IFN may stimulate dendritic cells maturation, and activation of cytotoxic T-lymphocytes and enhancement of memory T-cell survival which are characteristics of anti-tumor cytokines [11]. Breast cancer metastasis and TME are majorly associated with type-1 immune response. The lack of type -1 immune response helps tumor cells to escape from the immune-mediated anti-tumor response [12]. Decreased infiltration of CD8+ T lymphocyte in TME is associated with poor prognosis in cancer [13]. Activation of the IFN pathway in tumor cells recruits CD8+ T lymphocytes and enhances anti-tumor immunogenic response [14]. Hence stimulation of the cGAS-STING-IFN pathway has become a central target for the development of anticancer therapeutics [11]. The cDNs produced by intracellular pathogens can also activate STING-mediated innate immune and inflammatory response [15]. Since cGAMP is an endogenous molecule hence its level may be altered by several feedback mechanisms hence its signaling strength may determine its potential outcome in different pathological conditions [16, 17]. Therefore the potential of other cDNs molecules for activation of cGAS/STING/IFN pathway should be investigated further for an anti-tumorigenic response. c-di-AMP produced by *Listeria monocytogenes* in host cells activates type-1 immune response via STING and IRF-3 [18]. Similarly, intracellular infection of *Chlamydia* synthesizes cyclic di-AMP (c-di-AMP), which also acts as a ligand for STING that activates IFN responses during infection [19].

Though cyclic di-nucleotides of prokaryotic origin can effectively stimulate STING signaling and activate the downstream pathway [20], their potential as modulators of tumor cell survival and death mediated by STING pathway had not been explored. In the current study, we demonstrate that bacterial origin c-di-AMP, the analogue of cGAMP, activates STING mediated type-1 immune response and cell death in estrogen- receptor negative breast cancer cells. Moreover, the c-di-AMP induced cell death directly correlates with STING expression in breast cancer cells. c-di-AMP treated cells show caspase activation and PARP cleavage in STING expressing cell line independent of cGAS expression. Further c-di-AMP induces IRF-3 translocation to mitochondria to induce cell death.

Materials and methods

Cells line maintenance and culture

MCF-7, T-47D, ZR75, BT-474, MDA-MB-231 purchased from ATCC. MCF-7 cultured in EMEM media while T-47D, ZR75 and BT-474 maintained in RPMI medium. MX-1 obtained from CLS, Germany and cultured in F12K media. MDA-MB-231 was cultured in Leibovitz's L-15 media (HI-MEDIA, India). The media used were supplemented with 10% FBS (Life Technologies, USA) and 1% penicillin, streptomycin, and neomycin (PSN) antibiotic mixture (Life Technologies, USA). Cells were incubated at 37 °C, 5% CO₂ in specified media. All cell lines were checked for mycoplasma contamination by Universal Mycoplasma detection kit ATCC.

Plasmids and reagents

STING cloned in pCMV6 ENTRY plasmid was gift from Dr. Hong Bing Su (Wuhan University China), p65-shRNA and control shRNA were received from Dr. Ederne Berra Ramírez (Gene Silencing Platform, CICbioGUNE, Derio, Spain). STING-shRNA and IRF-3-shRNA were a generous gift from Dr. Peter Chumakov (Engelhardt Institute of Molecular Biology, Russian Academy of Sciences).

Primary antibody against STING was purchased from Proteintech, USA, cGAS and HRP-conjugated secondary anti-rabbit and anti-mouse antibodies were purchased from Thermo Scientific, USA. Antibodies against PARP, Caspase 9, Caspase 3, and, NF-kB p65 were purchased from Cell signalling, Inc., USA, 2' 3'-cGAMP and c-di-AMP from Sigma, PrestobluTM cell viability reagent from Invitrogen, USA and Caspase 3/7 luciferase reporter activity kit was purchased from Promega, USA.

Generation of cGAS-sgRNA clones

cGAS-sgRNA clones were generated using protocol described by Ran et al. [21]. The guide-RNAs targeting the first exon of cGAS was designed using GPP sgRNA Designer tool (Broad institute) [21]. sg-RNA-top and sg-RNA-bottom strands were synthesized as described earlier [21]. Synthesized oligos were annealed and cloned into BbsI-linearized pSpCa9(BB)-2A-Puro (PX459) V2.0 vector. cGAS-sgRNA clones were transformed into competent Stbl3 *E. coli* strain and transformants were screened by colony PCR using U6 sequencing primer and sg-RNA-bottom. Positive clones were finally confirmed by Sanger sequencing.

cGAS:

5'caccgAGACTCGGTGGGATCCATCG'3.

5'aaacCGATGGATCCCACCGAGTCTc'3.

Transfection

MCF-7, T-47D, ZR75, BT-474, MX-1 and MDA-MB-231 transfected with X-treamGENE (Sigma, USA) using manufacturer's protocol.

Quantitative analysis of gene expression

Total RNA was isolated using Tri Reagent (Life Technologies, USA) and was reverse transcribed to synthesize cDNA using Transcriptor First Strand cDNA synthesis kit (Roche, Germany) or SuperScript VILO cDNA Synthesis Kit (Life Technologies, USA) according to the manufacturer's instructions. Real-time PCR was performed using SYBR Premix Ex Taq TM (Takara, Japan) or SYBR mix (Life Technologies, USA) or Applied Biosystems as per manufacturer's instructions. Specific primers of the genes are listed below.

STING: Fwd 5'-CGCCTCATTGCCTACCAG-3';
Rev, 5'-ACATCGTGGAGGTACTGGG-3';
cGAS: Fwd 5'-GGGAGCCCTGCTGTAACACTTCTT
AT-3';
Rev 5'-CCTTTGCATGCTTGGGTACAAGGT-3';
β-Actin: Fwd 5'-TCGTGCGTGACATTAAGGGG-3';
Rev 5'-GTAAGGCTGCGCTCAGGAGGAG-3';
GAPDH: Fwd 5'-AGAAGGCTGGGGCTCATTTG-3';
Rev 5'-AGGGGCCATCCACAGTCTTC 3'.

Western blot

Cells were plated at a density of 4.5×10^5 cells/well in the six-well plate and transfected with indicated expression plasmid or shRNAs/sgRNA using X-treamGENE (Sigma, USA). After 48 h of transfection, the cells were harvested, washed with ice-cold PBS and lysed in buffer A (150 mM NaCl, 30 mM Tris-Cl, 10% Triton X-100, 10% Glycerol, 1 × Protease Inhibitor (Roche, Germany)). The equal protein was loaded and resolved on 11% SDS-PAGE. Protein was electro blotted on PVDF membrane at 110 V for 1 h at 4 °C. The membrane was blocked with 5% blocking buffer (5% non-fat dried milk and 0.1% Tween-20 in TBS) or 5% BSA (BSA (Sigma-Aldrich, USA), 0.1% Tween-20 in TBS-0.02 M Tris-Cl, 0.15 M NaCl) for 1 h at room temperature. The membrane was incubated overnight with a specific primary antibody. After incubation, the membrane was washed three times with TBS-T (TBS containing 0.1% Tween-20) for 10 min and incubated with a secondary antibody at room temperature for 1 h. The membrane was washed three times with TBS-T and the signal was visualized by using EZ-ECL

chemiluminescence detection kit for HRP (Biological Industries, Israel) by exposing it to UVTEC gel documentation system.

IFN-β and NF-κB luciferase assay

MCF-7, MX-1, BT-474 and MDA MB 231 were seeded at density of 1×10^5 cells in 24 well-plated, next day co-transfected with IFN-β firefly luciferase or NF-κB firefly luciferase using gene X-tream GENE (Sigma) and treated with 200 μM c-di-AMP for 24 h IFN-β or NF-κB activity measured using as per manufacturer's instructions (Promega, USA).

Caspase 3/7 activity assay and Caspase 3/7 green assay for microscopy

The activity was performed using Caspase-Glo® 3/7 Assay kit (Promega, USA) or Caspase-Glo® 8 Assay kit (Promega, USA). Cells were plated at the density of 4×10^4 cells per well in 96 well in white clear-bottom plates and transfected with indicated expression plasmids or shRNAs and respective controls. Caspase-Glo® 3/7 (10 μl) reagent was added to each well and luminescence was measured with a Centro LB 960 Luminometer (Berthold Technologies, Germany). Caspase 3/7 green assay for microscopy performed as per manufacturer protocol (ThermoFisher, USA).

Cell growth inhibition assay and clonogenic assay

All cell lines were seeded at a density of 5000 cells/well in 96 well plates and treated with different concentrations of c-di-AMP for 4 days. At the end of treatment, cell viability was measured using Presto blue cell viability reagent (Invitrogen, USA). The clonogenic assay has been performed as described previously [22].

Molecular docking and cellular thermal shift assay

a) Binding of c-di-AMP with STING was further analysed by Molecular Docking using Maestro ver11.9, Schrodinger Suite. Crystal structure of STING [4KSY (Homo sapiens)] with a bound ligand having resolution 1.88 Å was retrieved from Protein Data Bank and prepared using the Protein Preparation Wizard and minimized using OPLS3e force field. All the heteroatoms and water molecules were removed except the conserved water molecules within 5 Å and the hydrogen atoms were added. Each structure was minimized for all-atom

constrained minimization using Ligprep module with OPLS3e force field

- b) *Cellular thermal shift assay* MDA-MB 231 cells were lysed in HBSS via three freeze–thaw cycles in liquid nitrogen. Total protein was quantified and an equal protein (Cell lysate) was aliquoted into PCR tubes and incubated with and without 30 µg/ml c-di-AMP for 1 h. After incubation suspension was transferred into PCR tubes subjected to specific temperature treatment for 3 min. Precipitated protein was separated using centrifugation at 17000×g for 20 min at 4 °C then supernatant of each sample was collected and analyzed by western blot.

Fluorescent microscopy

MDA-MB-231 cells were seeded in an optical bottom dish. After overnight incubation, the cells were imaged using NIKON (Japan) Eclipse Ti2-E inverted fluorescent microscope.

Results

c-di AMP induces STING mediated IFN pathway in breast cancer cell lines

We investigated if c-di-AMP can activate the STING pathway in breast cancer cells and modulate the IFN pathway. Firstly, we monitored the expression of STING in ER-positive and negative breast cancer cells. The analysis of transcript level of cGAS by RT-qPCR (Fig. 1b) showed ubiquitous expression in both ER-positive (MCF-7, T-47D, ZR75) as well as negative breast cancer cell lines (MDA-MB-231, BT-474 and MX-1). In consonance with RT-qPCR data, western blotting showed the expression of cGAS protein in all selected breast cancer cells. Interestingly, we found that STING mRNA expression was lower in ER-positive breast cancer cell lines (MCF-7, T-47D, ZR75) compared to ER-negative breast cancer cell lines (MDA-MB-231, BT-474 and MX-1) (Fig. 1a). Gene expression correlation using TCGA database showed negative correlation between STING and estrogen receptor. The *r* value is represented in different color in different types of breast cancer (Fig. 1c). In agreement with RNA expression, protein expression of STING was undetectable in ER-positive breast cancer cell lines (MCF-7, T-47D and ZR75), whereas, its expression was high in ER-negative breast cancer cell lines (MDA-MB-231, BT-474, MX-1) (Fig. 1d).

Further, we analyzed whether the STING-IFN pathway is intact in breast cancer cell lines. MCF-7 cells (cGAS +ve/STING –ve) and MDA-MB-231 (cGAS +ve/STING +ve) were treated with c-di-AMP and monitored the activation of both NF-κB and IFN pathway using luciferase assay.

Interestingly c-di-AMP showed no activation of both NF-κB and IFN pathways in MCF-7 whereas it activated both pathways in MDA-MB-231 cells (Fig. 1e, f). In further experiments, we selected MDA-MB-231 as STING positive cell line and MCF-7 as STING negative cell line. This further suggests that the STING pathway is intact in MDA-MB-231 (cGAS +ve/STING +ve) and is inhibited in MCF-7 cells (cGAS +ve/STING –ve) by downregulation of STING.

c-di-AMP binds to STING

As c-GAMP is known to bind to STING hence we hypothesized its analog c-di-AMP may also bind to STING expressed in human cells. To understand the binding of c-di-AMP as compared to other dinucleotides with STING, we performed docking of c-di-AMP with STING. The pyrimidine ring of purine forms two hydrogen bonds with Arg238 of STING. The amino group on the pyrimidine ring forms the hydrogen bond with Val239 which is bridged through the conserved water molecule to Ser241 and the oxygen of phosphate group forms the hydrogen bond and salt bridge with Arg238. Further amino group on the pyrimidine ring of purine forms a hydrogen bond with Tyr 167 and Ser 241. The oxygen of phosphate forms the hydrogen bond with Arg238. The imidazole ring of purine shows the pi–pi interaction with Tyr167 and the oxygen atom of phosphate forms the hydrogen bond with Arg238. Interestingly, the purine ring of c-di-GMP shows the pi–pi interaction with Tyr167 and the oxygen atom of phosphate forms the hydrogen bond with Ser162. In di-nucleotide, the amino group on the pyrimidine ring of purine forms a hydrogen bond with Ser241 same as molecule c-di-AMP. The conserved water molecule forms the hydrogen bond with Ser241 and Val239 and oxygen atoms of phosphate form two hydrogen bonds and a salt bridge with Arg238. Apart from these interactions, the molecules also have hydrophobic interactions with Tyr167, Tyr240, Val239, Tyr163 and Leu159 similar to the bound ligand (Fig. 2a–d). The docking score of c-di-AMP and c-di-GMP was found comparable and near to the docking score of the co-crystal ligand.

Further, we used cellular thermal shift assay which measures the thermal stability of a target protein and the binding of a ligand to the protein causes an increase in protein melting temperature, hence quantitative measure of binding of a ligand. The natural ligand 2', 3'-cGAMP synthesized by cGAS binds to STING and stabilizes it as reported previously [23]. We used a similar method to detect c-di-AMP binding to STING. We observed that binding of c-di-AMP stabilized STING protein with increasing temperature whereas unbound STING denatured fast (Fig. 2f) suggesting the binding of c-di-AMP to STING.

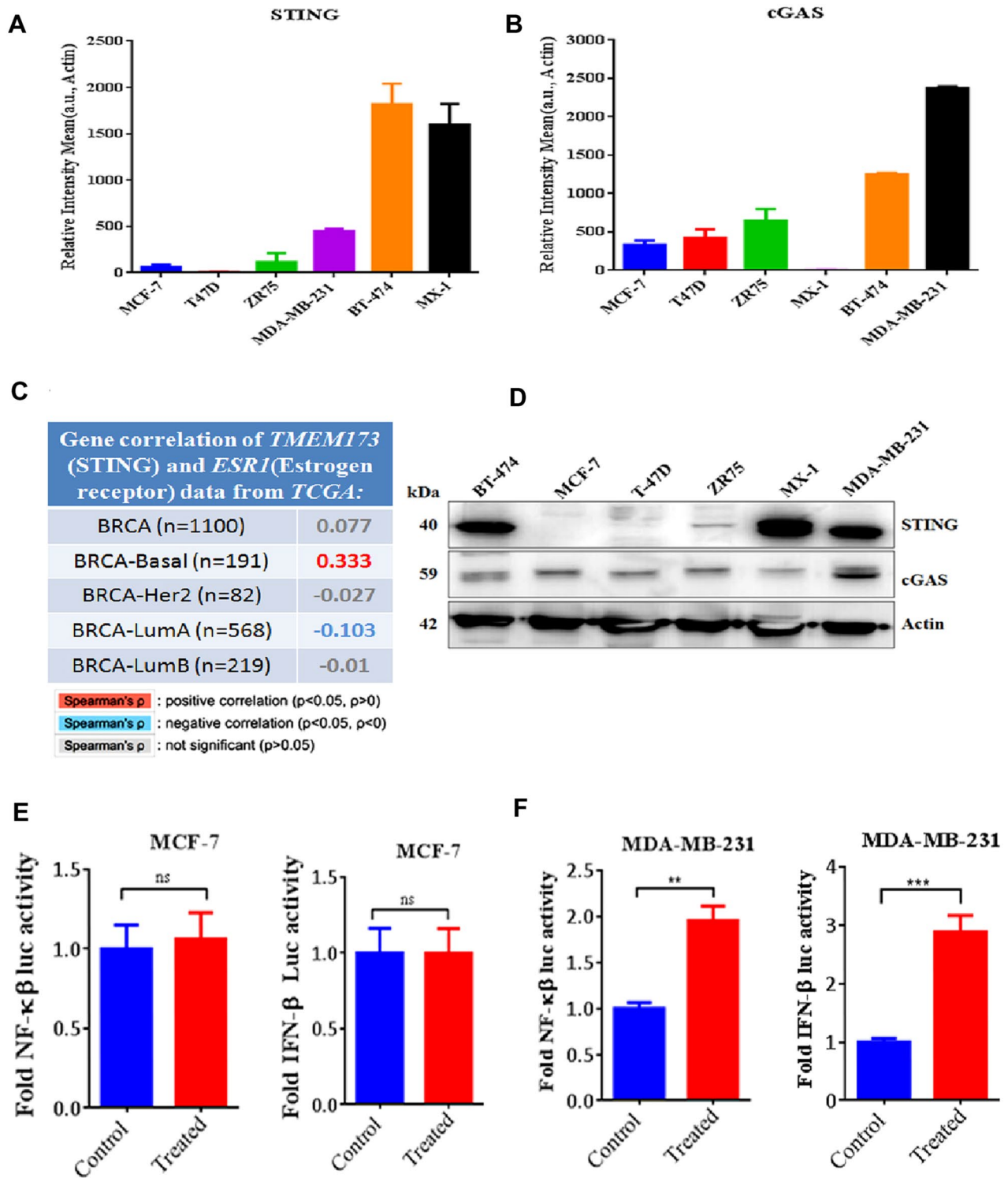
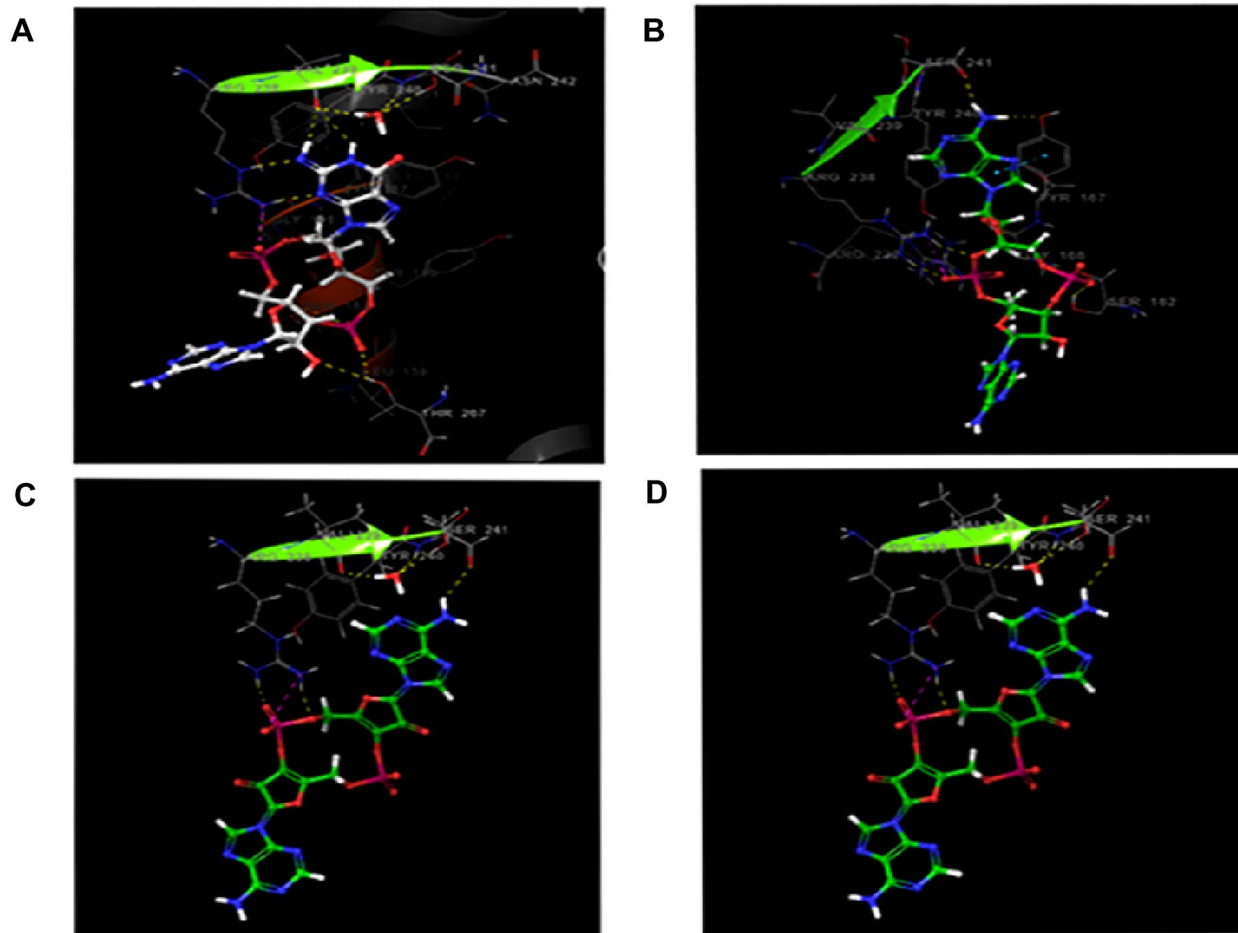
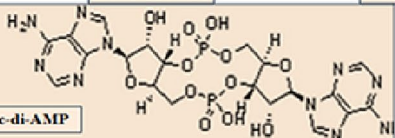
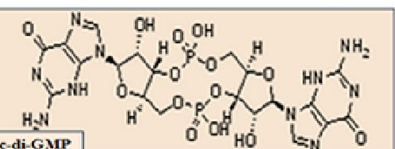
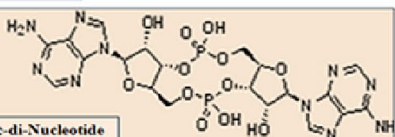
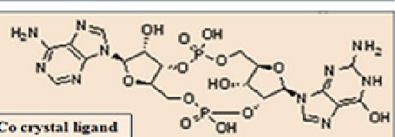


Fig. 1 c-di-AMP induces STING mediated IFN response in breast cancer cell lines. **a** Relative expression of STING in ER-positive (MCF-7, ZR75, T-47D) and ER-negative breast cancer cell lines (BT-474, MX-1 MDA-MB-231). **b** Relative expression of cGAS in ER-positive (MCF-7, ZR75, T-47D) and ER-negative breast cancer cell lines (BT-474, MX-1 MDA-MB-231). **c** Pearson correlation (r) between *TMEM173* and *ESR1* using TCGA database. **d** Western blot

analysis of cGAS and STING proteins in breast cancer cell lines. **e, f** MCF-7 [STING (–ve)], MDA-MB-231 [STING (+ve)] breast cancer cell lines were transfected with IFN- β and NF- κ B reporter constructs and treated with c-di-AMP (200 μ M) for 24 h and IFN- β and NF- κ B activity was measured. Data represent mean fold change compared to control (n = 3, mean \pm SD); *P < 0.05, **P < 0.01 and ***P < 0.001, based on a Student's t-test



Structure	Docking Score
 c-di-AMP	-4.720
 c-di-GMP	-4.825
 c-di-Nucleotide	-4.288
 Co crystal ligand	-5.551

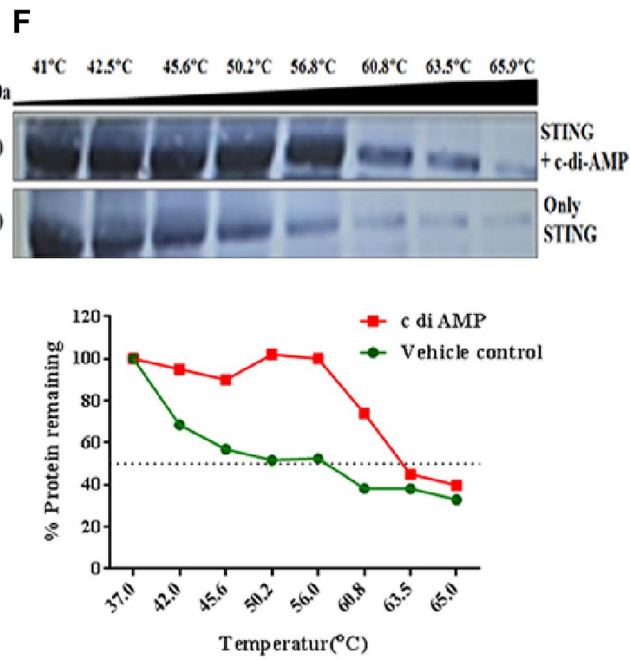


Fig. 2 c-di-AMP binds to STING directly. **a** Protein (PDB: 4KSY). Protein (STING) is represented in the wire model and ligands (c-di-AMP) are shown in a ball and stick model where the color represents atoms (Carbon-green, Nitrogen-blue, Oxygen-red, Hydrogen-white, Phosphorus-pink). The dotted lines indicate the protein–ligand interactions (Yellow- hydrogen bond, Pink- salt bridge, Blue- pi–pi interaction). **b–d** Shows the ligand interactions of molecule A, B and C with the protein (PDB: 4KSY) respectively. Protein is represented in the wire model and ligands are shown in the ball and stick model where the color represents atoms (carbon-green, nitrogen-blue, oxygen-red, hydrogen-white, phosphorus-pink). The dotted lines indicate the protein–ligand interactions (yellow- hydrogen bond, Pink- salt bridge, Blue- pi–pi interaction). **e** Respective dinucleotide and their Docking score. **f** Cellular thermal Shift assay was performed using MDA-MB-231 lysate incubated with c-di-AMP and western blotting was performed (Color figure online)

c-di- AMP activates cell death in ER/PR negative breast cancer cell lines

We and others have previously reported that STING can act as a tumor suppressor by sensitizing the cells to TNF- α induced cell death pathway [24]. We assessed whether c-di-AMP can activate the STING pathway and induce cell death in breast cancer cells. MCF-7 (ER-positive) breast cancer cell line, having an undetectable expression of STING, treated with c-di-AMP showed no effect on cell survival and caspase 3/7 activity (Fig. 3a). MX-1, BT-474, MDA- MB-231 (ER-negative), STING positive breast cancer cell lines showed a significant decrease in cell survival and increased caspase 3/7 activity (Fig. 3b–d). We analysed if c-di-AMP can activate the apoptotic cell death in breast cancer cells by monitoring PARP cleavage by western blotting. The band of 89 kDa corresponding to the cleaved subunit of PARP was observed in MDA-MB-231 and MX-1 cells whereas no band was detected in MCF-7 cells (Fig. 3e). The representative images of the fourth day after treatment of c-di-AMP (Fig. 3f) suggest that c-di-AMP inhibits the proliferation of STING positive tumor cells and induces apoptosis.

STING is essential for c-di-AMP induced cell death

As we observed here that c-di-AMP inhibited cell proliferation, we further characterized the role of STING in the initiation of the cell death pathway. STING was knockdown using shRNA in MDA-MB-231 and BT-474. After the knockdown of STING, cells were treated with c-di-AMP and monitored cellular viability caspase 3/7 activity. We observed that c-di-AMP treatment showed a significant reduction in cell viability in MDA-MB-231 and BT-474 cells, (Fig. 4a, d) which was rescued after STING knockdown both in MDA-MB-231 and BT-474 cells. Similarly, the caspase-3/7 activity increased significantly in c-di-AMP treated MDA-MB-231 cells and BT-474 cells (Fig. 4b, e). The knockdown of STING in MDA-MB-231 and BT-474

rescued cell proliferation and Caspase-3/7 activity of both the cell types. The knockdown of STING (Fig. 4c, f) was confirmed by western blotting. These experiments strongly suggest that STING is essential for c-di-AMP mediated cell death in MDA-MB-231 and BT-474 cells.

IRF-3 is indispensable for c-di-AMP induced apoptosis in ER-negative breast cancer cells

The implication of c-di-AMP regulated NF- κ B and IFN pathway for induction of cell death in breast cancer cells is not understood hence we explored the implication of these pathways in cell death. MDA-MB-231 and MX-1 cells were transfected with p65 and IRF-3 shRNA to inhibit NF- κ B and IFN pathway respectively. cGAS, p65 and IRF-3 were knocked out using CRISPR/Cas-9 sgRNA/shRNA and its role in the regulation of cell death was monitored. The knockdown of cGAS, p65 and IRF-3 was confirmed by western blotting (Fig. 5a, b). The knockdown of p65 showed no significant change in cell death both in c-di-AMP treated MDA-MB-231 and MX-1. Interestingly, the knockdown of IRF-3 significantly enhanced the cell survival in c-di-AMP treated MDA-MB-231 and MX-1 cells as observed. Similarly, IRF-3 knockdown also inhibited caspase activity in c-di-AMP treated MDA-MB-231 and MX-1 cells (Fig. 5e, f). We also analyzed the role of cGAS in the regulation of cell death, hence we knockdown cGAS and monitored cell death. The knockdown of cGAS in both cell lines showed no significant change in c-di-AMP induced cell death suggesting that cGAS acts upstream and is dispensable. These results suggest that IRF-3 is indispensable for c-di-AMP induced STING-mediated apoptosis in triple-negative breast cancer cells.

c-di-AMP induces IRF-3 translocation to mitochondria and induce the mitochondrial-mediated intrinsic pathway of apoptosis

The above experiment strongly suggests the indispensable role of IRF-3 in c-di-AMP induced cell death in STING positive MDA-MB-231 and MX-1 cells. It had been observed previously that IRF-3 activates mitochondrial-mediated apoptosis in viral infected cells [25]. IRF-3 plays a critical role in STING-mediated apoptosis via mitochondrial cytochrome c release [26]. We also monitored the subcellular localization of IRF3-GFP both in MCF-7 and MDA-MB-231 in the presence/absence of c-di-AMP. IRF-3-GFP showed diffused cytoplasmic localization both in MCF-7 and MDA-MB-231. Interestingly c-di-AMP treated cells show distinct puncta of IRF-3-GFP 3 both in MX-1 and MDA-MB-231 cells. The increased numbers of IRF-3 puncta in IRF-3-GFP positive

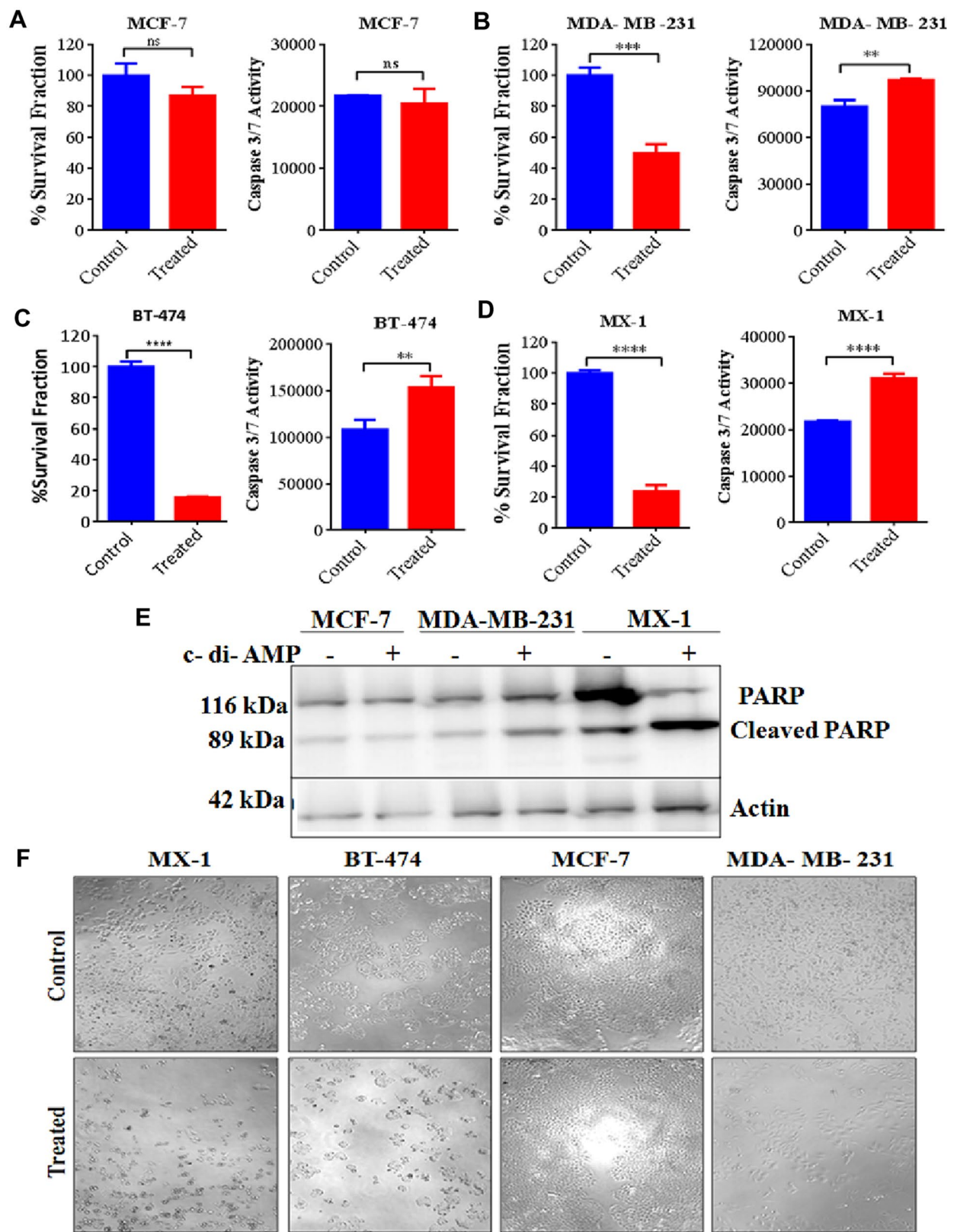


Fig. 3 c-di-AMP activates cell death in ER-negative breast cancer cell lines: Breast cancer cell lines treated with c-di-AMP (200 μ M) and cell survival was monitored by cell viability assay and Caspase3/7 activity (n=3, mean \pm SD). **a** MCF-7, **b** MDA-MB-231, **c** BT-474; **d**; MX-1 n=3, mean \pm SD). **e** MCF-7, MDA-MB-231, MX-1 treated with c-di-AMP (200 μ M) for 24 h and PARP cleavage was analysed by western blotting. **f** MCF-7, BT-474, MDA-MB-231 and MX-1 treated with c-di-AMP (200 μ M) and analysed by phase contrast microscopy image captured on the fourth day. *P<0.05, **P<0.01, ***P<0.001 and ****P<0.0001 based on a Student's t test

cells were observed in the presence of c-di-AMP as compared to untreated in both MDA-MB-231 cells and MX-1 (Fig. 6a). The co-localization of IRF-3 at mitochondria was checked by coexpressing IRF-3-GFP and mt-RFP constructs in MDA-MB-231 cells. Colocalization was measured by fluorescence microscopy in the presence and absence of c-di-AMP. We observed that localization of IRF-3 to mitochondria was significantly increased in c-di-AMP treatment condition in MDA-MB-231 cells (Fig. 6b).

Hence, we further analyzed if c-di-AMP induces mitochondrial-mediated apoptosis by measuring PARP cleavage and caspase-9 activation (Fig. 6c) Treatment of MDA-MB-231 and MX-1 cells with c-di-AMP cells showed the band of 89 kDa corresponding to a cleaved subunit of PARP predominantly in both cells whereas it was not observed in untreated cells. Further, we monitored the cleavage of Caspase-3 in similar conditions. The cleaved subunit of 17 kDa subunit was predominantly observed in c-di-AMP treated both MDA-MB-231 cells and MX1 cells (Fig. 6d). This was further confirmed by increased caspase 3/7 green fluorescence activity in both cells showing enhanced apoptotic cell death (Fig. 6e). Caspase-9 is activated upstream of executioner Caspase-3. Interestingly the cleaved subunit of 35 and 37 kDa was observed in c-di-AMP treated both MDA-MB-231 cells and MX1 cells. To further monitor the effect of c-di-AMP on the clonogenic ability of both MDA-MB-231 and MX-1 cells we performed a colony-forming assay in presence of c-di-AMP. The clonogenic ability of both MDA-MB-231 and MX-1 cells significantly decreased in presence of c-di-AMP (Fig. 6f). Overall, these results show that c-di-AMP enhances IRF-3 translocation to mitochondria and induces mitochondrial-mediated intrinsic pathway of apoptosis, inhibiting the clonogenic ability of STING positive breast cancer cells.

Discussion

Highly proliferating tumor cells show a high level of chromosomal instability which has become the hallmark of cancers of different origins [27]. Previous reports from

our lab and others had shown that ER-positive breast cancer cells are STING negative and using TCGA database we found negative gene expression correlation between *TMEM173* (STING) and *ESR1* (estrogen receptor) in breast cancer patients. This strongly suggests that ER expressing breast cancer cells have low expression of STING [28], whereas highly proliferative cells ER/PR/Her-2 negative, MDA-MB-231 and MX1 cells, are STING positive [24]. It has been observed that chromosomal instability promotes errors in chromosome segregation which leads to micronuclei formation and leakage of genomic DNA into the cytosol [9–14]. This leads to the activation of the cGAS–STING cytosolic DNA-sensing pathway and downstream noncanonical NF- κ B [29] signaling leading to proliferation and metastasis. Cyclic dinucleotide, cGAMP, is an endogenous high-affinity ligand for the adaptor protein STING [2]. The synthesis of the cGAMP analog like c-di-AMP in bacteria is an interesting phenomenon and modulate the STING pathway during infection however its potential in regulating these pathways and modulation of cell death in breast cancer cells has not been well studied.

We observed that c-di-AMP can activate NF- κ B and IFN pathways in breast cancer cells depending upon the presence of STING. It was observed that ER-positive cells are low STING or negative expressing cells and ER-negative cells show high STING positivity. The evidence here suggests that STING is eliminated or down-regulated during the early stage of the growth hormone ER/PR positive cells where some cells retained STING and became growth hormone-independent [30]. This supports the emerging hypothesis of clonal evolution of the cells which positively determines the tumor growth and metastasis by clonal amplification and retaining the gene expression at the different stages of cancer. The basal STING activation is essential for cell proliferation and metastasis by promoting non-canonical activation of NF- κ B [31]. This hypothesis is in consonance with earlier reports where STING positive cells showed enhanced proliferation, brain metastasis cells and chemoresistance in breast cancer cells and lung cancer cells [32]. Previously it had been observed that cGAMP can be transferred from the metastatic cells to brain astrocytes through cellular GAP junctions [29]. The intactness of the type-I IFN pathway and NF- κ B may play an essential role in tumor cells which can be therapeutically targeted. STING-NF- κ B and/IRF-3 pathway is intact in triple-negative breast cancer as compared to ER/PR-positive cells as observed in this study and can be differentially modulated by c-di-AMP. This is an interesting characteristic of aggressive breast cancer cells which can be further investigated and can be exploited therapeutically.

Interestingly sustained activation of the STING pathway by c-di-AMP shows the activation of cell death specifically in ER/PR negative cells and not in ER-positive cells where

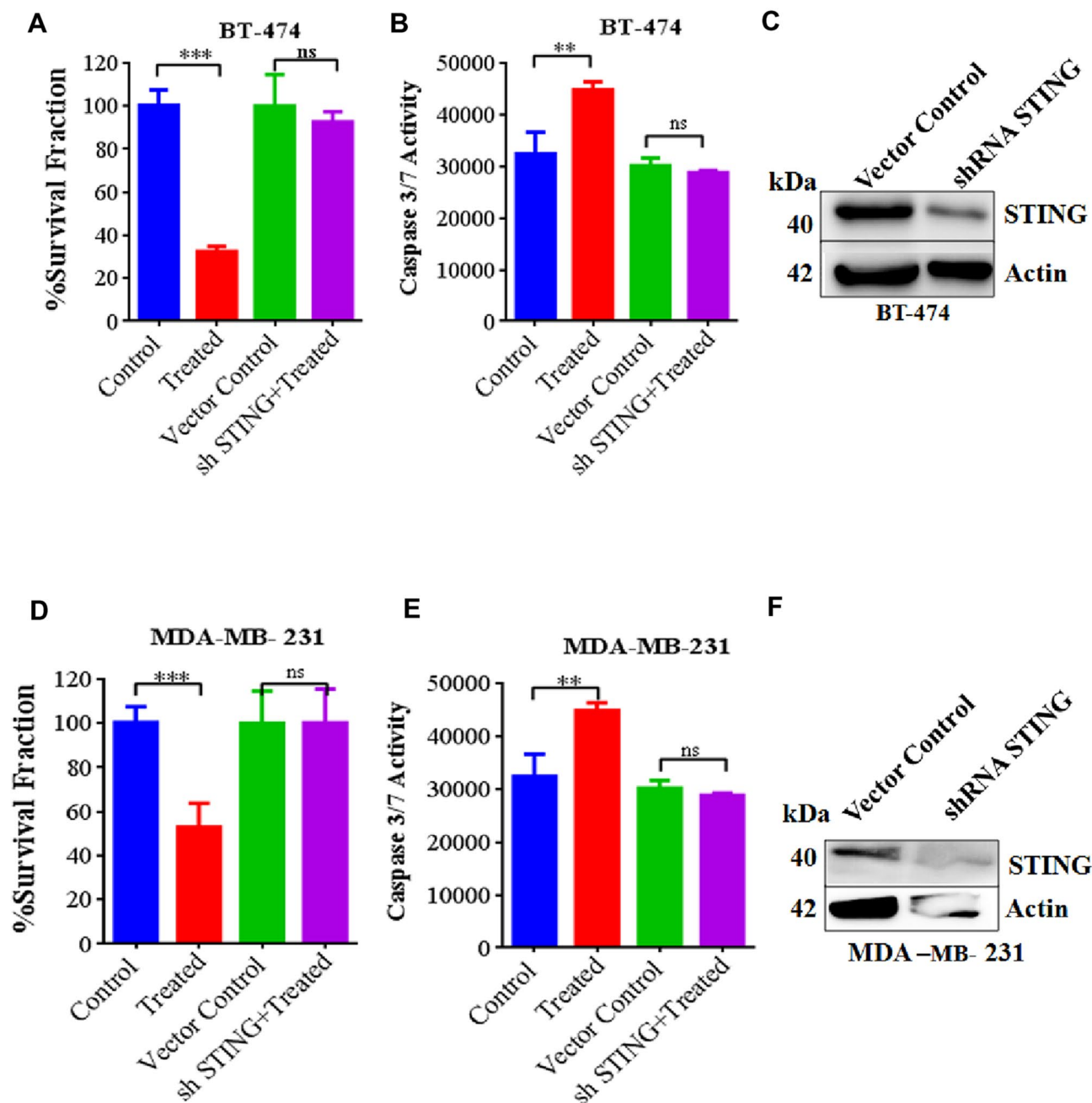


Fig. 4 STING is essential for c-di-AMP induced cell death: **a, d** BT-474 and MDA-MB-231 were transfected with STING shRNA and treated with c-di-AMP (200 μ M) for 4 days and cell survival was analysed (n=3, mean \pm SD). **b, e** BT-474 and MDA-MB-231 were transfected with STING shRNA and treated with 200 μ M c-di-AMP for

24 h and Caspase 3/7 activity was measured (n=3, mean \pm SD). **c, f** Western blot was performed to show the level of STING knockdown in BT-474 and MDA-MB-231 breast cancer cell lines.*P<0.05, **P<0.01 and ***P<0.001, based on a Student's t test

the IRF-3 pathway seems to be essential for the cell death pathway. Interestingly, c-di-AMP induces translocation of IRF-3 to mitochondria and activation of mitochondrial pathway in ER-negative cells, which is in consonance with the earlier observation of IRF-3 translocation to mitochondria during viral infection induced apoptosis [25]. This pathway

is although independent of the DNA binding ability and is dependent upon mitochondrial localization [33]. We also observed that mitochondrial functions are compromised leading to the activation of Caspase-9 mediated Caspase-3 activation in MDA-MB-231 cells and MX-1 cells. This pathway is not activated in MCF-7 and other ER-positive cells.

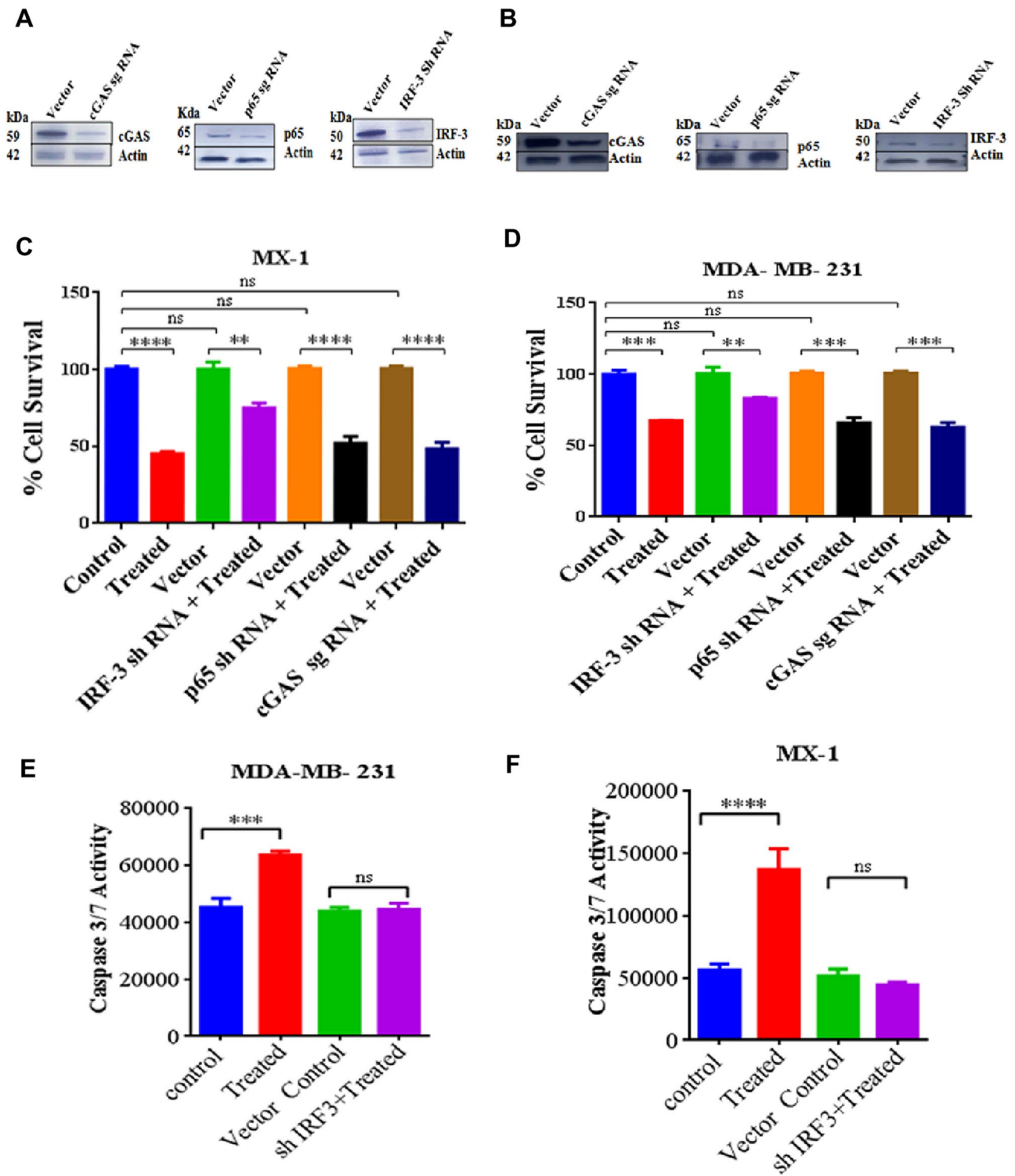
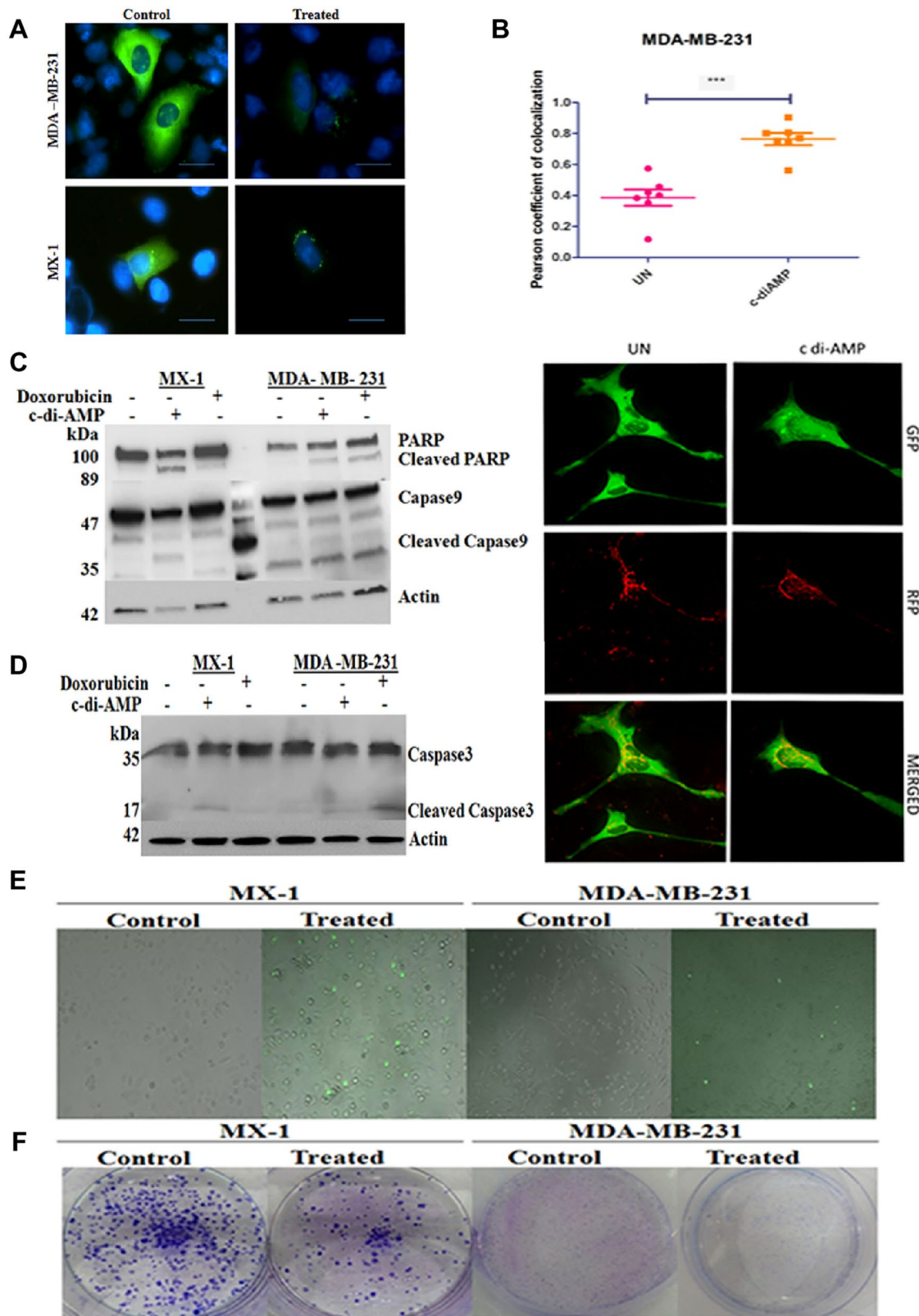


Fig. 5 c-di-AMP induces IRF-3 mediated apoptosis in STING positive, ER- negative breast cancer cells. cGAS, p65 and IRF-3 were knockdown MDA-MB-231 (a) and MX-1 (b) breast cell lines. MDA-MB-231 (c) and MX1 (d) with cGAS, p65 and IRF-3 knockdown were treated with c-di-AMP (200 μ M) and cell viability was measured by presto blue (n=3, mean \pm SD), cGAS, p65 and IRF-3 knock-

down MDA-MB-231 and MX-1 were knockdown in breast cell line and treated with c-di-AMP 200 μ M and caspase 3/7 activity measured (n=3, mean \pm SD). e MDA-MB-231, f MX-1 cells were knockdown with IRF-3 and treated with c-di-AMP (200 μ M) after 24 h caspase 3/7 activity measured *P < 0.05, **P < 0.01 and ***P < 0.001, based on a Student's t-test



MCF-7 is also IRF-3 positive cells however ER/PR positive cells are either less/negative STING, this suggests that a critical level of STING is required for c-di-AMP induced

cell death in breast cancer cells. The sustained activation of STING mediated pathways with fewer side effects is a requirement that may activate the immunogenic cell death

Fig. 6 c-di-AMP activates STING mediated mitochondrial apoptosis **a** MDA-MB-231 and MX-1 STING expressing cell lines treated with c-di-AMP (200 μ M) for 24 h and IRF-3 puncta was analysed using fluorescent microscope. **b** MDA-MB-231 cells were transfected with IRF-GFP and mt-RFP constructs and their colocalization was measured using fluorescent microscopy in presence and absence of c-di-AMP. **c, d** Western blotting was performed in MDA-MB-231 and MX-1 STING expressing cell lines by treating with c-di-AMP 200 μ M after 24 h to measure cleaved PARP, Caspase 9 and cleaved caspase 3. **e** STING expressing cell lines MDA-MB-231 and MX-1 were treated with c-di-AMP (200 μ M) for 24 h and caspase 3/7 green activity was measured using microscopy. **f** MDA-MB-231 and MX-1 cells were treated with c-di-AMP (200 μ M) and the colony-forming assay was performed

pathway [34] specifically in triple-negative breast cancer cells which are highly proliferative and metastatic and show high-level chromosomal instability. It had been observed previously due to chromothripsis and formation of micro nuclei, there is a release of DNA in cytoplasm leading to cGAS/cGAMP/STING activation however no type-I IFN activation [35]. However release of DNA leads to activation of the non-canonical NF- κ B pathway which may be determined by the strength of cGAMP induced signaling and which is enzymatically regulated and determine the outcome. Therefore the sustained activation of this pathway by cGAMP analog-like c-di-AMP which may induce IRF3 translocation to mitochondria and induce intrinsic pathway of apoptosis is of therapeutic importance for immunogenic cell death in solid tumors. There is no direct comparison of cGAMP with cDNs however isolated studies suggest cGAMP rather than therapeutic beneficial it may further support growth [36, 37].

This study provides a rationale for screening the bacterial origin cyclic dinucleotides which may activate the intrinsic cell death pathway and may activate the immunogenic cell death pathway. Therefore, the bacterial-derived c-di-AMP and other analogues should be screened for their potential as combinatorial therapy with DNA damaging agent for therapeutic potential in breast cancer cell lines and patient-derived xenograft model. Previously, the potential of c-di-GAMP increased the expression levels of maturation markers CD80/CD86 and MHC-II on DCs isolated from spleens of 4T1 tumor-bearing mice, which is important for the presentation of tumor-associated antigens (TAAs) and activation of TAA-specific T cells and can cause tumor regression. The potential of c-di-AMP and other bacterial-derived nucleotide and human origin di-nucleotide should be explored for the potential in antigen presentation and tumor cell-intrinsic cell death mechanism and should be exploited for therapeutic potential.

Acknowledgements This work was partially supported by the Department of Science and Technology, Govt. of India, Grant Number INT/Korea/P-39 to Prof. Rajesh Singh. Authors acknowledge the

instrumentation facility at the Department of Biochemistry, The M. S. University of Baroda, Vadodara. Kritarth Singh received a Senior Research Fellowship from the University Grants Commission (UGC), Govt. of India. We also acknowledge DST FIST for providing an instrumentation facility for the work. Anjali Shinde received her fellowship from ICMR, India. Minal Mane received her fellowship from CSIR, Govt. of India. Dhruv Gohel received his fellowship from ICMR, India. Fatema Currim received her fellowship from INSPIRE, India.

Declarations

Conflict of interest The authors declare no conflict of interest.

References

- Soysal SD, Tzankov A, Muenst SE (2015) Role of the tumor microenvironment in breast cancer. *Pathobiol J Immunopathol Mol Cell Biol* 82(3–4):142–152
- Sormendi S, Wielockx B (2018) Hypoxia pathway proteins as central mediators of metabolism in the tumor cells and their microenvironment. *Front Immunol*. <https://doi.org/10.3389/fimmu.2018.00040/full>
- Sachet M, Liang YY, Oehler R (2019) The immune response to secondary necrotic cells. *Apoptosis*. <https://doi.org/10.1007/s10495-017-1413-z>
- Woo S-R, Corrales L, Gajewski TF (2015) Innate immune recognition of cancer. *Annu Rev Immunol* 33:445–474
- Weinberg SE, Sena LA, Chandel NS (2015) Mitochondria in the regulation of innate and adaptive immunity. *Immunity* 42(3):406–417
- Singh K, Sripada L, Lipatova A, Roy M, Prajapati P, Gohel D et al (2018) NLRX1 resides in mitochondrial RNA granules and regulates mitochondrial RNA processing and bioenergetic adaptation. *Biochim Biophys Acta Mol Cell Res* 1865:1260–1276
- Li A, Yi M, Qin S, Song Y, Chu Q, Wu K (2019) Activating cGAS-STING pathway for the optimal effect of cancer immunotherapy. *J Hematol Oncol*. <https://doi.org/10.1186/s13045-019-0721-x>
- Corrales L, McWhirter SM, Dubensky TW, Gajewski TF (2016) The host STING pathway at the interface of cancer and immunity. *J Clin Invest* 126(7):2404–2411
- Basit A, Cho M-G, Kim E-Y, Kwon D, Kang S-J, Lee J-H (2020) The cGAS/STING/TBK1/IRF3 innate immunity pathway maintains chromosomal stability through regulation of p21 levels. *Exp Mol Med* 52(4):643–657
- Medrano RFV, Hunger A, Mendonça SA, Barbuto JAM, Strauss BE (2017) Immunomodulatory and antitumor effects of type I interferons and their application in cancer therapy. *Oncotarget* 8(41):71249–71284
- Lu C, Klement JD, Ibrahim ML, Xiao W, Redd PS, Nayak-Kapoor A et al (2019) Type I interferon suppresses tumor growth through activating the STAT3-granzyme B pathway in tumor-infiltrating cytotoxic T lymphocytes. *J Immunother Cancer* 7(1):157
- Fuertes MB, Woo S-R, Burnett B, Fu Y-X, Gajewski TF (2013) Type I interferon response and innate immune sensing of cancer. *Trends Immunol* 34(2):67–73
- Maimela NR, Liu S, Zhang Y (2018) Fates of CD8+ T cells in tumor microenvironment. *Comput Struct Biotechnol J* 22(17):1–13
- Zhu Y, An X, Zhang X, Qiao Y, Zheng T, Li X (2019) STING: a master regulator in the cancer-immunity cycle. *Mol Cancer*. <https://doi.org/10.1186/s12943-019-1087-y>

15. Andrade WA, Firon A, Schmidt T, Hornung V, Fitzgerald KA, Kurt-Jones EA et al (2016) Group B streptococcus degrades cyclic-di-AMP to modulate STING-dependent type I interferon production. *Cell Host Microbe* 20(1):49–59
16. Ma F, Li B, Liu SY, Iyer SS, Yu Y, Wu A, Cheng G (2015) Positive feedback regulation of type I IFN production by the IFN-inducible DNA sensor cGAS. *J Immunol* (Baltimore, Md.: 1950) 194(4):1545–1554. <https://doi.org/10.4049/jimmunol.1402066>
17. Ablasser A, Hur S (2020) Regulation of cGAS- and RLR-mediated immunity to nucleic acids. *Nat Immunol* 21:17–29
18. Archer KA, Durack J, Portnoy DA (2014) STING-dependent type I IFN production inhibits cell-mediated immunity to listeria monocytogenes. *PLoS Pathog.* <https://doi.org/10.1371/journal.ppat.1003861>
19. Barker JR, Koestler BJ, Carpenter VK, Burdette DL, Waters CM, Vance RE et al (2013) STING-dependent recognition of cyclic di-AMP mediates type I interferon responses during chlamydia trachomatis infection. *mBio.* <https://doi.org/10.1128/mBio.00018-13>
20. Ahn J, Barber GN (2019) STING signaling and host defense against microbial infection. *Exp Mol Med* 51(12):1–10
21. Ran FA, Hsu PD, Wright J, Agarwala V, Scott DA, Zhang F (2013) Genome engineering using the CRISPR-Cas9 system. *Nat Protoc* 8(11):2281–2308
22. Tomar D, Singh R, Singh AK, Pandya CD, Singh R (2012) TRIM13 regulates ER stress induced autophagy and clonogenic ability of the cells. *Biochim Biophys Acta—Mol Cell Res* 1823(2):316–326
23. Huber KVM, Olek KM, Müller AC, Soon Heng Tan C, Bennett KL, Colinge J et al (2015) Proteome-wide small molecule and metabolite interaction mapping. *Nat Methods* 12(11):1055–1057
24. Bhatelia K, Singh A, Tomar D, Singh K, Sripada L, Chagtoo M et al (2014) Antiviral signaling protein MITA acts as a tumor suppressor in breast cancer by regulating NF- κ B induced cell death. *Biochim Biophys Acta.* <https://doi.org/10.1016/j.bbadis.2013.11.006>
25. Chattopadhyay S, Sen GC (2017) RIG-I-like receptor-induced IRF3 mediated pathway of apoptosis (RIPA): a new antiviral pathway. *Protein Cell* 8(3):165–168
26. Sun F, Liu Z, Yang Z, Liu S, Guan W (2019) The emerging role of STING-dependent signaling on cell death. *Immunol Res* 67(2–3):290–296
27. Vargas-Rondón N, Villegas VE, Rondón-Lagos M (2017) The role of chromosomal instability in cancer and therapeutic responses. *Cancers.* <https://doi.org/10.3390/cancers10010004>
28. Li T, Fu J, Zeng Z, Cohen D, Li J, Chen Q, Li B, Liu XS (2020) TIMER2.0 for analysis of tumor-infiltrating immune cells. *Nucleic Acids Res.* <https://doi.org/10.1093/nar/gkaa407>
29. Chen Q, Boire A, Jin X, Valiente M, Er EE, Lopez-Soto A, Jacob LS, Patwa R, Shah H, Xu K, Cross JR, Massagué J (2020) Carcinoma–astrocyte gap junctions promote brain metastasis by cGAMP transfer. *Nature.* <https://doi.org/10.1038/nature18268>
30. Zhang M, Lee AV, Rosen JM (2017) The cellular origin and evolution of breast cancer. *Cold Spring Harb Perspect Med.* <https://doi.org/10.1101/cshperspect.a027128>
31. Dunphy G, Flannery SM, Almine JF, Connolly DJ, Paulus C, Jønsen KL et al (2018) Non-canonical activation of the DNA sensing adaptor STING by ATM and IFI16 mediates NF- κ B signaling after nuclear DNA damage. *Mol Cell* 71(5):745–760.e5
32. Su T, Zhang Y, Valerie K, Wang X-Y, Lin S, Zhu G (2019) STING activation in cancer immunotherapy. *Theranostics* 9(25):7759–7771
33. Yanai H, Chiba S, Hangai S, Kometani K, Inoue A, Kimura Y et al (2018) Revisiting the role of IRF3 in inflammation and immunity by conditional and specifically targeted gene ablation in mice. *Proc Natl Acad Sci* 115(20):5253–5258
34. Gulen MF, Koch U, Haag SM, Schuler F, Apetoh L, Villunger A et al (2017) Signalling strength determines proapoptotic functions of STING. *Nat Commun* 8(1):1–10
35. Bakhom SF, Ngo B, Laughney AM, Cavallo JA, Murphy CJ, Ly P, Shah P, Sriram RK, Watkins TBK, Taunk NK, Duran M, Pauli C, Shaw C, Chadalavada K, Rajasekhar VK, Genovese G, Venkatesan S, Birkbak NJ, McGranahan N, Lundquist M, LaPlant Q, Healey JH, Elemento O, Chung CH, Lee NY, Imielenski M, Nanjangud G, Pe'er D, Cleveland DW, Powell SN, Lammerding J, Swanton C, Cantley LC (2018) Chromosomal instability drives metastasis through a cytosolic DNA response. *Nature* 553(7689):467–472. <https://doi.org/10.1038/nature25432>
36. Chen Q, Boire A, Jin X, Valiente M, Er EE, Lopez-Soto A, Jacob L, Patwa R, Shah H, Xu K, Cross JR, Massagué J (2016) Carcinoma-astrocyte gap junctions promote brain metastasis by cGAMP transfer. *Nature* 533(7604):493–498. <https://doi.org/10.1038/nature18268>
37. Kwon J, Bakhom SF (2020) The cytosolic DNA-sensing cGAS-STING pathway in cancer. *Cancer Discov* 10(1):26–39

Publisher's Note Springer Nature remains neutral with regard to jurisdictional claims in published maps and institutional affiliations.



DNA damage induces STING mediated IL-6-STAT3 survival pathway in triple-negative breast cancer cells and decreased survival of breast cancer patients

Hitesh Vasiyani¹ · Minal Mane¹ · Khushboo Rana² · Anjali Shinde¹ · Milton Roy³ · Jyoti Singh¹ · Dhruv Gohel¹ · Fatema Currim¹ · Ratika Srivastava² · Rajesh Singh^{1,4}

Accepted: 10 August 2022

© The Author(s), under exclusive licence to Springer Science+Business Media, LLC, part of Springer Nature 2022

Abstract

Triple-negative breast cancer is aggressive and metastatic breast cancer type and shows immune evasion, drug resistance, relapse and poor survival. Anti-cancer therapy like ionizing radiation and chemotherapeutic drug majorly induces DNA damage hence, alteration in DNA damage repair and downstream pathways may contribute to tumor cell survival. DNA damage during chemotherapy is sensed by cyclic GMP-AMP synthase(cGAS)-stimulator of interferon genes (STING), which determines the anti-tumor immune response by modulating the expression of programmed cell death ligand-1 (PD-L1), immune suppressor, in the tumor microenvironment. Triple-negative breast cancer cells are cGAS-STING positive and modulation of this pathway during DNA damage response for survival and immune escape mechanism is not well understood. Here we demonstrate that doxorubicin-mediated DNA damage induces STING mediated NF- κ B activation in triple-negative as compared to ER/PR positive breast cancer cells. STING-mediated NF- κ B induces the expression of IL-6 in triple-negative breast cancer cells and activates pSTAT3, which enhances cell survival and PD-L1 expression. Doxorubicin and STAT3 inhibitor act synergistically and inhibit cell survival and clonogenicity in triple-negative breast cancer cells. Knockdown of STING in triple-negative breast cancer cells enhances CD8 mediated immune cell death of breast cancer cells. The combinatorial treatment of triple-negative breast cells with doxorubicin and STAT3 inhibitor reduces PD-L1 expression and activates immune cell-mediated cancer cell death. Further STING and IL-6 levels show a positive correlation in breast cancer patients and poor survival outcomes. The study here strongly suggests that STING mediated activation of NF- κ B enhances IL-6 mediated STAT3 in triple-negative breast cancer cells which induces cell survival and immune-suppressive mechanism.

✉ Rajesh Singh
rajesh.singh-biochem@msubaroda.ac.in;
singhraj1975@gmail.com

Hitesh Vasiyani
hiteshvasiyani@yahoo.com

Minal Mane
meenalmene14cir@gmail.com

Khushboo Rana
khoshboorana612@gmail.com

Anjali Shinde
anjalisshinde4891@gmail.com

Milton Roy
roymilton1989@gmail.com

Jyoti Singh
singhjyoti9315@gmail.com

Dhruv Gohel
dhruvgohilbaroda@gmail.com

Fatema Currim
currimfatema53@gmail.com

Ratika Srivastava
srivastava.ratika@gmail.com

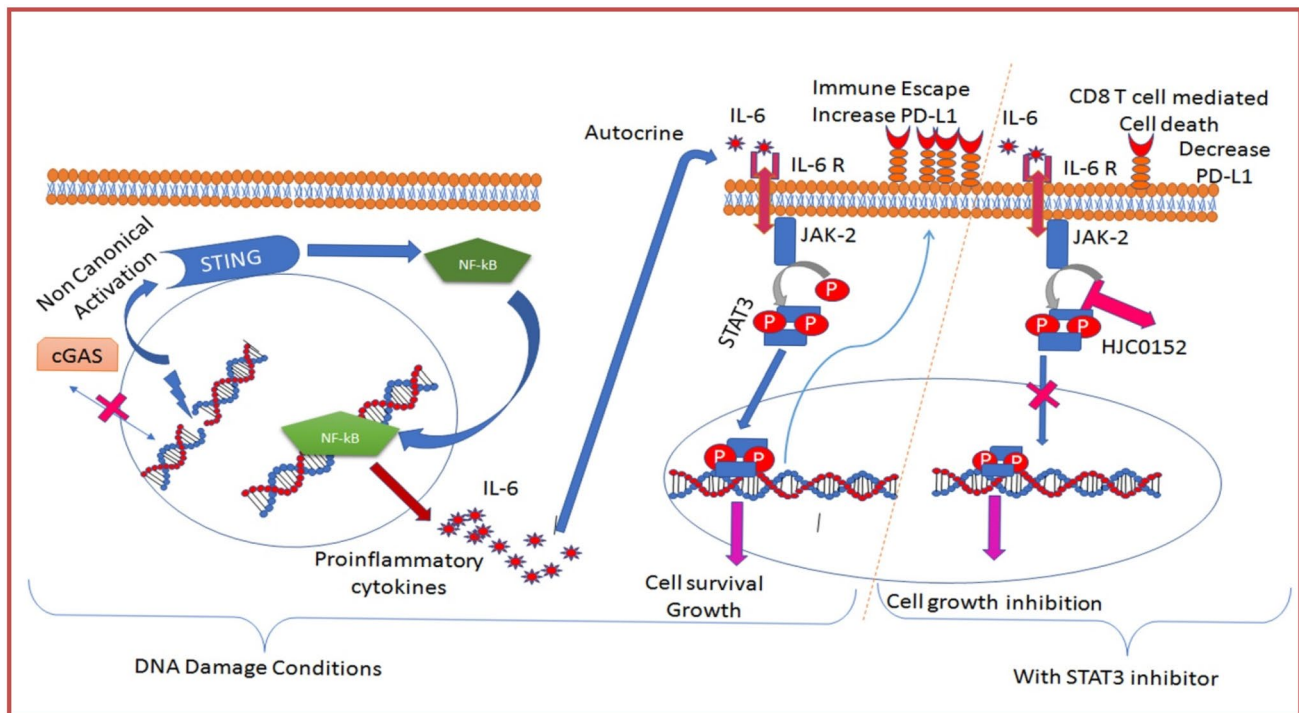
¹ Department of Biochemistry, Faculty of Science, The Maharaja Sayajirao University of Baroda, Vadodara, Gujarat 390002, India

² Department of Microbiology & Biotechnology Center, The M.S. University of Baroda, Vadodara, Gujarat 390002, India

³ Institute for Cell Engineering, John Hopkins University School of Medicine, 733 North Broadway, MRB 731, Baltimore, MD 21205, USA

⁴ Department of Mol and Human Genetics, Banaras Hindu University, Varanasi, UP 221005, India

Graphical abstract



Keywords STING · IL-6 · STAT3 · PD-L1 · Drug resistance · Immune escape

Introduction

The tumor microenvironment (TME) of solid tumors plays a significant role in progression and metastasis [1, 2]. The recruitment of the immune cells in TME of the solid tumor suggests the role of host immunity either to promote or inhibit the progression of cancer depending upon the stage of the tumor [3]. The cells of innate and adaptive immune response maintain strict surveillance of tumor cells and eliminate them. Hence immune regulation in the tumor microenvironment plays a critical role in determining the outcome of tumor progression [4]. The TME of different solid tumors shows a distinct pattern of cytokines, which may play a key role in supporting tumor cell growth and immune escape mechanisms [5, 6]. Many key cytokines act in the autocrine and paracrine mechanisms regulating tumor cell proliferation and growth in hostile TME [7]. High levels of IL-6 in serum and tumor have been associated with aggressiveness and poor outcome in cancer patients [8, 9]. IL-6 signaling is hyper-activated in many tumors including breast cancers [10]. Aberrant expression of IL-6 mediated STAT3 pY705 is seen in tumors having low prognostic value [11]. The potential of IL-6 as a modulator of anti-cancer

immune responses during genotoxic stress and tumor progression is not understood.

Chemotherapeutic agents like 5-fluorouracil and cisplatin induce DNA damage leading to NF-κB mediated expression and secretion of IL-6. Hyperactivation of IL-6 mediated downstream pathway leads to cell proliferation and invasiveness and develops chemoresistance in breast cancer [12]. During DNA damage conditions, nuclear DNA fragment leaks into the cytoplasm which can be recognized by cGAS, the cytoplasmic DNA sensor, to activate STING mediated inflammatory pathway [13]. Highly proliferative and malignant triple-negative breast cancer cells have high chromosomal instability which leads to increased micronuclei formation. This activates the cGAS-STING pathway which is associated with cell proliferation, invasiveness and migration [14]. Moreover, the tumor outcome also depends upon the activation of the immune evasion mechanism in the hostile TME by expression of PD-L1 on the tumor cell surface. Tumor cells engage with the PD-1 receptor of T cells which arrest the proliferation and inhibit their cytotoxic activity [15]. Moreover, the STING-mediated activation of IFN and NF-κB pathway may differentially regulate this immune checkpoint mechanism in TME. The previous report from our lab had observed that breast cancer cells show a

differential level of STING [16], however, their relevance in tumor survival advantage is still not well understood. It is important current to understand the molecular mechanisms by which DNA damage may escape the immune surveillance and promote tumor progression [17, 18].

Here we demonstrate that triple-negative breast cancer expressing a high level of STING induces NF- κ B activation under genotoxic stress conditions and enhances IL-6 levels. Sustained IL-6 autocrine signaling shows up-regulation of PD-L1 through the STAT3 pathway in the STING expressing ER-negative breast cancer cell lines which inhibit immune cell-mediated cancer cell death. STAT3 inhibitor HJC0152, with doxorubicin shows synergistic growth inhibition as well as reduction of PD-L1 expression and immune cell-mediated cancer cell death.

Materials and method

Cells line and culture

MCF-7, T47D, ZR75, BT-549, MDA-MB-231 and MDA-MB-468 were purchased from ATCC, USA. MCF-7 was cultured in EMEM media while T47D, ZR75 and BT-549 were maintained in RPMI medium. MX-1 was obtained from cell line service, Germany and cultured in F12K media. MDA-MB-231 and MDA-MB-468 were cultured in DMEM media (HI-MEDIA, India). The media were supplemented with 10% FBS (Life Technologies, USA) and 1% penicillin, streptomycin, and neomycin (PSN) antibiotic mixture (Life Technologies, USA). MDA-MB-231 STING knockdown stable cell lines generated via puromycin selection (2–4 μ g/mL). Cells were incubated at 37 °C, 5% CO₂ in specified media. All cell lines were checked for mycoplasma contamination by the Universal Mycoplasma detection kit (ATCC, USA).

Plasmids and reagents

STING-shRNA and IRF-3-shRNA were a generous gift from Dr. Peter Chumakov (Engelhardt Institute of Molecular Biology, Russian Academy of Sciences). STING cloned in pCMV6 ENTRY plasmid was a gift from Dr. Hong Bing Su (Wuhan University China), p65-GFP, p65-shRNA and control shRNA were received from Dr. Edurne Berra Ramirez (Gene Silencing Platform, CICbioGUNE, Derio, Spain). Primary antibody against STING was purchased from Proteintech, USA, cGAS and HRP-conjugated secondary anti-rabbit and anti-mouse antibodies were purchased from Thermo Scientific, Anti-PD-L1 antibody and secondary Alexa Flour 594 tag antibody purchased from abcam USA. Antibodies against PARP, pSTAT3Y705, total STAT3, Histone3, NF- κ B p65 and phospho-histone H2A.X were purchased from Cell signaling USA, Inc. PrestobluTM cell viability reagent from

Invitrogen, USA and Caspase-Glo[®] 3/7 Assay kit was purchased from Promega, USA, IL-6 ELISA R&D systems, USA. STAT3 inhibitor as HJC0152 purchased from selleckem, USA. Doxorubicin was purchased from Sigma, USA.

Generation of cGAS -sgRNA and p65-sgRNA clones

cGAS-sgRNA clones were generated using the protocol described by Ran et al. 2013. The guide-RNAs targeting the first exon of cGAS, p65 were designed using the GPP sgRNA Designer tool (Broad Institute) [19]. sg-RNA-top and sg-RNA-bottom strands were synthesized as described earlier [19]. Synthesized oligos were annealed and cloned into BbsI -linearized pSpCa9(BB)-2A-Puro (PX459) V2.0 vector. cGAS-sgRNA, p65-sgRNA clones were transformed into competent Stbl3 E. coli strain and transformants were screened by colony PCR using U6 sequencing primer and sg-RNA-bottom. Positive clones were confirmed by Sanger sequencing. Guide RNA sequence of p65 and cGAS are as following:

cGAS

5'CACCGAGACTC GGTGGGATCCATCG'3.
5'AAACCGA TGG ATC CCA CCG AGTCTC'3.

p65

5'CACCGTCAATGGCTACACAGGACCA'3
5'AAACTGGTCCTGTGTAGCCATTGAC'3

Transfection

MCF-7, T-47D, ZR75, BT-474, MX-1 and MDA-MB-231 were transfected with sgRNA cGAS, shRNA STING, STING-flag, p65-GFP, NF- κ B Luc, Renilla luc and control sgRNA, shRNA and Vector control using the manufacturer's protocol. X-treamGENE (Sigma, USA).

Western blot

Cells were plated at a density of 4.5 X 10⁵ cells/well in the six-well plate and transfected with indicated expression plasmid or shRNA/sgRNA using X-treamGENE (Sigma, USA). After 48 h of transfection, cells were harvested, washed with ice-cold PBS and lysed in buffer A (150 mM NaCl, 30 mM Tris-Cl, 10% Triton X-100, 10% Glycerol. Protease Inhibitor (Roche, Germany). The equal protein was loaded and resolved on 11% SDS-PAGE. Protein was electroblotted on the PVDF membrane at 110 V for 1 h at 4 °C. The membrane was blocked with 5% blocking buffer (5% non-fat dried milk and 0.1% Tween-20 in TBS) or 5% BSA (BSA (Sigma-Aldrich, USA), 0.1% Tween-20 in TBS-0.02 M

Tris-Cl, 0.15 M NaCl) for 1 h at room temperature. The membrane was incubated overnight with a specific primary antibody and washed three times with TBS-T (TBS containing 0.1% Tween-20) and incubated with a secondary antibody at room temperature for 1 h. The membrane was washed three times with TBS-T and the signal was visualized by using an EZ-ECL chemiluminescence detection kit for HRP (Biological Industries, Israel) by exposing it to UVTEC gel documentation system.

NF- κ B luciferase assay and IL-6 ELISA

To assess NF- κ B activity, MCF-7, MDA-MB-231 and MX-1 cells were plated at a density of 1×10^5 cells/well in 24 well plates and treated with doxorubicin and luciferase assay was performed using Dual-Glo luciferase assay system (Promega, USA) [20]. IL-6 levels were analyzed using ELISA as per the manufacturer's protocol (R&D systems USA).

Caspase3/7 activity

The activity was performed using Caspase-Glo® 3/7 Assay kit (Promega, USA), Cells were plated at the density of 5×10^3 cells per well in 96 well in white clear-bottom plates and treated with Doxorubicin and HJC0152 and a combination of both after 24 h Caspase-Glo® 3/7 (50 μ l) reagent was added to each well and luminescence was measured with a Centro LB 960 Luminometer (Berthold Technologies, Germany).

Cell growth inhibition assay and clonogenic assay

Cells were seeded at a density of 5000 cells/well in 96 well plates and treated with different concentrations of Doxorubicin and HJC0152 and a combination of both for 4 days. At the end of treatment, cell viability was analyzed using Presto blue cell viability reagent (Invitrogen, USA). The clonogenic assay has been performed as described previously [21].

Analysis of tumor-induced T cell suppression and colony formation assay

Human PBMCs were isolated from the blood of healthy volunteers using the Ficoll gradient centrifugation method. Briefly, 24-well plates were coated overnight with 5 μ g/ml anti-CD3 (BD Bioscience, USA), then washed twice with PBS. PBMCs were plated in complete DMEM medium (10% heat-inactivated fetal bovine serum, penicillin–streptomycin

and considered as Effectors cells. MDA-MB-231 control cell line and MDA-MB-231 shSTING stable cell lines plated in PBMC containing 24- well plates as Targets with target-to-effectors ratios of 1:0, 1:4, 1:16 in triplicates. Additionally, to analyze the PD-L1 mediated effect, the PD-L1 blocking antibody was also used in the same settings. After 4 days of co-incubation, 24-well plate wells were rinsed with PBS twice to harvest PBMCs. Further, plate with survived adherent tumor cells were fixed and stained with Giemsa staining solution. The dried plates were scanned and quantified the intensity. PBMCs were stained for CD45, CD4 and CD8 first, followed by fixation, permeabilization and intracellular staining of IFN- γ using fluorochrome-conjugated antibodies. 10,000 cells were acquired to assess the expression of IFN- γ by flow cytometer (BD FACS Calibur, Singapore).

Cell surface expression of PD-L1

To assess the expression of cell surface PD-L1, MDA-MB-231 and MDA-MB-231 STING knockdown stable cells were incubated with primary antibody (1:100) and washed with PBS and followed with incubation with secondary antibody and analyzed by flow cytometer. 10,000 cells were acquired to access the expression of PD-L1 by flow cytometer (BD FACS Calibur, Singapore).

Fluorescent microscopy

MDA-MB-231 and MCF-7 cells were seeded in an optical bottom dish and transfected with p65-GFP. After overnight incubation transfected cells were treated with doxorubicin and imaged using NIKON (Japan) Eclipse Ti2-E inverted fluorescent microscope.

PARP cleavage

MDA-MB-231 and MX-1 were seeded at density with 1×10^5 cells/well in 24 well plates and treated with doxorubicin and HJC0152 and a combination of both. After treatment of 24 Hrs, cells were collected, lysed and PARP cleavage was analyzed using western blotting as described above.

3D spheroid inhibition assay

MDA-MB-231 and shRNA-STING-MDA-MB-231 cells 3D spheroids were generated. 2000 cells were seeded per well in NunclonSphera plate in 100 μ L and the plate was centrifuged at 290 \times g for 3 min and incubated in a complete

medium containing 3 µg/ml collagen-I. The next day plate was centrifuged at 100Xg for 3 min and incubated for 24 h followed by treatment with doxorubicin. After 7 days the cell viability was measured as per CellTiter-Glo® 3D Cell Viability AssayPromega, USA.

Subcellular fractionation

MCF-7, MDA-MB-231 and MDA-MB-468 cells were resuspended in buffer A (10 mM HEBES, 0.1 mM EDTA, 10 mM KCL, 0.4%NP40, 0.5 mM DTT and 1 mM PMSF) and incubated for 20 min on ice. The lysates were centrifuged for 5 min at 200×g at 4 °C, and the supernatant was collected (cytosolic fraction). The nuclear fraction was resuspended in buffer B (2 mM HEPS,400 mM NaCl,1 mM EDTA,1 mM DTT,1 mM PMSF) and incubated on ice for 20 min and centrifuged at 15000xg at 4 °C and the supernatant was collected and analyzed further by western blotting.

Survival analysis

Breast cancer patients in The Cancer Genome Atlas (TCGA) database were ranked by chemotherapy (Adjuvant therapy) These groups were analyzed in a Kaplan–Meier survival plot to estimate the correlation between the gene’s expression level and survival of patients. The KM plots for each probe along with Hazard Ratio (HR) and P value were plotted [22].

TIMER database analysis

Tumor Immune Estimation Resource (TIMER) is a web server for Comprehensive Analysis of Tumor-Infiltrating Immune Cells [23]. We used the “Correlation” module to get the expression scatterplots, Spearman’s correlation and estimated statistical significance between TMEM173 STING and CD274(PD-L1) expression, and also for correlation between CD274(PD-L1) and IL6 expression in breast cancer. Finally, TMEM173(STING) directly correlated with gene CD274(PD-L1), ESR1(Estrogen receptor) and IL6. Partial correlation conditioned was adjusted to none.

Statistical analysis

The experiments were repeated independently and represented by Mean ± SD. Comparisons between two groups or multiple groups were performed by Student’s t-test or one-way ANOVA (Kruskal–Wallis post- hoc Dunn multiple comparisons), respectively. The experiments

were performed a minimum of two times independently. Statistically significant differences are indicated as follows: *p < 0.05; **p < 0.01; ***p < 0.001; ****p < 0.0001. Statistical details of experiments can be found in the figure legends.

Results

DNA damage induces NF-κB activation in STING positive triple-negative breast cancer cells

DNA damaging agents acting on the genome of the rapidly proliferating cancer cells had been the preferred target for developing chemotherapeutic anti-tumor drugs. Doxorubicin, a topoisomerase inhibitor, stalls the replication fork causing toxic DSBs and cell death [24]. Doxorubicin is one of the most effective agents for the treatment of breast cancer however, it can not eliminate all the breast cancer cells at the late stage and may provide a survival advantage Hence, we used doxorubicin-induced stress to understand its implication in DNA damage-induced inflammation, immune-suppressive mechanisms and cell death. We analyzed the expression of cGAS and STING using western blotting in breast cancer cells. We used ER-positive: MCF-7, T47D and ZR75, PR positive: MX-1, HER2 Positive: BT-549, and triple-negative: MDA-MB-468, MDA-MB-231 breast cancer cells. The 59 kDa band corresponding to cGAS was observed in all the breast cancer cell lines (Fig. 1A). Western blotting showed that ER/PR positive cell lines: MCF-7, T47D, and ZR75 show low or undetectable STING expression, whereas HER2 positive: BT-549 and TNBC cell line: MDA-MB-468, MDA-MB-231 showed higher expression of STING (Fig. 1B). Double-stranded breaks induced by DNA damaging agent lead to phosphorylation of Ser-139 residue of the histone variant H2AX, forming γH2AX, which is observed in different cell types and recruits proteins of DNA damage repair pathway. The detection of γH2AX has become an established marker of a double-stranded break during DNA damage [25]. Hence, we analyzed γH2AX in doxorubicin-treated breast cancer cells. We observed doxorubicin-induced upregulation of γH2AX in a time-dependent manner (Fig. 1C). We further used MCF-7 as STING negative and MDA-MB-231 as STING expressing cell line for analysis of STING mediated NF-κB activation during DNA damage. MDA-MB-231 showed higher activation of the NF-κB pathway, whereas it remained at basal level in the MCF-7 cell line. DNA damage-induced NF-κB

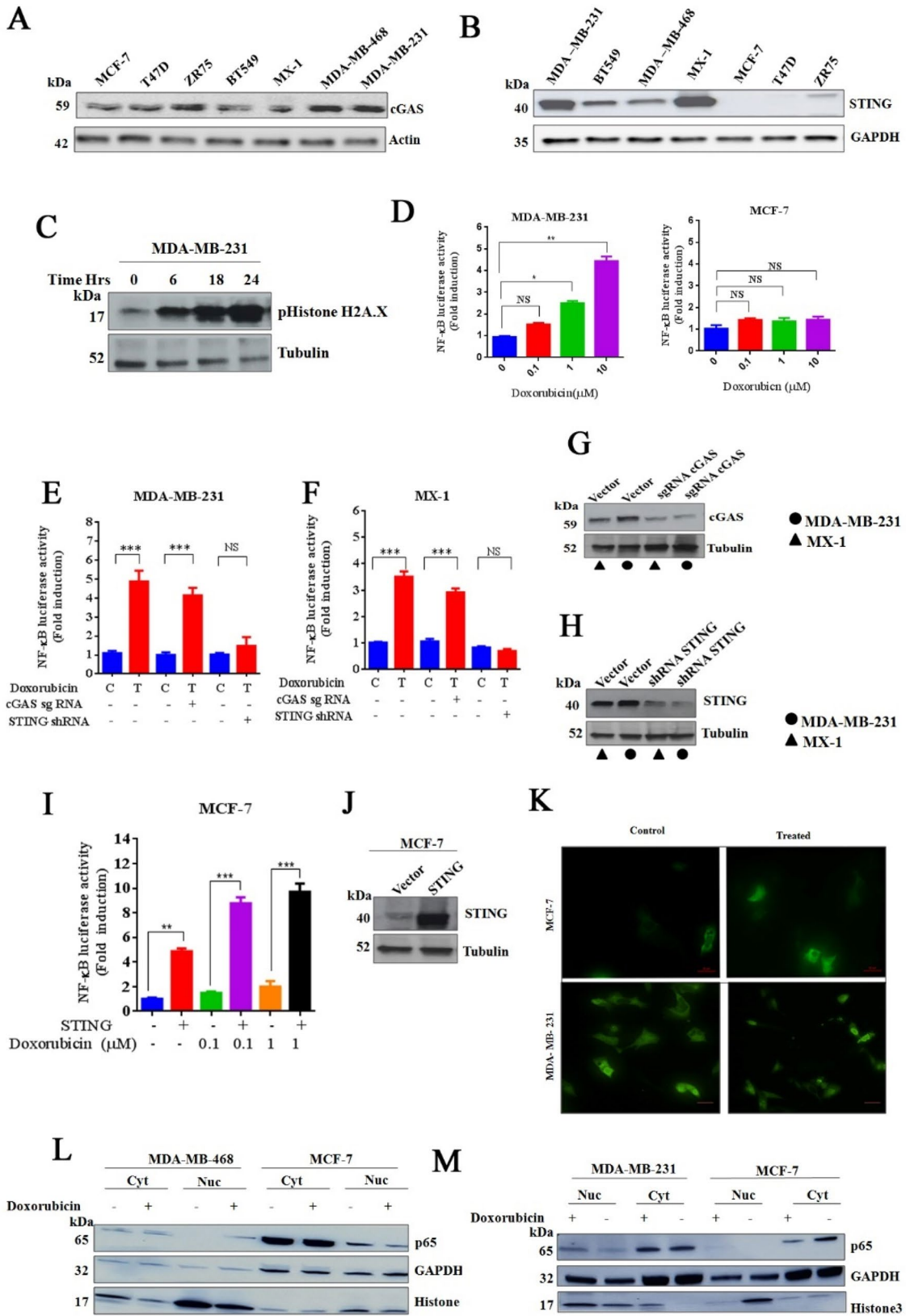


Fig. 1 DNA damage induces NF- κ B activation in STING positive triple-negative breast cancer cells. Analysis of expression of cGAS and STING in breast cancer cells: Expression of cGAS and STING was analyzed by western blotting in MCF-7, T47D, ZR75 ER (+ve), MX-1 PR(+ve), BT549 HER2 (+ve), and MDA-MB-231, MDA-MB-468 as triple-negative cell lines (A) and for STING (B). Doxorubicin induced activation of phospho-Histone H2A.X in a time-dependent manner: MDA-MB-231 cells were treated with doxorubicin, cell lysate was collected at different time points and western blot was performed (C). Analysis of STING mediated NF- κ B activation by luciferase assay: MCF-7 and MDA-MB-231 were transfected with 5X-NF- κ B-Luc and treated with doxorubicin for 24 h and luciferase activity was analyzed using DLR assay. Data represent mean fold change compared to control (n=3, mean \pm SD); *p<0.05, **p<0.01 and ***p<0.001, based on a one-way ANOVA (Kruskal–Wallis post-hoc Dunn multiple comparisons) (D). Effect of cGAS and STING knockdown on NF- κ B activation: Sequentially cGAS and STING knockdown in MDA-MB-231 and MX-1, cells were transfected with 5X-NF- κ B-Luc and treated with doxorubicin for 24 h and luciferase activity was analyzed using DLR assay. Data represent mean fold change compared to control (n=3, mean \pm SD): *p<0.05, **p<0.01 and ***p<0.001, based on a Student's t-test (E, F). Representative western blot for knockdown of cGAS and STING in MDA-MB-231 and MX-1 (G, H). Effect of STING overexpression on NF- κ B activation in MCF-7 cells: MCF-7 cells were co-transfected with STING and 5X-NF- κ B-Luc and treated with doxorubicin for 24 h and luciferase activity was analyzed using DLR assay. Data represent mean fold change compared to control (n=3, mean \pm SD); *p<0.05, **p<0.01 and ***p<0.001, based on a Student's t-test (I) and representative western blot image for overexpression of STING in MCF-7 (J). Analysis of p65 translocation during DNA damage in breast cancer cells: MCF-7 and MDA-MB-231 were transfected with p65-GFP and treated with doxorubicin for 6 Hrs and translocation of p65 was analyzed under a fluorescent microscope (K). Nuclear translocation of p65 to the nucleus by western blotting: MCF-7 and MDA-MB-231 and MDA-MB-468 cells were treated with doxorubicin for 6 Hrs and subcellular fractions were prepared and analyzed by western blotting using specific antibodies (L, M)

activity was further enhanced in MDA-MB-231 cells as compared to MCF-7 cells (Fig. 1D). DNA damage-induced NF- κ B activation may be essential for survival during genotoxic stress conditions [26], hence, we analyzed the role of cGAS/STING in NF- κ B expression in different cell lines. The knockdown of cGAS and STING in MDA-MB-231 and MX-1 cell lines, cGAS knockdown showed no effect on NF- κ B activation during DNA damage whereas STING knockdown inhibits NF- κ B activation (Fig. E, F). The knockdown of cGAS and STING in MDA-MB-231 and MX-1 was confirmed by western blotting (Fig. 1G, H). Nuclear translocation of p65-GFP was observed in doxorubicin treated MDA-MB-231 (STING +ve cell line), whereas it remained in cytoplasm both in control and doxorubicin treated, MCF-7, (STING -ve cell line) (Fig. 1K). We further confirmed the nucleus translocation of p65 by subcellular fractionation

and western blotting. MDA-MB-231 and MDA-MB-468 show higher levels of p65 in the nucleus as compared to the MCF-7 STING negative cell line (Fig. 1L, M). To confirm if STING was essential for NF- κ B activation in MCF-7 (ER/PR +ve breast cancer cells), we overexpressed STING in MCF-7 and monitored NF- κ B activation. The expression of STING in MCF-7 shows upregulation of NF- κ B (Fig. 1I, J). The evidence here suggest STING is highly expressed in triple-negative breast cancer cells as compared to ER/PR positive cells and is essential for NF- κ B activation during DNA damage conditions.

STING mediated NF- κ B activation induces IL-6 expression in triple-negative breast cancer cells in DNA damage conditions

The activation of NF- κ B in breast cancer cells in the tumor microenvironment leads to expression of several cytokines which may amplify survival signals and leads to resistance to cell death during stress conditions [27]. Hence, we analyzed the possible role of STING mediated differential NF- κ B activation modulating the expression of IL-6, a key cytokine that is essential for survival and drug resistance in breast cancer cells [28]. Different sub-types of breast cancer cells were treated with doxorubicin and analyzed for IL-6 secretion by ELISA. Interestingly, MCF-7, T47D, and ZR75 (ER/PR positive cells) show basal IL-6 levels whereas MX-1, BT549, MDA-MB-231, and MDA-MB-468 (Triple-negative cells) showed significant elevated IL-6 levels (Fig. 2A). The expression and secretion of IL-6 increased with time in presence of doxorubicin in MDA-MB-231 (STING +ve cell line) as compared to T47D (STING -ve cell line) suggesting that STING is essential for the expression of IL-6 (Fig. 2B). IL-6 binds to its cognate receptor complex IL6R/gp130 and activates downstream Janus kinases (JAKs), which activate downstream STAT3 through phosphorylation of Tyrosine 705 [29]. We investigated if IL-6 differentially activates a downstream pathway in the STING high/low breast cancer cells. We treated the cells with doxorubicin and monitored pSTAT3 Y705 phosphorylation by western blotting using a phospho-STAT3 specific antibody. The phosphorylation of STAT3 was significantly enhanced in MDA -MB-231, STING positive cells whereas was not detected in T47D as STING negative cell line (Fig. 2C). Previous reports suggested that DNA damage-induced IL-6 may activate downstream JAK-STAT pathway STAT3 via an autocrine mechanism [30]. STING was knockdown both in MDA-MB-231 and MX-1 and monitored pSTAT3 Y705 using a

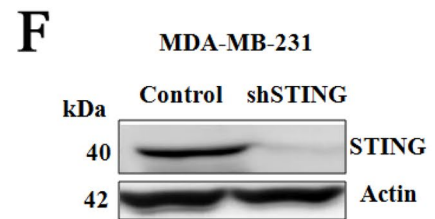
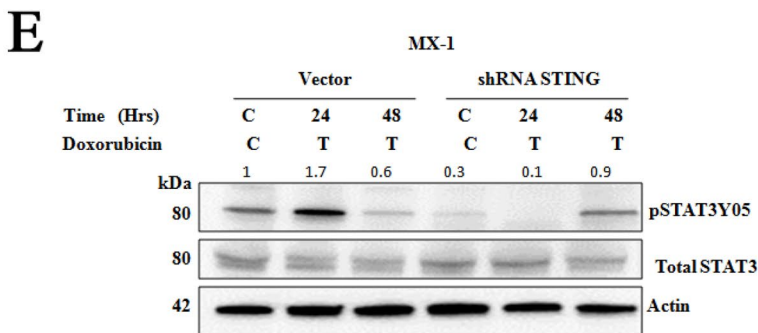
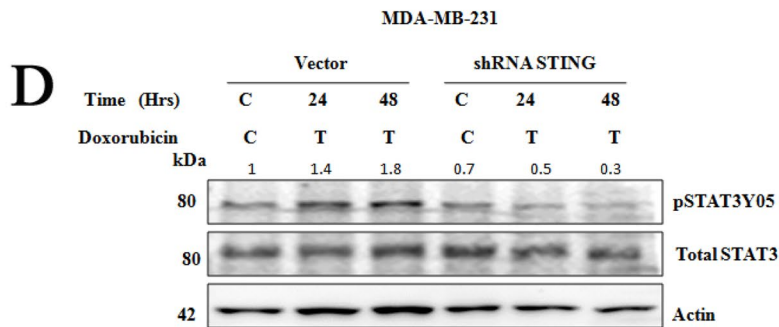
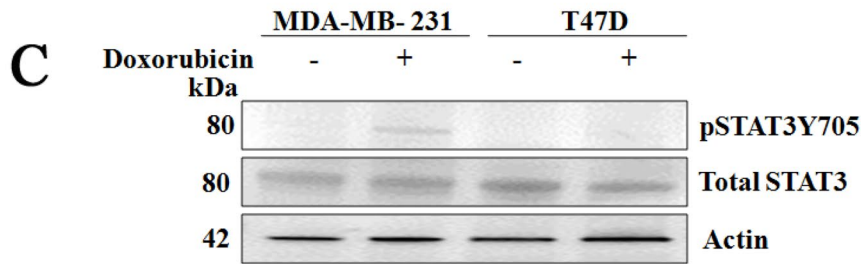
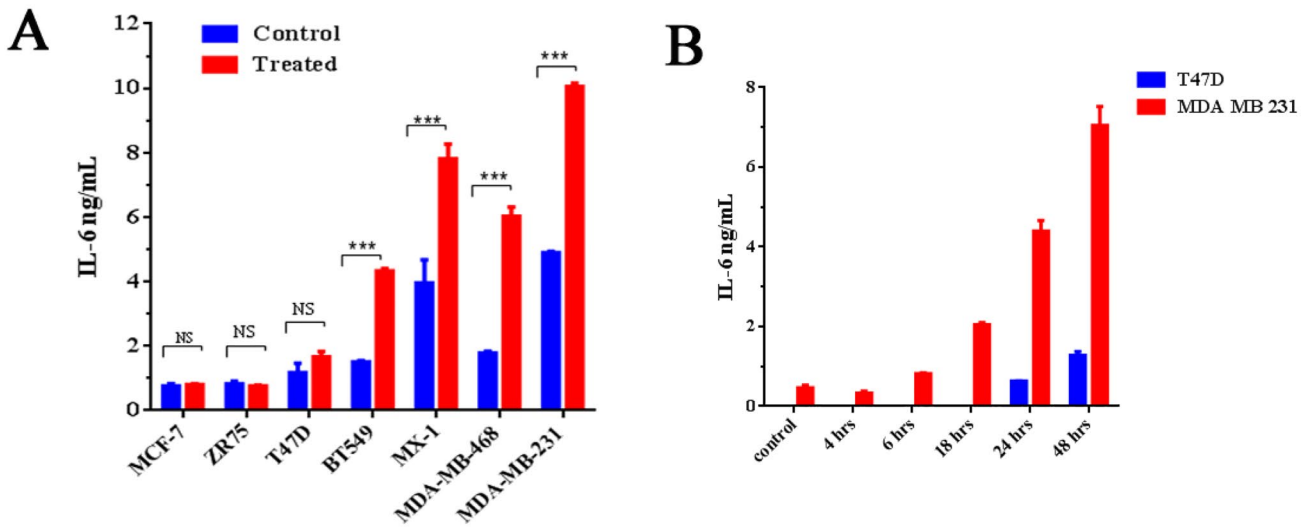


Fig. 2 STING mediated NF- κ B activation induces IL-6 expression in triple-negative breast cancer cells in DNA damage conditions. Analysis of IL-6 during DNA damage: Breast cancer cell lines treated with doxorubicin and IL-6 levels were analyzed in media by ELISA, Data represent mean change compared to control (n=3, mean \pm SD): *p<0.05, **p<0.01 and ***p<0.001, based on a Student's t-test (A). Analysis of IL-6 levels during DNA damage at different time points: T47D and MDA-MB-231 cell lines were treated with doxorubicin and IL-6 was analyzed by ELISA at the different time points (B). Analysis of pSTAT3Y705 during DNA damage: T47D and MDA-MB-231 cell lines were treated with doxorubicin for 24 h and pSTAT3Y705 levels were analyzed via western blotting (C). Effect of STING knockdown on level pSTAT3Y705 during DNA damage: MDA-MB-231 and MX-1 were transfected with shRNA of STING and treated with doxorubicin for 24 and 48 h and levels of pSTAT3Y705 were analyzed by western blotting (D, E). Analysis of STING knockdown: Western blot was performed to show the level of STING knockdown in MDA-MB-231 (F) and MX-1 (G) breast cancer cell lines.

specific antibody. Interestingly, pSTAT3 Y705 levels were elevated in MDA-MB-231 and MX-1 control cells and were undetectable in STING knockdown conditions (Fig. 2D, E). The knockdown of STING expression was also confirmed in both cell lines (Fig. 2F, G). The evidence here suggests DNA damage induces STING mediated IL-6 expression and autocrine activation of downstream STAT3 pathway in triple-negative breast cancer cells.

The knockdown of STING sensitizes breast cancer cells to genotoxic stress and inhibits clonogenicity

The activation of the IL-6/STAT3/NF- κ B pro-inflammatory circuit in tumor cells, other cell types in TME, and cancer-associated fibroblasts isolated from breast cancer patients play a critical role in tumor progression [27]. We investigated if STING-mediated NF- κ B/IL-6/STAT3 activation is important for the resistance to genotoxic drugs in breast cancer cells. We knockdown STING in MDA-MB-231 and MX-1 and treated them with doxorubicin and monitored cell viability. Knockdown of STING sensitized both MDA-MB-231 and MX-1 cells to doxorubicin (Fig. 3A, C). IC₅₀ of doxorubicin shifted 0.126 μ M to 0.066 μ M in STING knockdown in MDA-MB-231, a similar IC₅₀ shift was also observed in MX-1 with 0.07 μ M to 0.03 μ M in STING knockdown conditions (Fig. 3B, D). We generated a stable knockdown of STING in MDA-MB-231(shSTING) and monitored its ability to generate a 3D spheroid. Further MDA-MB-231 form a strong and dense spheroid whereas MDA-MB-231(shSTING) formed dispersed spheroid and showed inhibition of spheroid formation in the presence of doxorubicin (Fig. 3E). We also analyzed the sensitivity of the MDA-MB-231(shSTING) to doxorubicin by analyzing the

cell viability and observed that MDA-MB-231(shSTING) cells were more sensitive and showed decreased viability as compared to control MDA-MB-231 cells (Fig. 3F). We also analyzed the clonogenic abilities of both MDA-MB-231 cells and BT-549 cells in STING knockdown cells. Interestingly reduced STING levels reduce the clonogenic abilities of both MDA-MB-231 (Fig. 3G) and BT-549 cells (Fig. 3H).

STING mediated IL-6 induction enhances PD-L1 expression during DNA damage in triple-negative breast cancer cells

Genotoxic stress may induce the release of nuclear DNA in the cytosol and the formation of micronuclei which activate the STING mediated NF- κ B pathway further modulating the survival pathway and immune suppression mechanism by regulating PD-L1 [31, 31]. We analyzed if STING modulates the immune suppressive mechanisms in breast cancer cells in the presence of doxorubicin. Interestingly, MDA-MB-231 cells treated with doxorubicin showed an enhanced level of 45 kDa band corresponding to PD-L1 (Fig. 4A). As we observed above doxorubicin-induced IL-6 expression and release hence we hypothesized that STING regulated IL-6-STAT3 pathway may regulate the expression of PD-L1. Hence, we treated MDA-MB-231 cells with IL-6 and monitored the expression of PD-L1 by western blotting. The western blotting showed that PD-L1 expression was directly proportional to the dosage of IL-6 (Fig. 4B). To confirm if the expression of PD-L1 is mediated through STING/IL-6/STAT3 pathway, STING was knockdown in MDA-MB-231 and monitored PD-L1 expression. The knockdown of STING in MDA-MB-231 cells decreased PD-L1 expression (Fig. 4C). We used HJC0152, an Anti-helminthic drug that inhibits STAT3 phosphorylation and hence inhibits the STAT3 pathway [33]. MDA-MB-231 cells treated with HJC0152 and showed a decreased level of PD-L1 (Fig. 4D). Flow cytometry analysis also showed decreased surface expression of PD-L1 in STING knockdown MDA-MB-231 (Fig. 4E), as monitored by mean fluorescence Intensity (Fig. 4F). These experiments suggest that STING-mediated IL-6 production during DNA damage conditions induces PD-L1 expression which may be one of the immune escape and suppression mechanisms in breast cancer cells during DNA damage. Overexpression of PD-L1 on cancer cells helps to escape the cell-mediated immune response, hence we tested further inhibiting PD-L1/PD1 interaction using an anti-PD-L1 antibody. MDA-MB-231 (control) and MDA-MB-231(shRNA STING) knockdown cells were incubated with PD-L1 antibody and activated lymphocytes. The activated lymphocytes were able to

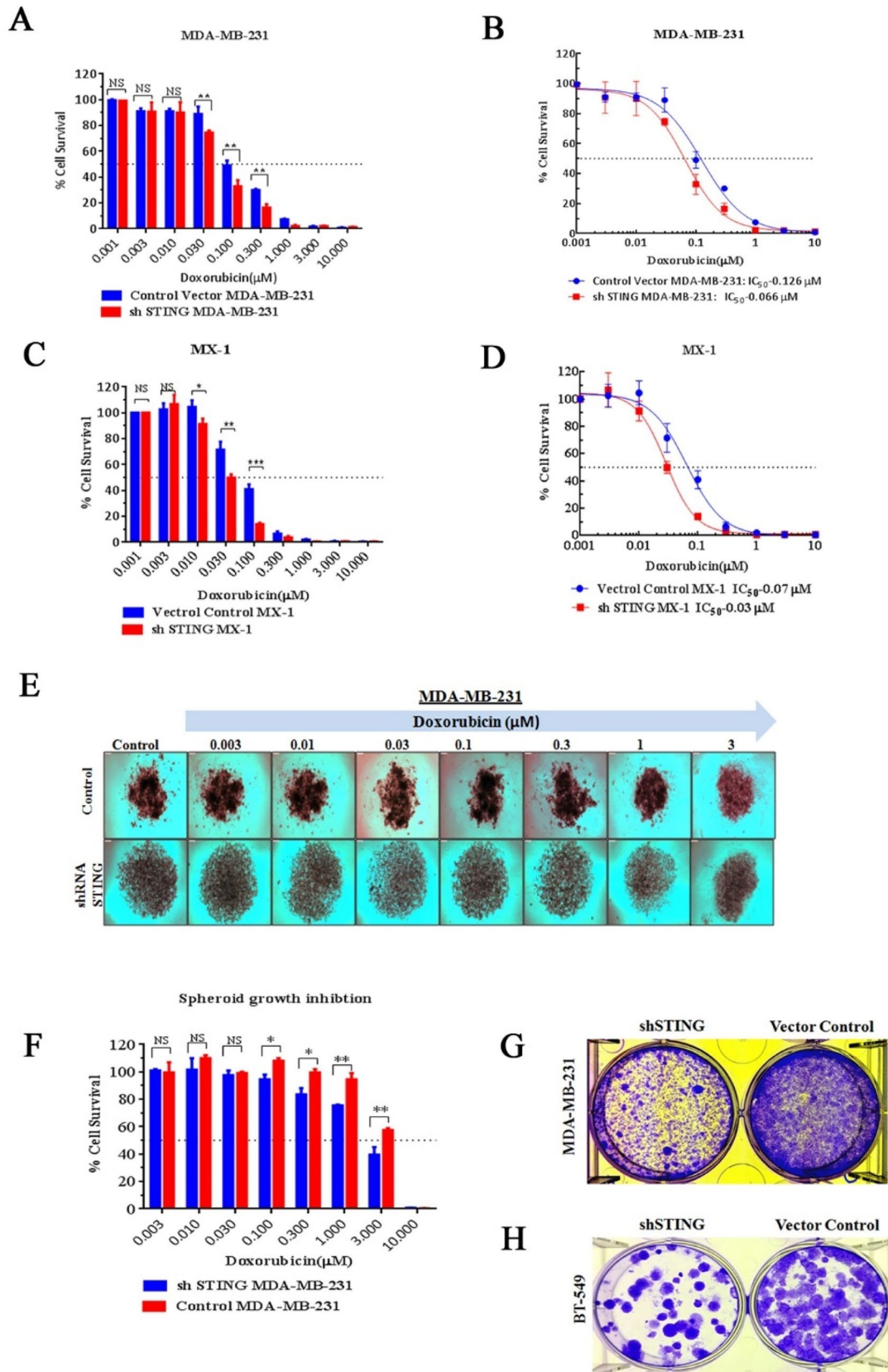


Fig. 3 The knockdown of STING sensitizes breast cancer cells to genotoxic stress and inhibits clonogenicity. Effect of STING knockdown on cell survival in presence of doxorubicin: MDA-MB-231 and MX-1 were transfected with STING shRNA and treated with different concentrations of doxorubicin for 4 days and % viability was analyzed. Data represent mean treated change compared to control (n=3, mean±SD): *p<0.05, **p<0.01 and ***p<0.001, based on a Student's t-test (A) and (C). Effect of knockdown of STING on growth in presence of doxorubicin and IC₅₀ was calculated (B) and (D) Effect of doxorubicin on 3D spheroid condition: MDA-MB-231 and MDA-MB-231 (shSTING) cells were seeded to form spheroid as described in the method section, spheroid generation at different concentrations of doxorubicin was analyzed after 7 days (E). Cell viability is plotted as Bar plot. Data represent mean treated change compared to control (n=3, mean±SD): *p<0.05, **p<0.01 and ***p<0.001, based on a Student's t-test (F) Effect of STING knockdown on clonogenicity: MDA-MB-231 and BT-549 were transfected with STING shRNA and colony formation assay was performed (G, H).

induce immune cell death in anti-PD-L1 treated cells. Interestingly MDA-MB-231(shRNA STING) cells with lymphocytes show a similar level of activated PBMCs mediated cell death. This further supports our hypothesis that STING expression in triple-negative breast cancer provides an immune escape mechanism during DNA damage conditions. The stable cell line MDA-MB-231(STING shRNA) line showed decreased expression of PD-L1 as compared to the control MDA-MB-231(WT) parent cell line. Down-regulation of PD-L1 show enhanced T cell activity in CD4 and CD8 T cells reflected by higher cell death of target cells. Giemsa stained surface area plotted using ImageJ (Fig. 4G) and representative image of geimsa stain. (Fig. 4H) was plotted. Significantly higher amount of IFN- γ production by both CD8 and CD4 T cells was observed in response to sh STING target cells as compared to WT target cells at 1:16 target: effector ratio as assessed by intracellular staining and flow cytometry (Fig. 4I, J). Atezolizumab, FDA-approved PD-L1 inhibitor antibody was used as a positive control for the suppressive effect.

STAT3 inhibitor, HJC0152 and doxorubicin act synergistically in breast cancer cells to inhibit cell death

STAT3, a transcription factor, is hyper-activated in many tumor cells including breast cancer [34], and its inhibition has been proposed as a possible drug target in breast cancer [30, 35]. Hence, we analyzed the combinatorial cytotoxic potential of HJC0152, STAT3 inhibitor and doxorubicin against MDA-MB-231 and MX-1 cell lines. Interestingly combination of both the drug shows a synergistic effect in growth inhibi-

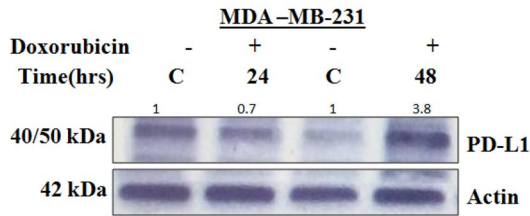
tion (Fig. 5A, B), Microscopic analysis also showed enhanced cell death in presence of combinatorial treatment of doxorubicin and HJC0152 (Fig. 5E). Caspase3/7 activity also increased in MDA-MB-231 and MX-1, STING +ve cell lines, in presence of both HJC0152 and doxorubicin as compared to individual treatments (Fig. 5C, D). We also checked the PARP cleavage as a marker of apoptosis in these conditions via western blotting. The band of 86 kDa corresponding to cleaved PARP cleavage increased significantly in combinatorial treatment conditions as compared to individual treatments (Fig. 5F, G)

STING expression positively correlates with IL6 and PD-L1 expression and high STING expression in chemotherapy shows poor survival

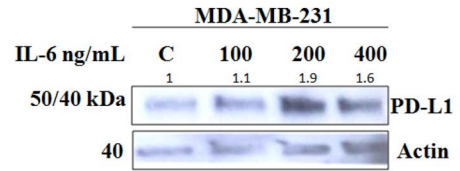
Tumor Immune Estimation Resource (TIMER) is a database of more than 32 cancer and is a web-based server to analyze the correlation between gene expression and immune cell infiltration. It also provides the gene expression and its correlation with breast cancer type and progression of the tumor [36]. We used the TIMER database to compare the mRNA expression of different genes such as STING and IL6 and PD-L1 genes in different breast cancer subtypes [23]. Interestingly, the expression of STING (TMEM173) positively correlates with CD274(PD-L1) and IL6 positively correlates with CD274 (PD-L1) levels in invasive carcinoma, Basal, luminal, HER2 type breast cancer (Fig. 6A). We also analyzed the correlation of the STING (TMEM173) gene with the expression of three genes as PD-L1, ESR1(Estrogen receptor) and IL6 in breast cancer. TMEM173 (STING) positively correlated for PD-L1, and IL6. Further TMEM173(STING) negatively correlated with ESR1 (Estrogen receptor) in invasive carcinoma, Basal, luminal, HER2 type breast cancer (Fig. 6B). This data in consonance with our *in-vitro* data higher expression of STING in ER-negative cell lines.

We analyzed the Kaplan- Meier survival curves of patients having STING expression using a web-based curator [22]. Patients having a higher expression of STING show poor outcomes in terms of survival as {HR = 1.54(0.93–2.53) log Rank p=0.089} during chemotherapy. Similarly, in the second database, TMEM173 (STING) expression worsens survival as the {HR = 1.41(0.92–2.49) log Rank p=0.1}. During chemotherapy, low expression of STING (TMEM173) (represented by black line) showed better survival where as higher expression of STING (TMEM173) (represented by red line) (Fig. 6C, D) worsened the survival.

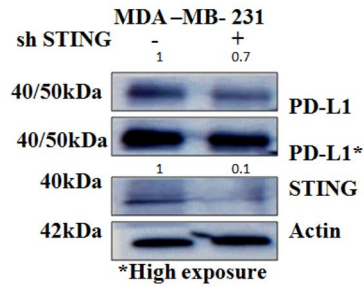
A



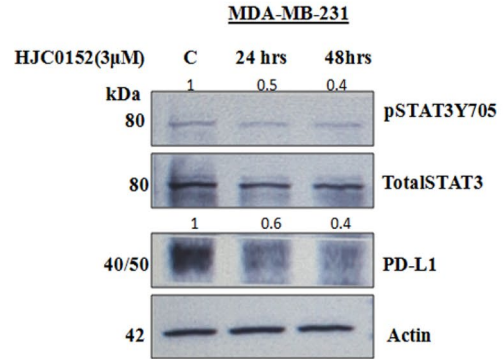
B



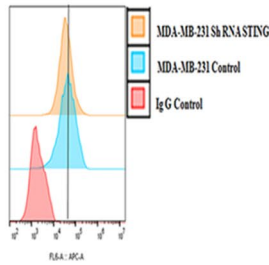
C



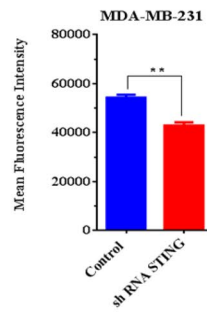
D



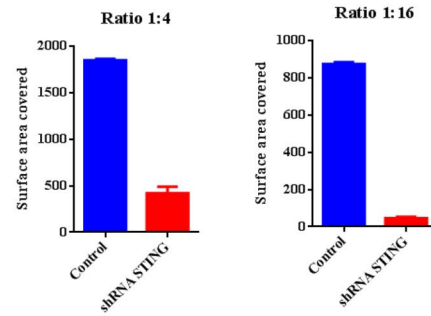
E



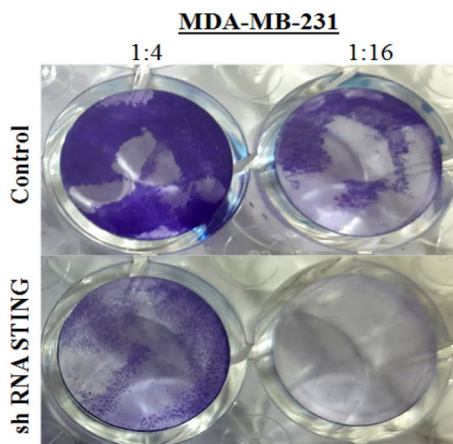
F



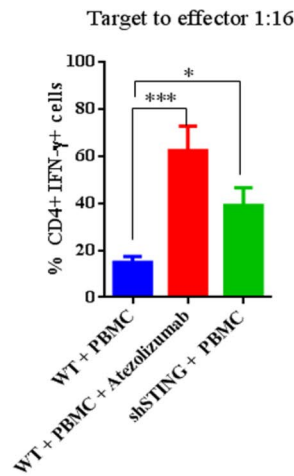
G



H



I



J

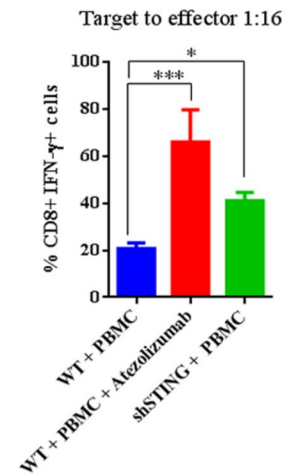


Fig. 4 STING mediated IL-6 induction enhances PD-L1 expression during DNA damage in triple-negative breast cancer cells. DNA damage induces PD-L1 expression: MDA-MB-231 was treated with doxorubicin for 24 h and 48 h and western blotting was performed for the expression of PD-L1 (A). IL-6 induces PD-L1 expression: MDA-MB-231 was treated with different concentrations of IL-6 for 24 h and PD-L1 expression was analyzed by western blotting (B). Effect of STING knockdown on PD-L1 expression: MDA-MB-231 was transfected with shRNA of STING and the expression of PD-L1 was analyzed via western blotting (C). Effect of HJC0152 on the expression of pSTAT3 and PD-L1: MDA-MB-231 cells were treated with HJC0152 (STAT3 Inhibitor) for 24 h and expression of total STAT3, pSTAT3 Y705 and expression of PD-L1 was analyzed via western blotting (D). Surface PD-L1 expression in STING knock-down condition: PD-L1 levels in MDA-MB-231, sh RNA STING and MDA-MB-231 (wt) cell lines were analyzed by flow cytometry. Data represent mean treated change compared to control (n=3, mean±SD); *p<0.05, **p<0.01 and ***p<0.001, based on a Student's t-test (E, F) T cell-mediated tumor cell death assay: MDA-MB-231 and MDA-MB-231-shRNA-STING cells were co-cultured with PBMCs (targeted cells: effectors cells=1:4, 1:16) in 24-well plates for 4 days and colonies were visualized by Giemsa staining surface area (G), and representative image (H). Interferon γ production by T cells: Both CD4 and CD8 T cells Interferon γ measured via flow cytometry. Data represent mean fold change compared to control (n=2, mean±SD); *p<0.05, **p<0.01 and ***p<0.001, based on a one-way ANOVA (Kruskal–Wallis post-hoc Dunn multiple comparisons) (I) and (J).

Discussion

The tumor microenvironment of solid tumors is complex and the constant interaction of tumor cells with immune cells determines the progression of tumors. The tumor cells are the major focus of such interactions which evolve and retain the expression of the key genes required for the immune evasion and cell survival pathway during stress conditions favoring tumor cell survival [37]. Similarly Triple-negative breast cancer cells are highly proliferative and show a high level of chromosomal instability [38], and retain the expression of key proteins of innate immune pathways: cytoplasmic sensors like cGAS and STING, which sense DNA and can reprogram signaling pathways in stress conditions for tumor cell survival [14]. In the current study, we demonstrate that STING activates IL-6 mediated STAT3 pathway during genotoxic stress and evade immune suppression via enhancing PD-L1 in malignant triple-negative breast cancer cells.

The activation of cGAS and STING pathways in tumor cells and immune cells recruited in the tumor microenvironment had been of major interest as it may help to modulate tumor intrinsic cell survival and death pathways [39]. Interestingly, STING was expressed at a higher level in TNBC and ER-negative breast cancer cells (MDA-MB-231, MX-1, BT-549, MDA-MB-468) and is low or undetectable in ER-positive cell lines like MCF-7, T47D, and ZR75. As we

observed here that different breast cancer cell lines show a similar expression level of cGAS whereas STING is only retained in triple-negative breast cancer cells which may provide a survival advantage specifically to triple-negative breast cancer cells. This agrees with the previous observation from our lab and others [14, 14]. Interestingly we observed that genotoxic stress conditions cGAS was dispensable for NF- κ B activation whereas STING was indispensable for NF- κ B activation in triple-negative breast cancer cells. The implication of the NF- κ B pathway in the survival pathway during genotoxic stress conditions can be either pro and anti-apoptotic depending upon the breast cancer cells subtypes and growth stage. Previously we demonstrated that enforced STING expression in ER/PR positive cells shows activation of caspase-8 mediated cell death [16]. Hence this probably explains the loss of STING in early phase triple-positive breast cancer cells. The response to NF- κ B during genotoxic stress conditions may be dependent upon the dosage and duration of stress induction in cells.

In breast cancer there is limited targeted therapy available for TNBC and chemotherapy is widely used for the treatment of TNBC [41]. The evidence, here suggests that doxorubicin which induces genotoxic stress conditions in highly proliferative cancer cells shows activation of STING mediated NF- κ B pathway and induces expression of IL-6 and STAT3 pathway in triple-negative breast cancer cells. This corroborates with earlier observation where highly proliferative breast cancer cells show high CIN leading to the formation of micronuclei sensed by cGAS/STING which activates the non-canonical STING pathway that induces NF- κ B and cell survival [14]. In the current study, we observed that DNA damage-induced alternate STING pathway of NF- κ B activation in triple-negative breast cancer cells where cGAS showed no major role. This is in agreement with previous observation where DNA damage-induced alternate pathway of NF- κ B activation rather than IFN pathway where STING binds to DNA binding protein IFI16 along with DNA damage response factors ATM and PARP-1 which forms an alternative STING signaling complex that includes the tumor suppressor p53 and TRAF6, E3 ubiquitin ligase [32]. It will be also interesting to investigate the assembly of alternate signaling complex and downstream co-operativity of p53 and p65 during DNA damage and their role in tumor progression. The evidence here suggests the DNA damage activates STING mediated alternate NF- κ B activation and further role of this pathway in cell survival, immune evasion and immune cell death was explored.

During DNA damage, STING induced the expression of IL-6, which binds to its cognate receptor leading to activation of phosphorylation of tyrosine (705) residue of STAT3 [30], suggesting the activation of the STING mediated IL-6/

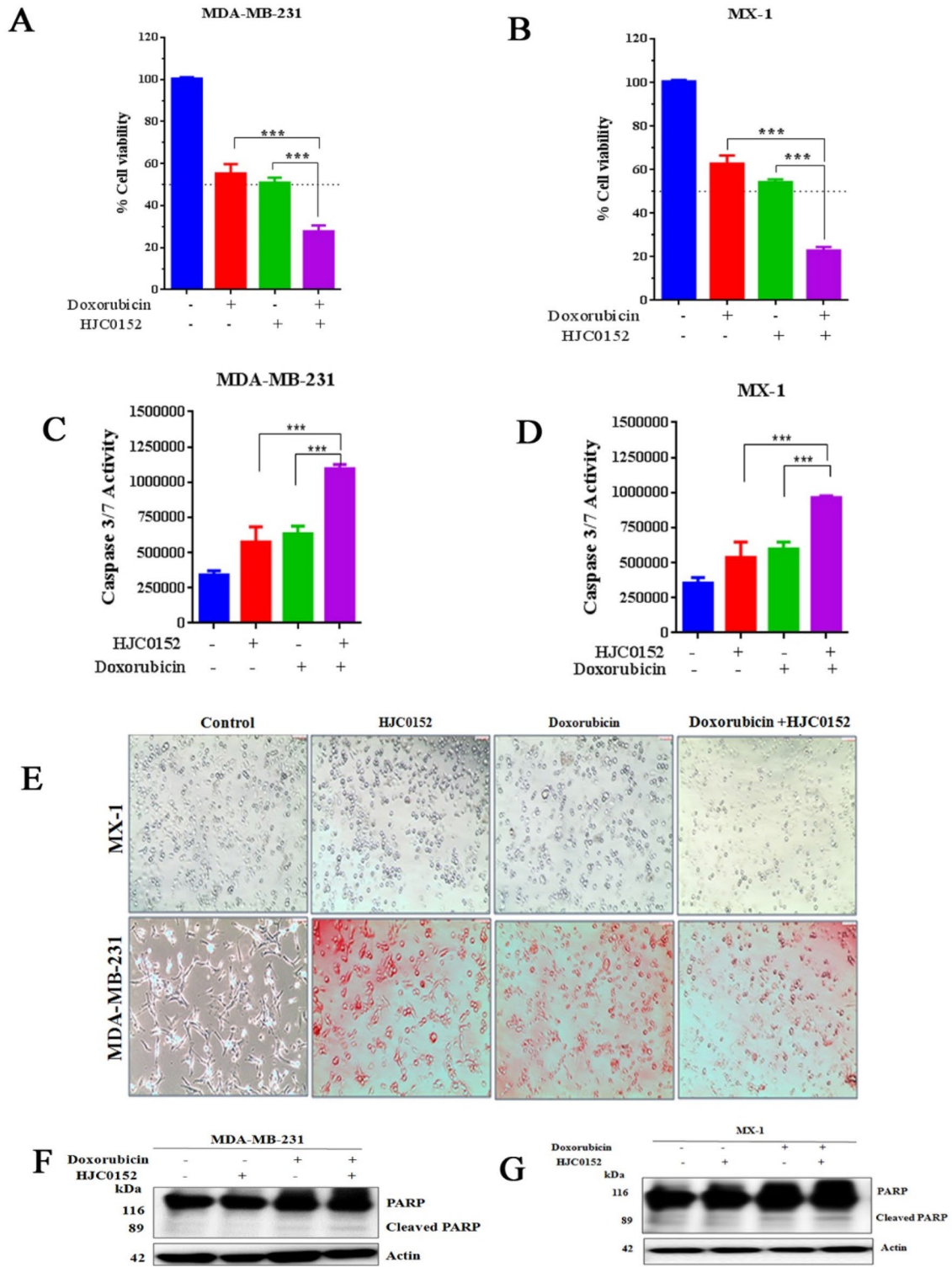


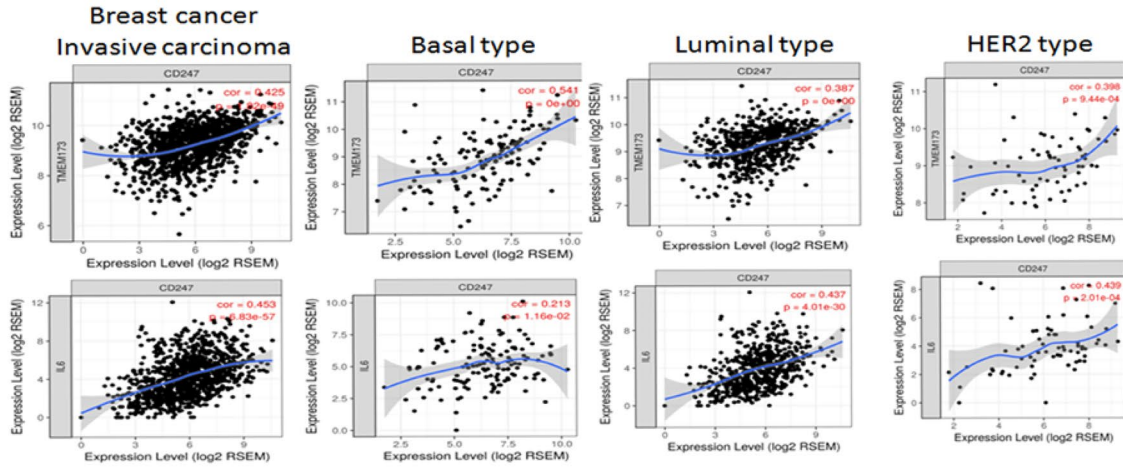
Fig. 5 STAT3 inhibitor, HJC0152 and doxorubicin act synergistically in breast cancer cells to inhibit cell death. Effect of combinatorial treatment of STAT3 inhibitor and doxorubicin on cell viability: MDA-MB-231 and MX-1 inhibition: MDA-MB-231 and MX-1 treated with doxorubicin, HJC0152 and combinations of both and % cell viability was analyzed. Data represent mean change compared to control ($n=3$, mean \pm SD); * $p < 0.05$, ** $p < 0.01$ and *** $p < 0.001$, based on a one-way ANOVA (Kruskal–Wallis post- hoc Dunn multiple comparisons) (A) and (B). Effect of combinatorial treatment of STAT3 inhibitor and doxorubicin on caspase3/7 activity: MDA-MB-231 and MX-1 treated with 1 μ M doxorubicin, 3 μ M of HJC0152 and combinations of both drugs and Caspase3/7 activity, Data represent mean change compared to control ($n=3$, mean \pm SD); * $p < 0.05$, ** $p < 0.01$ and *** $p < 0.001$, based on a one-way ANOVA (Kruskal–Wallis post- hoc Dunn multiple comparisons) (C) and (D). Effect of combinatorial treatment of STAT3 inhibitor and doxorubicin on growth: MDA-MB-231 and MX-1 were treated with 1 μ M doxorubicin, 3 μ M of HJC0152 and combinations and cells were analyzed using a microscope (E). Effect of combinatorial treatment of STAT3 inhibitor and doxorubicin on PARP cleavage: Cells were treated with 1 μ M doxorubicin, 3 μ M of HJC0152 and combinations of both for 24 h and cleaved PARP measured using western blotting (F, G)

STAT3 pathway in triple-negative breast cancer cells during genotoxic stress conditions. It is known that IL6/STAT3 signaling plays a critical role in tumor progression in many solid tumor types by inducing epithelial-to-mesenchymal transition (EMT) and angiogenesis [42]. Therefore IL6/STAT3 pathway is an attractive drug target in different solid tumors including breast cancer. Several approaches to target this pathway in different cancer are being pursued at different clinical stages. This includes the upstream targeting of JAKs, direct targeting of STAT3 phosphorylation and activation [35]. We investigated if inhibition of STAT3 pathway under genotoxic stress conditions sensitizes the ER-negative breast cancer cells to cell death. Niclosamide, a potent STAT3 inhibitor, suppresses STAT3 phosphorylation at Tyr705 and inhibit cell proliferation in adrenocortical carcinoma and prostate cancer [30]. HJC0152 is an improved derivative of niclosamide and a potent inhibitor of STAT3 activation was used in further study [43]. The evidence here suggests the combinatorial treatment of HJC0152 and doxorubicin sensitizes the breast cancer cells and shows

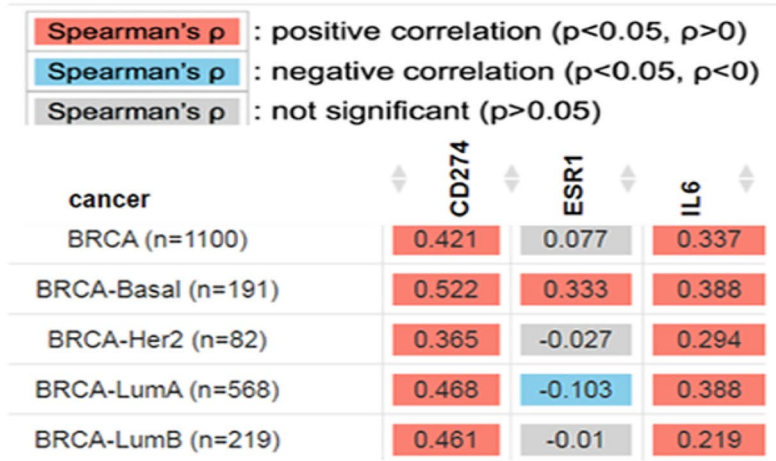
synergistic growth inhibition of MDA-MB-231 and MX-1, STING expressing cell line. Hence it may be further interesting to explore the potential of the combinatorial therapeutic regimen of STAT3 inhibitors and genotoxic drugs which may work at a low dosage and hence may avoid side effects.

DNA damage or high chromosomal instability as observed in highly malignant breast cancer cells show immune evasion suggesting the important role of DNA damage-induced activation of the STING pathway. Here we demonstrated DNA damage induces PD-L1 expression in STING positive triple-negative breast cancer cells. This is also in consonance with a previous report where DNA damage is known to induce PD-L1 where TBK1 had been shown to enhance the PD-L1 in tumor cells [44, 44]. The STAT3 pathway is closely associated with PD-L1, a major blocker for T cell-mediated immune suppression mechanism in the tumor [45, 45]. Our experiment clearly shows that down-regulation of STING sensitizes MDA-MB-231 cells to immune cell death mediated by activated lymphocytes. This suggest STING as central regulator of resistance to immune cell death in triple-negative metastatic breast cancer cells during DNA damage conditions. Hence, we also analyzed different TCGA and other databases which strongly show that STING positively correlated with IL-6 and show poor survival outcomes. Moreover, during chemotherapy, STING expression show poor survival outcome which should be also considered while deciding on the therapeutic regimen. Further, it is also important to screen further different types of chemotherapeutic agents and their survival outcomes in different subgroups of breast cancer. Further, we suggest that combination therapy of DNA damaging agent and STAT3 inhibitor may act synergistically in the clinical condition to induce immune cell death in STING expressing metastasis tumor cells. This needs further study to develop this combinatorial regimen and its possible analysis in a different model system for exploiting the STING pathway for clinical therapy in metastatic triple-negative breast cancer.

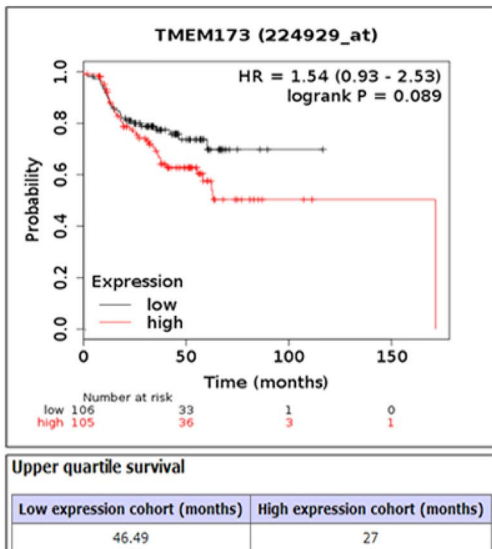
A



B



C



D

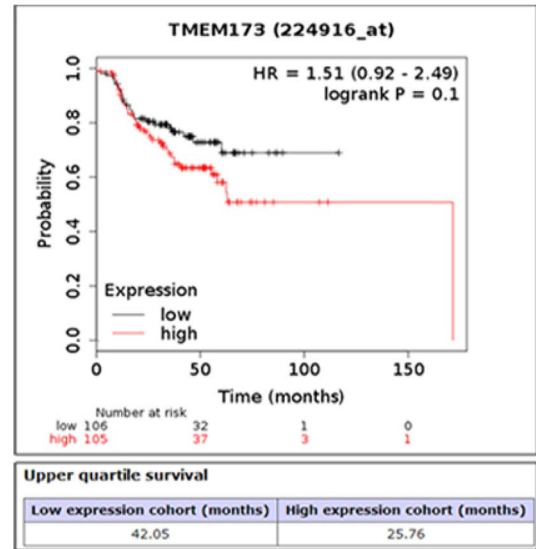


Fig. 6 STING expression positively correlates with IL6 and PD-L1 expression and high STING expression in chemotherapy shows poor survival. Gene expression correlation: Correlation of expression between STING and PD-L1(CD247) and IL-6 and PL-1(CD247) in Invasive Carcinoma, Basal Type, Luminal Type, HER2 type of Breast cancer was analyzed using TIMER database (A). Gene expression correlation: correlation in subtypes of breast cancer for CD274, ESR1 and IL6 using TIMER database (B) Kaplan Meier survival analysis: Plot for TMEM173 in breast cancer patients' survival with chemotherapy (C) and (D).

Acknowledgements This work was partially supported by the Department of Science and Technology, Govt. of India, Grant Number INT/Korea/P-39 to Prof. Rajesh Singh. Authors also acknowledged practical support from GSBTM, GJ, India The authors acknowledge the instrumentation facility at the Department of Biochemistry, The M. S. University of Baroda, Vadodara under the DST FIST program. DBT BUILDER program supported by Department of Biotechnology, Govt of India. Minal Mane received her fellowship from CSIR, Govt. of India. Dhruv Gohel received his fellowship from ICMR, India. Fatema Currim received her fellowship from the DST-INSPIRE program, India. Anjali Shinde is ICMR SRF.

Author contributions HV: conceptualization, methodology, formal analysis, investigation, writing—original draft, AS: data curation, writing—review and editing, resources; MR: writing—review and editing, resources; MM: resources; JS: resources; DG: resources; FC: resources; KR: data curation, resources; RS: resources; RS: funding acquisition, project administration, supervision, conceptualization, writing—review and editing.

Funding Department of Science and Technology, Govt. of India, Grant Number INT/Korea/P-39 to Prof. Rajesh Singh.

Data availability The data that support the findings of this study are available on request from the corresponding author.

Declarations

Ethical approval Not applicable.

Consent to participate Not applicable.

Consent of publication I, the undersigned, give my consent for the publication of identifiable details, which can include a photograph(s) and/or videos and/or case history and/or details within the text (“Material”) to be published in a journal of Apoptosis.

Conflict of interest Not applicable.

References

- Cacho-Díaz B, García-Botello DR, Wegman-Ostrosky T, Reyes-Soto G, Ortiz-Sánchez E, Herrera-Montalvo LA (2020) Tumor microenvironment differences between primary tumor and brain metastases. *J Med Transl*. <https://doi.org/10.1186/S12967-019-02189-8>
- Balkwill FR, Capasso M, Hagemann T (2012) The tumor micro-environment at a glance. *J Cell Sci*. <https://doi.org/10.1242/jcs.116392>
- Ostrand-Rosenberg S (2008) Immune surveillance: a balance between protumor and antitumor immunity. *Curr Opin Genet Dev* 18(1):11–18. <https://doi.org/10.1016/J.GDE.2007.12.007>
- Gonzalez H, Hagerling C, Werb Z (2018) Roles of the immune system in cancer: from tumor initiation to metastatic progression. *Genes Dev* 32(19–20):1267–1284. <https://doi.org/10.1101/GAD.314617.118>
- Kc C, Md M, Ta W (2019) Cytokines in the treatment of cancer. *J Interferon Cytokine Res* 39(1):6–21. <https://doi.org/10.1089/JIR.2018.0019>
- Chen W, Qin Y, Liu S (2018) Cytokines, breast cancer stem cells (BCSCs) and chemoresistance. *Clin Transl Med* 7(1):27. <https://doi.org/10.1186/S40169-018-0205-6>
- Lázár-Molnár E, Hegyesi H, Tóth S, Falus A (2000) Autocrine and paracrine regulation by cytokines and growth factors in melanoma. *Cytokine* 12(6):547–554. <https://doi.org/10.1006/CYTO.1999.0614>
- Dethlefsen C, Højfeldt G, Hojman P (2013) The role of intratumoral and systemic IL-6 in breast cancer. *Breast Cancer Res Treat* 138(3):657–664. <https://doi.org/10.1007/S10549-013-2488-Z>
- Ravishankaran P, Karunanithi R (2011) Clinical significance of preoperative serum interleukin-6 and C-reactive protein level in breast cancer patients. *World J Surg Oncol* 9:18. <https://doi.org/10.1186/1477-7819-9-18>
- Méndez-García LA, Nava-Castro KE, Ochoa-Mercado TDL, Palacios-Arreola MI, Ruiz-Manzano RA, Segovia-Mendoza M, Solleiro-Villavicencio H, Cázarez-Martínez C, Morales-Montor J (2019) Breast cancer metastasis: are cytokines important players during its development and progression? *J Interferon Cytokine Res* 39(1):39–55. <https://doi.org/10.1089/JIR.2018.0024>
- Pa J et al (2018) High content imaging assays for IL-6-induced STAT3 pathway activation in head and neck cancer cell lines. *Methods Mol Biol* 1683:229–244. https://doi.org/10.1007/978-1-4939-7357-6_14
- Saha S et al (2016) Aspirin suppresses the acquisition of chemoresistance in breast cancer by disrupting an NFκB–IL6 signaling axis responsible for the generation of cancer stem cells. *Cancer Res* 76(7):2000–2012. <https://doi.org/10.1158/0008-5472.CAN-15-1360>
- Mackenzie KJ et al (2017) cGAS surveillance of micronuclei links genome instability to innate immunity. *Nature* 548(7668):461. <https://doi.org/10.1038/NATURE23449>
- Sf B et al (2018) Chromosomal instability drives metastasis through a cytosolic DNA response. *Nature* 553(7689):467–472. <https://doi.org/10.1038/NATURE25432>
- Juneja VR et al (2017) PD-L1 on tumor cells is sufficient for immune evasion in immunogenic tumors and inhibits CD8 T cell cytotoxicity. *J Exp Med* 214(4):895. <https://doi.org/10.1084/JEM.20160801>
- Bhatelia K et al (2014) Antiviral signaling protein MITA acts as a tumor suppressor in breast cancer by regulating NF-κB induced cell death. *Biochim Biophys Acta*. <https://doi.org/10.1016/j.bbadis.2013.11.006>
- Pei J et al (2019) STAT3 inhibition enhances CDN-induced STING signaling and antitumor immunity. *Cancer Lett* 450:110–122. <https://doi.org/10.1016/J.CANLET.2019.02.029>
- Reisländer T, Groelly FJ, Tarsounas M (2020) DNA damage and cancer immunotherapy: a STING in the tale. *Mol Cell* 80(1):21–28. <https://doi.org/10.1016/J.MOLCEL.2020.07.026>
- Ran FAF, Hsu PD, Wright J, Agarwala V, Scott DA, Zhang F (2013) Genome engineering using the CRISPR-Cas9 system. *Nat*

- Protoc 8(11):2281–2308. <https://doi.org/10.1038/NPROT.2013.143>
20. Tomar D, Sripada L, Prajapati P, Singh R, Singh AK, Singh R (2012) Nucleo-cytoplasmic trafficking of TRIM8, a novel oncogene, is involved in positive regulation of TNF induced NF- κ B pathway. *PLoS ONE* 7(11):e48662. <https://doi.org/10.1371/JOURNAL.PONE.0048662>
 21. Tomar D, Singh R, Singh AK, Pandya CD, Singh R (2012) TRIM13 regulates ER stress induced autophagy and clonogenic ability of the cells. *Biochim Biophys Acta* 1823(2):316–326. <https://doi.org/10.1016/j.bbamer.2011.11.015>
 22. Nagy Á, Munkácsy G, Györfly B (2021) Pancancer survival analysis of cancer hallmark genes. *Sci Rep* 11(1):6047. <https://doi.org/10.1038/s41598-021-84787-5>
 23. Li T et al (2021) TIMER2.0 for analysis of tumor-infiltrating immune cells. *Nucleic Acids Res* 48(W1):W509–W514. <https://doi.org/10.1093/NAR/GKAA407>
 24. Wilkinson RDA et al (2019) Topoisomerase II inhibitors induce cGAS-STING dependent inflammation resulting in cytokine induction and immune checkpoint activation. *bioRxiv*: 764662
 25. Nagelkerke A, Span PN (2016) Staining against phospho-H2AX (γ -H2AX) as a marker for DNA damage and genomic instability in cancer tissues and cells. *Adv Exp Med Biol* 899:1–10. https://doi.org/10.1007/978-3-319-26666-4_1
 26. Wang W, Mani AM, Wu Z-H (2017) DNA damage-induced nuclear factor-kappa B activation and its roles in cancer progression. *J Cancer Metastasis Treat* 3(3):45. <https://doi.org/10.20517/2394-4722.2017.03>
 27. McFarland BC et al (2013) NF- κ B-induced IL-6 ensures STAT3 activation and tumor aggressiveness in glioblastoma. *PLoS ONE* 8(11):e78728. <https://doi.org/10.1371/JOURNAL.PONE.0078728>
 28. Xia L et al (2018) Role of the NF κ B-signaling pathway in cancer. *Onco Targets Ther* 11:2063. <https://doi.org/10.2147/OTT.S161109>
 29. Mauer J, Denson JL, Brüning JC (2015) Versatile functions for IL-6 in metabolism and cancer. *Trends Immunol* 36(2):92–101. <https://doi.org/10.1016/J.IT.2014.12.008>
 30. Zou S, Tong Q, Liu B, Huang W, Tian Y, Fu X (2020) Targeting STAT3 in cancer immunotherapy. *Mol Cancer* 19(1):1–19. <https://doi.org/10.1186/S12943-020-01258-7>
 31. Sato H et al (2017) DNA double-strand break repair pathway regulates PD-L1 expression in cancer cells. *Nat Commun* 8(1):1–11. <https://doi.org/10.1038/s41467-017-01883-9>
 32. Dunphy G, Flannery SM, Almine JF, Connolly DJ, Paulus C, Jønsen KL et al (2018) Non-canonical activation of the DNA sensing adaptor STING by ATM and IFI16 mediates NF- κ B signaling after nuclear DNA damage. *Mol Cell* 71(5):745–760. <https://doi.org/10.1016/J.MOLCEL.2018.07.034>
 33. Li Z et al (2019) A novel STAT3 inhibitor, HJC0152, exerts potent antitumor activity in glioblastoma. *Am J Cancer Res* 9(4):699
 34. Bromberg MWGDYZRPAJDJF (1999) Stat3 as an oncogene. *Cell* 98(3):295–303. [https://doi.org/10.1016/s0092-8674\(00\)81959-5](https://doi.org/10.1016/s0092-8674(00)81959-5)
 35. Gariboldi MB, Ravizza R, Molteni R, Osella D, Gabano E, Monti E (2007) Inhibition of Stat3 increases doxorubicin sensitivity in a human metastatic breast cancer cell line. *Cancer Lett* 258(2):181–188. <https://doi.org/10.1016/J.CANLET.2007.08.019>
 36. Li T et al (2017) TIMER: a web server for comprehensive analysis of tumor-infiltrating immune cells. *Cancer Res* 77(21):e108–e110. <https://doi.org/10.1158/0008-5472.CAN-17-0307/SUPPLEMENTARY-VIDEO-S1>
 37. Shen R et al (2022) DNA damage and activation of cGAS/STING pathway induce tumor microenvironment remodeling. *Front Cell Dev Biol* 9:3915. <https://doi.org/10.3389/FCCELL.2021.828657/BIBTEX>
 38. Bareche Y et al (2020) Unraveling triple-negative breast cancer tumor microenvironment heterogeneity: towards an optimized treatment approach. *JNCI J Natl Cancer Inst* 112(7):708–719. <https://doi.org/10.1093/JNCI/DJZ208>
 39. da Hoong BY, Gan YH, Liu H, Chen ES (2020) cGAS-STING pathway in oncogenesis and cancer therapeutics. *Oncotarget* 11(30):2930–2955. <https://doi.org/10.18632/oncotarget.27673>
 40. Cheradame L et al (2020) STING promotes breast cancer cell survival by an inflammatory-independent nuclear pathway enhancing the DNA damage response. *bioRxiv*. <https://doi.org/10.1101/2020.07.11.196790>
 41. Wahba HA, El-Hadaad HA (2015) Current approaches in treatment of triple-negative breast cancer. *Cancer Biol Med* 12(2):106. <https://doi.org/10.7497/J.ISSN.2095-3941.2015.0030>
 42. Johnson DE, O'Keefe RA, Grandis JR (2018) Targeting the IL-6/JAK/STAT3 signalling axis in cancer. *Nat Rev Clin Oncol* 15(4):234. <https://doi.org/10.1038/NRCLINONC.2018.8>
 43. Jiang X et al (2018) HJC0152, a novel STAT3 inhibitor with promising anti-tumor effect in gastric cancer. *Cancer Manag Res* 10:6857. <https://doi.org/10.2147/CMAR.S188364>
 44. Parkes EE et al (2016) Activation of STING-dependent innate immune signaling by S-phase-specific DNA damage in breast cancer. *J Natl Cancer Inst*. <https://doi.org/10.1093/JNCI/DJW199>
 45. Bu LL et al (2017) STAT3 induces immunosuppression by upregulating PD-1/PD-L1 in HNSCC. *J Dent Res* 96(9):1027. <https://doi.org/10.1177/0022034517712435>
 46. Zerdes I et al (2019) STAT3 activity promotes programmed-death ligand 1 expression and suppresses immune responses in breast cancer. *Cancers (Basel)*. <https://doi.org/10.3390/CANCERS11101479>

Publisher's Note Springer Nature remains neutral with regard to jurisdictional claims in published maps and institutional affiliations.

Springer Nature or its licensor holds exclusive rights to this article under a publishing agreement with the author(s) or other rightsholder(s); author self-archiving of the accepted manuscript version of this article is solely governed by the terms of such publishing agreement and applicable law.



Exosome Release Is Modulated by the Mitochondrial-Lysosomal Crosstalk in Parkinson's Disease Stress Conditions

Fatema Currim¹ · Jyoti Singh¹ · Anjali Shinde¹ · Dhruv Gohel¹ · Milton Roy¹ · Kritarth Singh² · Shatakshi Shukla¹ · Minal Mane¹ · Hitesh Vasiyani¹ · Rajesh Singh¹

Received: 21 April 2020 / Accepted: 2 December 2020 / Published online: 6 January 2021
© The Author(s), under exclusive licence to Springer Science+Business Media, LLC part of Springer Nature 2021

Abstract

Parkinson's disease (PD) is a neurodegenerative disorder characterized by the progressive loss of dopaminergic neurons in the substantia nigra (SN) pars compacta region of the brain. The main pathological hallmark involves cytoplasmic inclusions of α -synuclein and mitochondrial dysfunction, which is observed in other part of the central nervous system other than SN suggesting the spread of pathogenesis to bystander neurons. The inter-neuronal communication through exosomes may play an important role in the spread of the disease; however, the mechanisms are not well elucidated. Mitochondria and its role in inter-organellar crosstalk with multivesicular body (MVB) and lysosome and its role in modulation of exosome release in PD is not well understood. In the current study, we investigated the mitochondria-lysosome crosstalk modulating the exosome release in neuronal and glial cells. We observed that PD stress showed enhanced release of exosomes in dopaminergic neurons and glial cells. The PD stress condition in these cells showed fragmented network and mitochondrial dysfunction which further leads to functional deficit of lysosomes and hence inhibition of autophagy flux. Neuronal and glial cells treated with rapamycin showed enhanced autophagy and inhibited the exosomal release. The results here suggest that maintenance of mitochondrial function is important for the lysosomal function and hence exosomal release which is important for the pathogenesis of PD.

Keywords Mitochondrial dysfunctions · Mitochondria-lysosome crosstalk · Exosome release · Parkinson's disease

Introduction

Parkinson's disease (PD) is a chronic, progressive, neurodegenerative movement disorder including motor as well as non-motor symptoms. It affects 1% of the population of over 60 years of age and 3% of people over 80 years of age, and an estimated seven to ten million people are affected worldwide [1, 2]. Neuronal loss in the substantia nigra leads to a decrease in the dopamine levels in the corpus striatum, which leads to the motor symptoms, namely, tremor, rigidity and bradykinesia. The cellular hallmark of PD is the presence of the intracytoplasmic Lewy bodies and Lewy neurites, composed of protein aggregates, fats and polysaccharides. The protein aggregates contain α -synuclein, neurofilaments,

ubiquitin, Parkin and Synphilin [3]. There are emerging evidences which show that misfolded proteins spread through the brain along anatomically connected networks to other neuronal regions thereby promoting progressive decline [4]. PD occurs sporadically as well as in a familial form. Mutations in genes like SNCA, LRRK2 and VPS35 are related to autosomal dominant forms of PD, while PARKIN, PINK1 and DJ1 are associated with autosomal recessive form of PD [5]. The key molecular pathways regulated by these genes involved in PD are emerging; however, their role in progression to different brain regions is not well understood.

The dopaminergic neurons are specifically vulnerable in PD; however, α -synuclein aggregation and neuronal degeneration are observed in non-dopaminergic parts of the brain as well, like neocortex, brain stem and olfactory bulb [6], suggesting that the pathology spreads to other types of brain cells including microglia and astrocytes and other parts of the brain. Emerging studies suggest that exosomes play a major role in inter-neuronal and neuron-glia communication in the brain [7]. Exosomes are a class of extracellular vesicles ranging in the size approximately 30–150 nm, which are released from almost all cell types including neuron, glial and astrocytes [8].

✉ Rajesh Singh
singhraj1975@gmail.com

¹ Department of Biochemistry, Faculty of Science, The MS University of Baroda, Vadodara, Gujarat 390002, India

² Department of Cell and Developmental Biology, University College London, Gower Street, London WC1E 6BT, UK

The exosomes are generated within multivesicular bodies (MVBs) that contain intra-luminal vesicles (ILVs) in the endosomal system. A variety of mRNAs, small non-coding RNAs, DNA and proteins, are selectively enriched into the ILVs of the MVBs, when the MVB fuses with the plasma membrane, ILVs in the form of exosomes are released [9]. In PD-insulted neurons, α -synuclein is predominantly enriched in exosomes, transferred to nearby neurons leading to neuronal dysfunction [10]. Further exosomes loaded with α -synuclein along with other components like miRNA, mRNA and DNA are uptaken by the glial cells and induce inflammation [11]. Overall, these evidences suggest that exosomes play a major role in inter-neuronal and neuronal-glial communication; however, the intracellular pathway regulating the exosomal release in neuronal and glial cells in the PD stress conditions are unclear.

Mitochondria is a dynamic organelle which has been implicated in various cellular functions including maintenance of bioenergetics by oxidative phosphorylation (OXPHOS), calcium homeostasis, apoptosis and inflammation [12]. Given its vital role in the cellular homeostasis and neuronal survival, mitochondrial dysfunction plays a central role in PD and other neurodegenerative diseases. The dysfunction is mainly characterized by a decrease in the complex I activity of the OXPHOS complex, generation of ROS (reactive oxygen species), ATP depletion and apoptosis. The turnover of dysfunctional mitochondria through selective process of autophagy called as mitophagy is important in neuronal survival including dopaminergic neurons [13]. Interestingly, genes involved in familial PD like PINK1 and PARKIN play essential role in turnover of mitochondria through mitophagy; hence, mutations in these genes lead to accumulation of damaged mitochondria [14, 15]. The effective turnover of dysfunctional mitochondria and alpha-syn aggregates requires efficient autophagy flux and in turn functional lysosomes. There are emerging studies which show that the autophagy-lysosome pathway is altered in PD [16]. Mutations in genes like ATP13A2/PARK9, cause of familial PD, also show impairment of lysosomal functions and accumulation of autophagosomes [17, 18]. LRRK2-mutant PD patient neurons (iPSCs) show altered macro autophagy and increased levels of α -synuclein in the cell [19, 20]. These evidences suggest that autophagy is important for neuronal homeostasis; however, its role in exosome release and inter-neuronal communication is not understood.

Multivesicular body is known to play critical role in exosome biogenesis and recruitment of the misfolded protein and its degradation through the endo-lysosomal pathway [21]. MVBs fuse with the lysosome where their content is degraded and recycled back [22] and may also fuse with the plasma membrane, releasing the ILV content in the form of exosomes [23]. The mitochondria-lysosomal crosstalk is important for

the process of autophagy and cellular homeostasis which in turn plays a role in exosomal release [24]. This crosstalk between mitochondria, lysosome and exosome in neuronal cells are yet to be investigated systematically in PD stress conditions. In this study, we analysed the mitochondrial-lysosome crosstalk in PD stress conditions and its role in exosome release from the neuronal cell in PD stress conditions.

Materials and Methods

Cell Culture and Reagents

SH-SY5Y, human neuroblastoma cells were grown at 37 °C, 5% CO₂ in Ham's F-12 Kaighn's Modification (F-12K, HyClone, GE Lifesciences) supplemented with 10% (v/v) heat-inactivated foetal bovine serum (FBS) (Gibco, Invitrogen) and 1% (v/v) penicillin, streptomycin and neomycin (PSN) antibiotic mixture (Gibco, Invitrogen). U-87 MG and SK-N-SH cells were grown at 37 °C, 5% CO₂ in MEM/EBSS (HyClone, GE Lifesciences) accompanied with 10% (v/v) heat-inactivated FBS, 1% (v/v) PSN and 1 mM sodium pyruvate (HyClone, GE Lifesciences). One-shot exosome-depleted FBS was obtained from Gibco, Invitrogen. All three cell lines were obtained from National Centre for Cell Sciences, Pune, India. mCherry-GFP-LC3 was provided by Dr. Terje Johansen (Dept. of Biochemistry, Institute of Medical Biology, University of Tromsø). The primary antibodies used were anti-LC3 (Sigma-Aldrich, USA), anti-p62 (Cell Signalling, USA), anti-NDP52 (Cell Signalling, USA), anti-CD63 (Santa Cruz, USA), anti-actin (GenScript, USA), and anti-calnexin (Cell Signalling, USA). Secondary antibodies HRP-conjugated anti-rabbit and anti-mouse antibodies (Jackson ImmunoResearch, USA) were used. Rotenone, 6-OHDA, Bafilomycin A1, rapamycin and wortmannin were all purchased from Sigma-Aldrich, USA. For transfection, Lipofectamine® 3000 (Invitrogen, USA) was used. SH-SY5Y dopaminergic neuronal cells and U-87 MG glial cells were treated with 75 μ M 6-OHDA and 0.01 μ M Rotenone, whereas SK-N-SH dopaminergic neuronal cells were treated with 5 μ M 6-OHDA and 0.1 μ M Rotenone.

Exosome Isolation

Cells were seeded at a density of 4.5×10^5 cells per well in 6-well plate and were treated with pre-conditioned media containing exosome-depleted serum. The exosomes were isolated using an affinity purification-based method. The pre-conditioned media was collected and centrifuged at 2000 g for 30 min to settle down the cell debris. The supernatant was collected and Total Exosome Isolation reagent (Thermo Fisher Scientific, Invitrogen, USA) was added in 2:1 ratio volume. The mixture was incubated at 4 °C overnight. Following incubation, the mixture

was centrifuged at 10,000 *g* for 1 h at 4 °C to obtain the exosome pellet. The exosome pellet was then used for either NTA or western blotting for further characterization.

Nanoparticle Tracking Analysis

Cells were seeded at a density of 2.5×10^5 cells per well in 12-well plate and were treated with the given chemicals along with the pre-conditioned media. The pre-conditioned media was collected, and exosomes were isolated by the method described above. Exosome pellet was resuspended in 1 ml of DPBS solution and was analysed by the NanoSight NS300 (Malvern Panalytical, UK), which shows both the particle size as well as concentration.

Western Blotting

Cells were seeded at a density of 4.5×10^5 cells per well in 6-well plate and were treated with the given chemicals for the particular time period. After treatment, cells were harvested, washed with ice cold PBS and lysed in NP40 lysis buffer (150 mM NaCl, 50 mM Tris–Cl, 5 mM EDTA, 1% NP40, 1% glycerol and $1 \times$ protease inhibitor cocktail (Sigma-Aldrich, USA). Protein concentration was determined by Bradford assay (Bio-Rad Protein Assay Dye Reagent Concentrate, Bio-Rad, USA), and equal amount of proteins were resolved on 12.5% SDS-PAGE. Proteins were electro-blotted on PVDF membrane (Immun-Blot@ PVDF Membrane, Bio-Rad, USA) at 110 V for 1 h at 4 °C. Following the transfer, the membrane was blocked with 5% blocking buffer (5% non-fat dried milk and 0.1% Tween-20 in TBS) for 1 h at room temperature. The membrane was incubated overnight with specific primary antibody. After incubation the membrane was washed three times with TBS-T (TBS containing 0.1% Tween-20) and incubated with a secondary antibody at room temperature for 1 h. The membrane was washed three times with TBS-T and signal visualized by using (Bio-Rad, USA) by exposing to X-ray film. The band intensity was quantified using ImageJ software and relative quantification was shown as compared to control samples.

Lysosomal Acid Phosphatase Assay

Cells were seeded at a density of 2.5×10^5 cells per well in 12-well plate and treated with the given chemicals. After treatment, cells were collected and lysed with Passive Lysis Buffer (25 mM Tris-HCl, pH 7.8, 2 mM DTT, 2 mM EDTA, 10% glycerol, 1% Triton X-100) for 30 min on ice. Protein concentration was determined by Bradford assay. Acid phosphatase activity was measured as a colorimetric assay. Ten micrograms of lysate was incubated with 5 mM pNPP in 100 μ l of citrate buffer (90 mM, pH 4.8) in 96-well plate for 30 min at

37 °C. The reaction was stopped with 100 mM NaOH solution, and absorbance was measured at 405 nm in a microplate reader (Thermo Fisher Scientific, USA).

Fluorescence Microscopy

Cells were seeded at a density of 1.5×10^5 cells per well in 24-well plate and transfected with mCherry-GFP-LC3 construct and subsequently treated with given chemicals, 24 h post transfection. Fluorescence microscopy was performed using Eclipse Ti2-E inverted fluorescence microscope (Nikon, Japan) and analysed by ImageJ. Detectors gain, offset levels and laser power were calibrated at identical levels and remain unchanged for a set of experiment. Numbers and types (yellow or red) of puncta per cell were counted in minimum 30 cells manually and graph plotted for the average number of LC3 puncta per cell.

Confocal Microscopy

For analysis of mitochondrial morphology, MT-RFP was transfected in cells and subsequently treated with the given chemicals, 24 h post transfection, and images were acquired using confocal microscope. All images were acquired with LSM 710 inverted confocal microscope (Carl Zeiss, Germany), and detectors gain, offset levels and laser power were calibrated at identical levels and remain unchanged for a set of experiment.

Similarly, cells were treated with the given chemicals for 24 h and stained with LysoTracker Blue (Invitrogen) post-treatment, and images were obtained using LSM 710 inverted confocal microscope, and detectors gain, offset levels and laser power were calibrated at identical levels and remain unchanged for a set of experiment. The number of lysosomes per cell was counted using the ITCN plugin in ImageJ software.

ATP Assay

The cellular ATP level was measured using ATP determination kit (Molecular Probes/Life Technologies, Canada) by using 1:10 diluted cell lysate in ATP determination master mix (25 mM Tricine buffer, pH 7.8, 5 mM MgSO₄, 0.5 mM D-luciferin, 1.25 μ g/ml firefly luciferase, 100 μ M EDTA and 1 mM DTT). The luminescence intensity was measured using TriStar² LB 942 Multimode Microplate Reader, Berthold Technologies, Germany. The protein content was determined by Bradford assay and normalized with obtained intensity.

Spectrophotometric Analysis of Mitochondrial Complex I Assay

The activity of mitochondrial complex I was analysed spectrophotometrically. Cells were seeded at the density of 9×10^5

cells in 60-mm dish. After treatment, cells were subjected to 2–3 freeze–thaw cycles in a freeze–thaw complete solution (0.25 M sucrose, 20 mM Tris-HCl (pH 7.4), 40 mM KCl, 2 mM EDTA supplemented with 1 mg/ml fatty acid-free BSA, 0.01% digitonin and 10% Percoll). The cells were washed again thrice with the freeze–thaw solution devoid of digitonin and resuspended in complex I assay buffer (35 mM potassium phosphate (pH 7.4), 1 mM EDTA, 2.5 mM NaN_3 , 1 mg/ml BSA, 2 $\mu\text{g/ml}$ antimycin A, 5 mM NADH). The reaction was started by adding 80 μg of cell lysate to 500 μl of assay buffer in 1-ml quartz cuvette. Complex I activity was measured for 2 min by monitoring the decrease in absorbance at 340 nm after the addition of 2.5 mM acceptor decylubiquinone indicating the oxidation of NADH.

Statistical Analysis

Data are shown as mean \pm SEM for number of times the experiment was repeated. Comparisons between two groups were performed using Student's *t* test for repeated measurements to determine the levels of significance for each group. The experiments were performed minimum two times independently and $p < 0.05$ was considered as statistically significant. GraphPad Prism (version 5) software was used to perform all the statistical analysis.

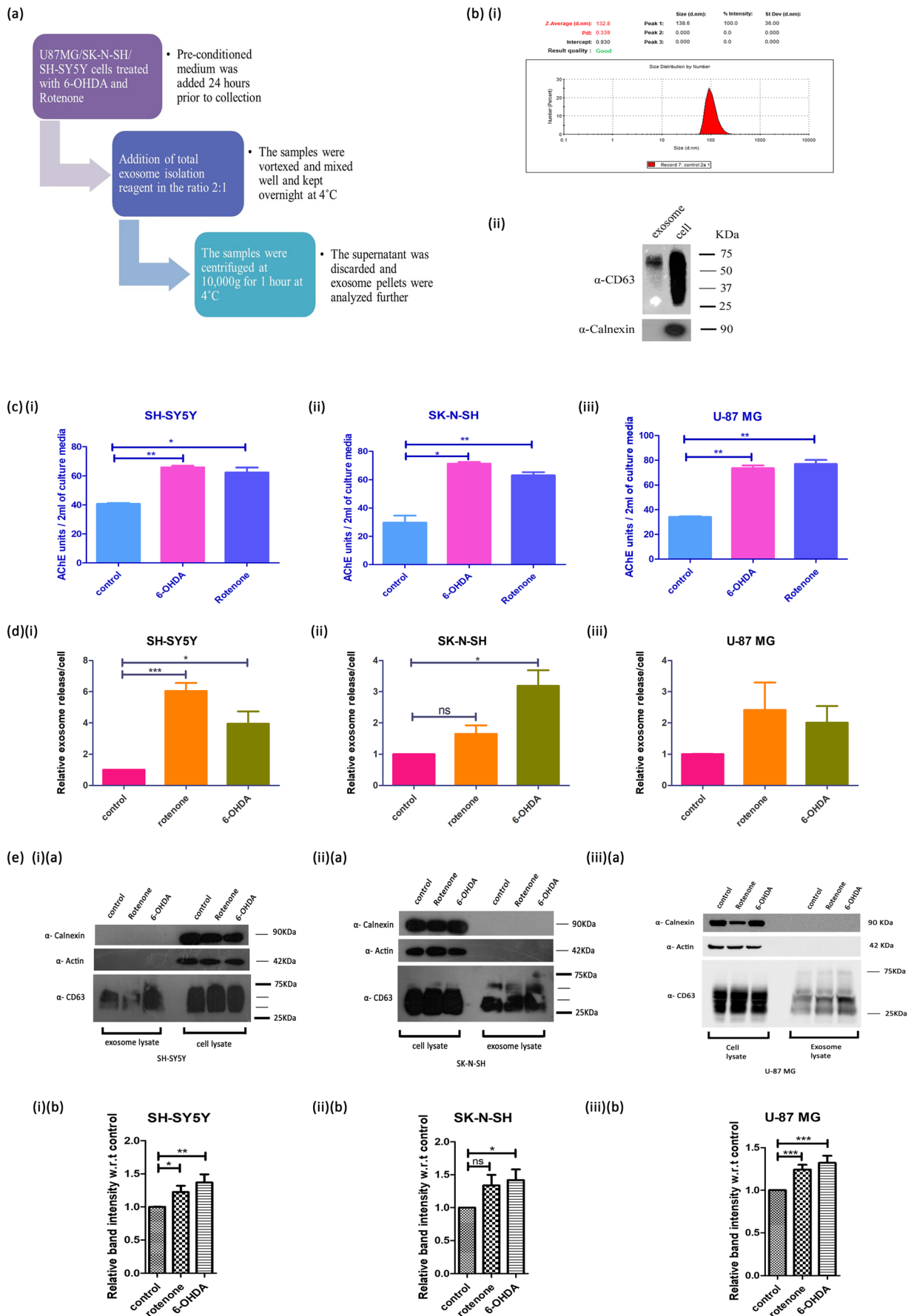
Results

Exosome Release Is Enhanced in Parkinson's Disease Stress Conditions

The release of exosomes and its modulation in PD stress conditions in different neuronal cell types in brain is not well understood. Hence, we first isolated the exosomes from three different cell lines, including U-87 MG (glial cell origin), SH-SY5Y and SK-N-SH (neuronal cell line; expresses high levels of dopamine β hydroxylase) (Fig. 1a) and subsequently characterized the exosomes by Nanoparticle Tracking Analysis (NTA) and western blotting. The NTA analysis showed the particle size ranging from 80 to 150 nm which is the size range of exosomes (Fig. 1b (i)) in U-87 MG. Recent evidences show that the exosome population is rather heterogeneous in nature, based on which the exosomes are categorized into subpopulations of large exosome vesicles, Exo-L, 90–120 nm; small exosome vesicles, Exo-S, 60–80 nm; and exomeres, \sim 35 nm [25]. In line with these reports, the nanoparticle plots of all cell lines in PD stress conditions also showed varying concentrations and population of different sizes, even including the microvesicles population (Supplementary Fig. S1). Western blot analysis shows bands of the size 30–60 kDa corresponding to CD-63, a well-characterized exosome marker in SK-N-

Fig. 1 Exosome release is enhanced in Parkinson's disease stress conditions: **a** Schematic flowchart of the exosome isolation. **b** Characterization of exosomes by (i) Nanoparticle Tracking Analysis—U-87 MG exosomes were suspended in DPBS and analysed by NTA. The exosome size was found to be in a range of 80–150 nm. (ii) Western Blotting—Exosomes were isolated from SK-N-SH cells, and western blotting was performed and blotted against antibodies as indicated. **c** Exosomes were isolated from (i) SH-SY5Y, (ii) SK-N-SH and (iii) U-87 MG cells treated with 6-OHDA and Rotenone, and exosome concentration was monitored by acetylcholine esterase activity. Asterisk (*) and (**) indicates units statistically significant from control; p value < 0.05 and < 0.01 (respectively), SEM of two independent experiments. **d** Exosomes were isolated from (i) SH-SY5Y, (ii) SK-N-SH and (iii) U-87 MG cells treated with 6-OHDA and Rotenone and subjected to NTA analysis. Asterisk (*) and (***) indicates levels statistically significant from control; p value < 0.05 and < 0.001 (respectively), SEM of three independent experiments. **e** Exosomes were isolated from (i)(a) SH-SY5Y, (ii)(a) SK-N-SH and (iii)(a) U-87 MG cells treated with 6-OHDA and Rotenone and were subjected to western blot analysis using the indicated antibodies. Relative quantification of CD63 as compared to untreated samples in (i)(b) SH-SY5Y, (ii)(b) SK-N-SH and (iii)(b) U-87 MG exosome lysates of cells treated with 6-OHDA and Rotenone. Asterisk (*), (**) and (***) indicates units statistically significant from control; p value < 0.05 , < 0.01 and < 0.001 (respectively), SEM of three independent experiments

SH dopaminergic neuronal cells. Calnexin (ER-resident protein) was used as a negative control for the exosome lysate. The absence of calnexin in the exosomal fraction further confirmed its purity (Fig. 1b (ii)). 6-OHDA and Rotenone are widely used to generate experimental models of PD in vitro [26, 27]. We further analysed the release of exosomes from these cell lines in PD stress conditions like 6-OHDA and Rotenone. Acetylcholine esterase has been previously described to be enriched in exosomes [28] and so has been used as marker for exosomes. Hence, we analysed acetylcholine esterase activity of the isolated exosomes in SH-SY5Y and SK-N-SH dopaminergic neuronal cells and U-87 MG glial cells in different PD stress conditions, 6-OHDA and Rotenone, to analyse the quantitative release of exosomes. We observed enhanced level of acetylcholine esterase activity in exosomal fraction isolated from all cells in presence of 6-OHDA and Rotenone as compared to untreated (Fig. 1c). We also used NTA analysis to quantify the release of the exosomes. Exosomes from cells treated with 6-OHDA and Rotenone subjected to NTA analysis showed increased concentration of exosomes in PD stress conditions in all the cell lines (Fig. 1d). Further, we analysed the levels of CD63 (a well-characterized exosome marker) in exosomes by western blotting in 6-OHDA and Rotenone conditions. Interestingly, increased level of exosomal CD63 was observed in 6-OHDA and Rotenone treated cells compared to control in all the cell lines (Fig. 1e). All the evidences provided here strongly suggest enhanced exosomal release in both neurons and glial cells in vitro in PD stress conditions.



Parkinson's Disease Stress Conditions Lead to Mitochondrial Dysfunctions

Mitochondrial dysfunctions affect a number of cellular pathways leading to cell death; hence, we monitored mitochondrial functions in PD stress conditions. We assessed the mitochondrial morphology in PD stress conditions in U-87 MG glial cells by confocal microscopy. The untreated cells show an extensive mitochondrial network, as compared to the cells treated with 6-OHDA and Rotenone, which show a fragmented mitochondrial network (Fig. 2a). Mitochondrial respiratory chain is the most important sites for ROS production, and alteration in complex I activity is one of the major ROS source as there are many electron transfer centres and possibilities of leakage of electron [29]. Hence, we analysed the complex I activity in PD stress conditions by spectrophotometric method in SH-SY5Y and SK-N-SH dopaminergic neuronal cells. Both SH-SY5Y and SK-N-SH showed a considerable decrease in the complex I activity in PD stress conditions (Fig. 2b). Complex I is the entry point of electrons from NADH in ETC (electron transport chain) in mitochondria and, hence, determines the level of ATP and ROS levels in cells. Therefore, we analysed the ATP levels in SH-SY5Y, SK-N-SH dopaminergic neuronal cells and U-87 MG glial cells. All the cell lines show a decrease in the ATP levels in the presence of 6-OHDA and Rotenone (Fig. 2c). These evidences clearly suggest that mitochondrial functions are altered in PD stress conditions.

Lysosomal Functions Are Altered in Parkinson's Disease Stress Conditions

The emerging evidences suggest that defect in OXPHOS activity leads to altered NADH/NAD ratio which also leads to lysosomal dysfunction [30]. This suggests that mitochondrial and lysosomal functions are linked [31]; however, this crosstalk between the lysosome and mitochondria is not well understood in PD; hence, we analysed the lysosomal functions in PD stress conditions. We assessed the lysosomes with LysoTracker Blue by confocal microscopy in the presence and absence of 6-OHDA and Rotenone in SH-SY5Y, SK-N-SH dopaminergic neuronal cells and U-87 MG glial cells. We observed significant decrease in the number of lysosomes, in all the three cell lines when treated with 6-OHDA and Rotenone (Fig. 3a).

The function of lysosomes is critical for autophagy and hence degradation of α -syn aggregates and turnover of mitochondria; hence, we monitored the acid phosphatase activity of both neuronal and glial cells. We observed significant decrease in lysosomal acid phosphatase activity in 6-OHDA- and Rotenone-treated cells in all the cell lines. U-87 MG glial

cells showed decreased lysosomal acid phosphatase activity in the PD stress conditions as compared to SK-N-SH and SH-SY5Y dopaminergic neuronal cells (Fig. 3b).

TFEB is a transcription factor and a master regulator of lysosome biogenesis and autophagy, and nuclear translocation of TFEB is essential for activating transcriptional programmes related to lysosomal biogenesis [32]; therefore, we assessed the nuclear localization of TFEB in PD stress conditions using western blotting. SH-SY5Y dopaminergic neuronal cells and U-87 MG glial cells were treated with Rotenone and 6-OHDA, and nuclear fractions were prepared, and the levels of TFEB were monitored using TFEB-specific antibody. Western blot analysis of the nuclear fractions showed decreased nuclear localization of TFEB in 6-OHDA conditions in both SH-SY5Y and U-87 MG cells (Fig. 3c (i)(a) and (ii)(a)), while no change could be observed in Rotenone-treated conditions. Relative quantification of the western blots confirm that the TFEB/Lamin ratio decreases in 6-OHDA treatment as compared to untreated, and no significant change is observed under Rotenone conditions (Fig. 3c (i)(b) and (ii)(b)).

Altered Autophagic Flux Modulates Exosome Release in PD Stress Conditions

Autophagy is a degradative mechanism used by all cell types to maintain protein homeostasis in the cells. Deficiency of basal autophagy results in neurodegeneration characterized by the accumulation of ubiquitinated-protein aggregates [33]. Above results strongly suggest the lysosomal dysfunction in PD stress conditions, which can lead to autophagy defect; hence, autophagy was monitored in neuronal and glial cells in PD stress conditions. We observed that 6-OHDA modulates the autophagy flux using tandem-mcherry-GFP-LC3 construct. The yellow puncta (red and green merge) indicate autophagosomes whereas red puncta indicate autophagosomes fused with lysosomes also called as autophagolysosomes [34]. All the cell lines were transfected with mCherry-GFP-LC3 and subsequently treated with 6-OHDA and Rotenone, and red/yellow puncta were monitored. In all the three cell lines, the number of red puncta decreased in 6-OHDA as well as Rotenone-treated cells as compared to untreated. Similarly, the yellow-coloured puncta increased per neurons in the 6-OHDA and Rotenone condition, indicating the reduced autophagic flux (Fig. 4a). We also examined autophagy using LC3 western blotting in cell lines treated with 6-OHDA and Rotenone. LC3, the cytosolic form of which (LC3-I) is conjugated to phosphatidylethanolamine to form LC3-phosphatidylethanolamine conjugate (LC3-II), is recruited to autophagosomal membranes [35]; hence, LC3 is an established marker of autophagy. In SH-SY5Y dopaminergic neuronal cells, enhanced conversion of LC3-I to LC3-II is observed in 6-OHDA-treated cells, and further accumulation is observed when the autophagy pathway is blocked by Bafilomycin (100 nM)

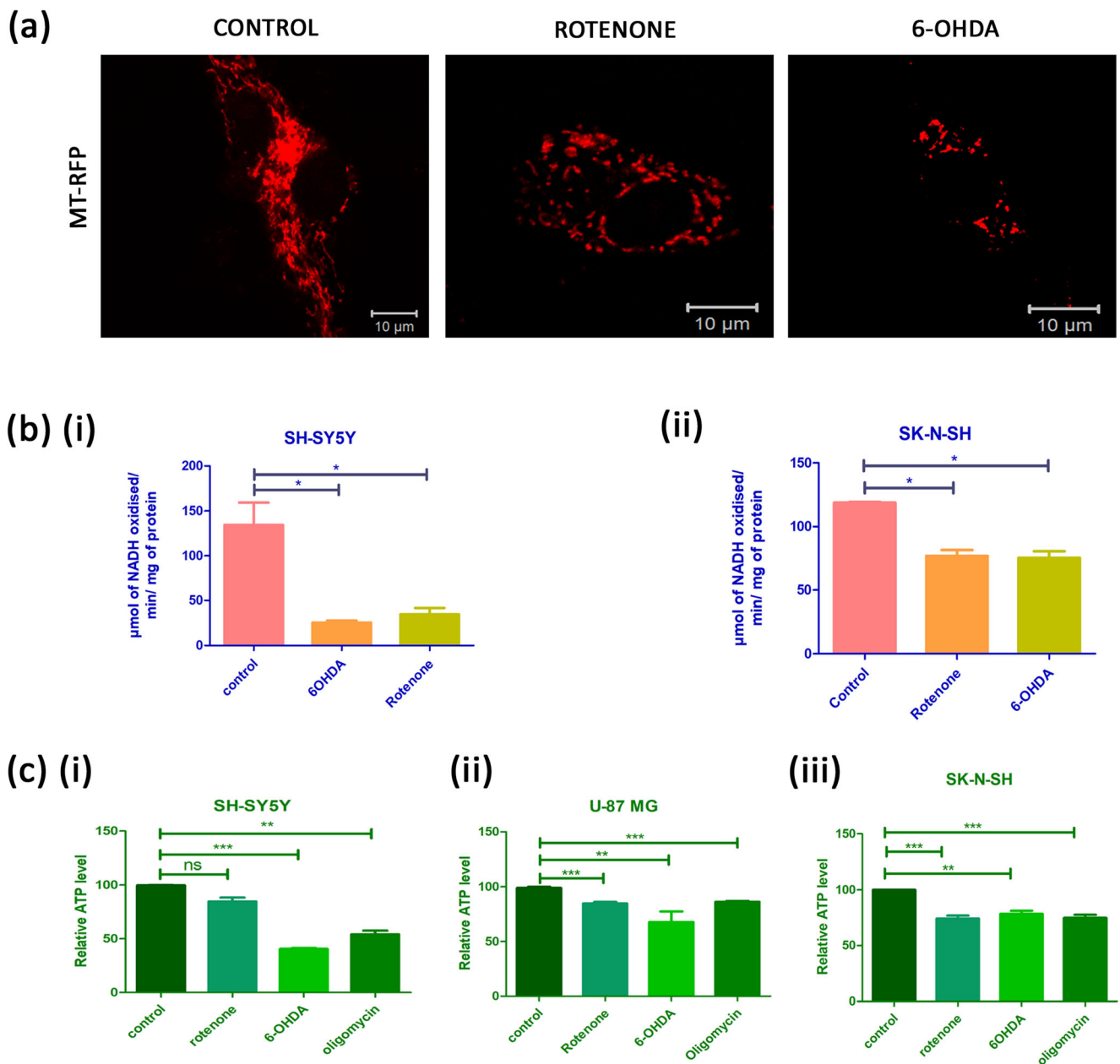
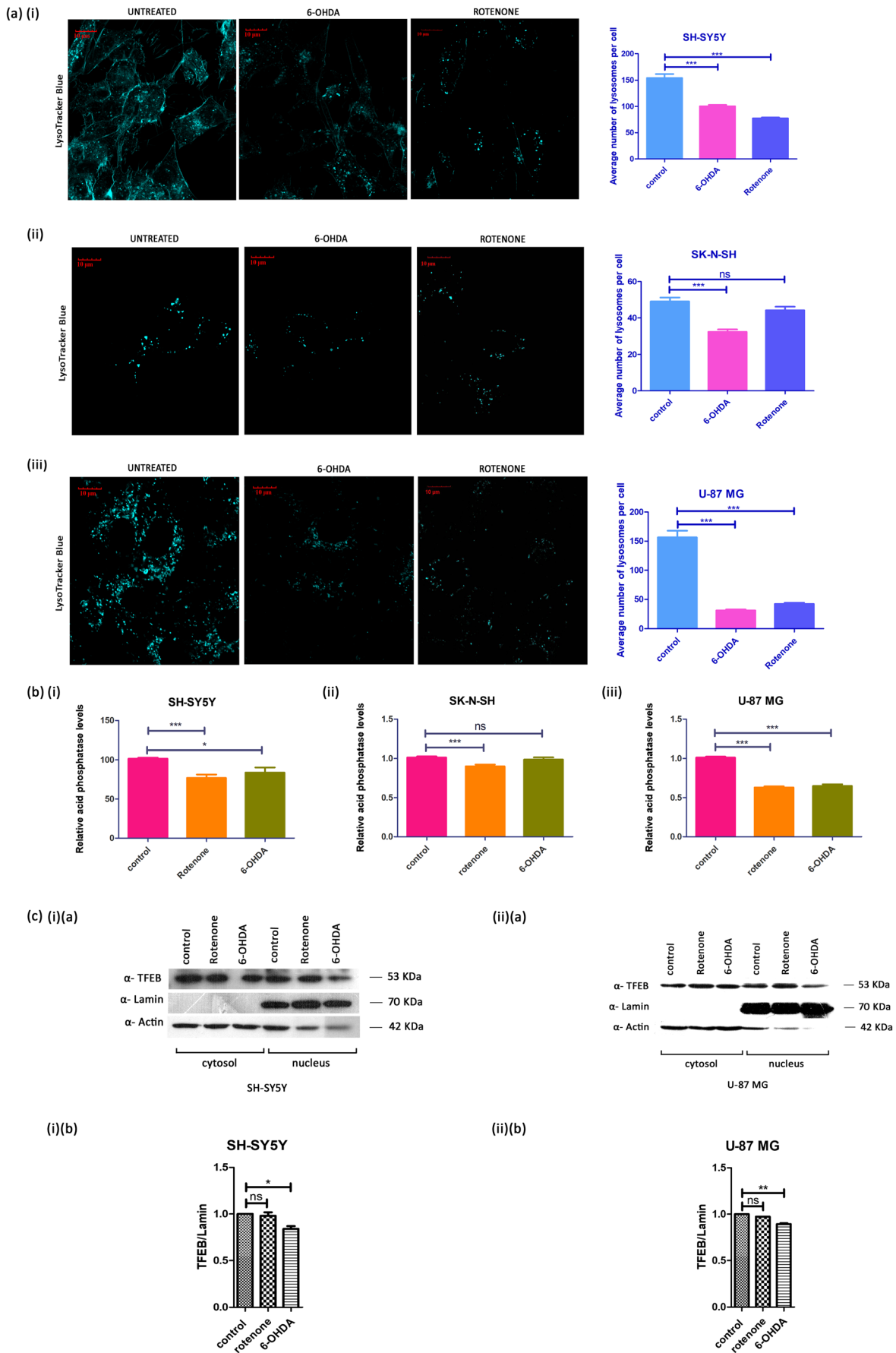


Fig. 2 Parkinson's disease stress conditions lead to mitochondrial dysfunctions: **a** MT-RFP transfected U-87 MG cells were treated with 6-OHDA and Rotenone and analysed by confocal microscopy. **b** (i) SH-SY5Y and (ii) SK-N-SH cells were treated with 6-OHDA and Rotenone, and complex I activity was measured by spectrophotometric method. Asterisk (*) indicates levels statistically significant from control; *p* value

< 0.05, SEM of three independent experiments. **c** (i) SH-SY5Y, (ii) SK-N-SH and (iii) U-87 MG cells were treated with 6-OHDA and Rotenone, and ATP levels were determined by luminescence method. Asterisk (**) and (***) indicates levels statistically significant from control; *p* value < 0.01 and < 0.001 (respectively), SEM of three independent experiments

(Fig. 4b (i)(a)) which is also evident by the LC3II/LC3I ratio (Fig. 4b (i)(b)). Similar results are obtained in SK-N-SH dopaminergic neuronal cells (Fig. 4b (ii)). However, a decrease in LC3-II levels are observed in U-87 MG glial cells, but LC3 accumulates when co-treated with Bafilomycin A1 (Fig. 4b (iii)(a) and (iii)(b)). These results indicate alteration of autophagic flux in all the cell lines under PD stress conditions. The

autophagic flux was also monitored using wortmannin, which is a widely used autophagy inhibitor. LC3-II accumulates in cells co-treated with 6-OHDA and wortmannin which indicates defect in autophagic flux in SH-SY5Y dopaminergic neuronal cells (Supplementary Fig. S2 (a)(i) and (a)(ii)). There are emerging evidences to show a molecular and functional crosstalk between autophagy pathways and exosome release [36]. Exosome release



◀ **Fig. 3** Lysosomal functions are altered in Parkinson's disease stress conditions: **a** (i) SH-SY5Y, (ii) SK-N-SH and (iii) U-87 MG cells were treated with 6-OHDA and Rotenone for 24 h. After treatment cells were stained with LysoTracker Blue as described in method section and were visualized by confocal microscopy and average number of lysosomes per cell was quantified using ImageJ software. Asterisk (***) indicates number of puncta statistically significant from control; p value < 0.001 , SEM of three independent experiments. **b** (i) SH-SY5Y, (ii) SK-N-SH and (iii) U-87 MG cells were treated with 6-OHDA and Rotenone for 24 h. After treatment, acid phosphatase activity was determined as described in the "Materials and methods" section. Asterisk (*) and (***) indicates acid phosphatase levels statistically significant from control; p value < 0.05 and < 0.001 (respectively), SEM of four independent experiments. **c** (i)(a) SH-SY5Y and (ii)(a) U-87 MG cells were treated with 6-OHDA and Rotenone, and nuclear fractionation was performed and subjected to western blot analysis using the indicated antibodies. Relative quantification of TFEB protein levels in (i)(b) SH-SY5Y and (ii)(b) U-87 MG cells treated with 6-OHDA and Rotenone. Asterisk (*) and (***) indicates units statistically significant from control; p value < 0.05 and < 0.01 (respectively), SEM of two independent experiments

may serve as a cellular mechanism to partially bypass the autophagic defect that occurs during pathological situations. To elucidate the crosstalk of the autophagy and exosome release pathways under PD stress conditions, SH-SY5Y and SK-N-SH dopaminergic neuronal cells and U-87 MG glial cells were treated with 6-OHDA and Rotenone, and autophagy pathway was blocked using Bafilomycin, and subsequent exosome release was monitored by western blotting. In all the cell lines, enhanced exosome release was observed when autophagy pathway is blocked by Bafilomycin and even more enhanced when the PD stress conditions are co-treated with Bafilomycin (Fig. 4c (i)(a), (ii)(a) and (iii)(a)). Relative quantification of the CD63 levels as compared to control confirms that there is a significant increase in the co-treated conditions (Fig. 4c (i)(b), (ii)(b) and (iii)(b)). Similarly, subsequent exosome release was checked in all the cell lines under PD stress conditions co-treated with wortmannin. The cells treated with wortmannin did not significantly alter the exosome release in the cells whereas decreased in cells co-treated with 6-OHDA and Rotenone with wortmannin (Supplementary Fig. S2 (d), (e), and (f)).

Enhancement of Autophagy Flux by Rapamycin Decreases the Release of Exosomes in PD Stress Conditions

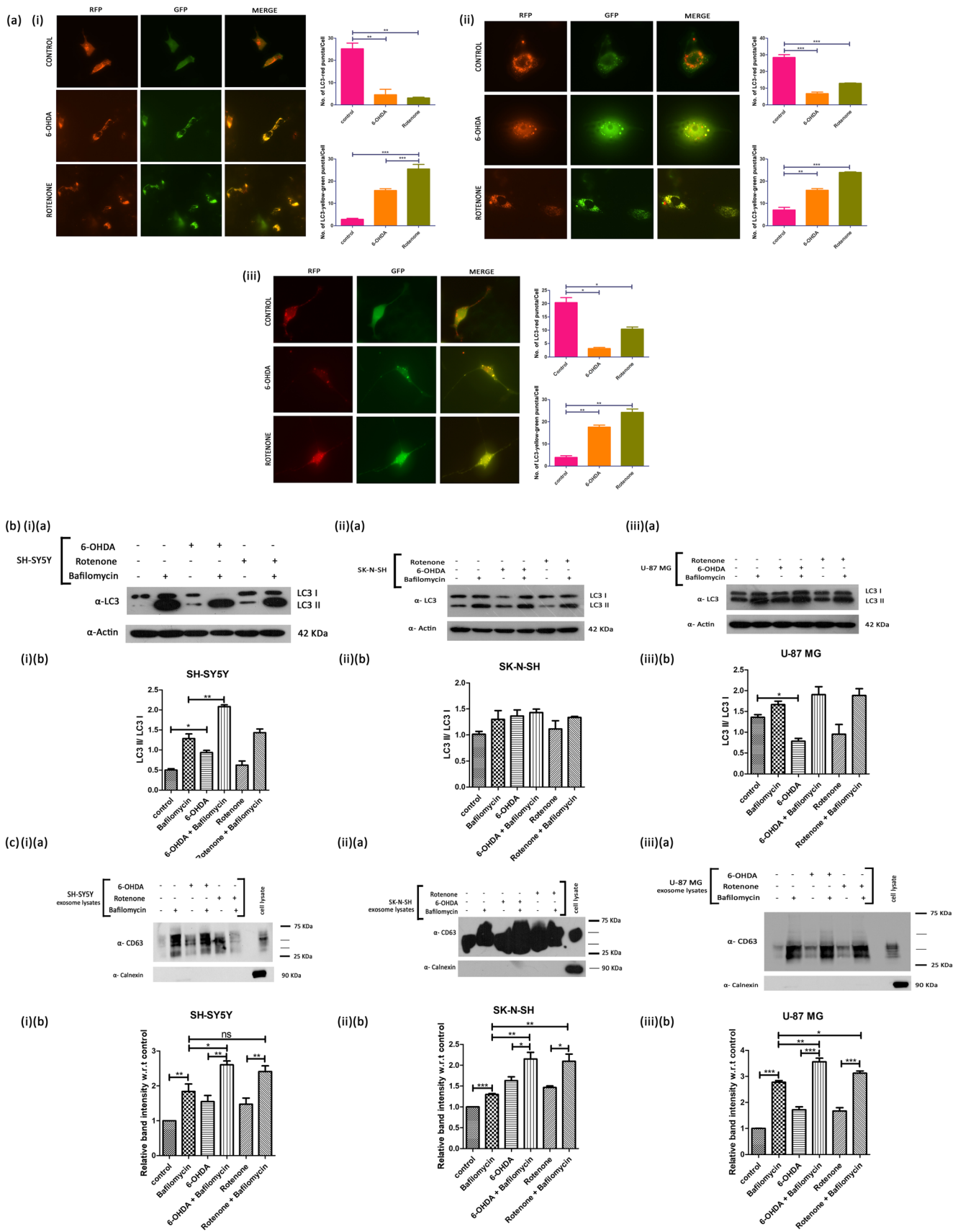
The experiments here showed that mitochondrial and lysosomal dysfunction can modulate the autophagic flux and hence also modulate the exosomal release in PD stress conditions. We hypothesized that enhancing the basal autophagic flux may decrease the exosomal release. Rapamycin is an allosteric inhibitor of mammalian target of rapamycin (mTOR), and inhibition of mTOR activity enhances autophagy, which in turn plays a role in maintaining metabolic homeostasis [37]; however, its implication in exosomal release in neuronal cells is not well understood.

Hence, we treated the cells with PD stress conditions in presence and absence of rapamycin and checked the exosome release. Firstly, we analysed if rapamycin can modulate the autophagy flux in both neurons and glial cells. SH-SY5Y dopaminergic neuronal cells treated with 6-OHDA showed enhanced level of LC3-II form which decreased when cells were co-treated with rapamycin (Fig. 5a (i)). Similarly, enhanced degradation of accumulated LC3-II forms was observed in U-87 MG glial cells (Fig. 5a (ii)). These evidences suggest that rapamycin enhances the autophagy flux both in neuronal and glial cells in the presence of PD stress conditions. As enhanced autophagy flux may modulate the release of exosomes, hence, we analysed the exosomal release in presence of PD stress conditions and rapamycin. In SH-SY5Y dopaminergic neuronal cells and U-87 MG glial cells, the level of CD63 marking the exosome release is enhanced in the presence of 6-OHDA and Rotenone and PD stress conditions. Interestingly, the level of CD63 is decreased in cells co-treated with 6-OHDA and Rotenone with rapamycin both in SH-SY5Y and U-87 MG cells (Fig. 5b (i) and (ii)). These experiments suggest that enhancing the autophagy through rapamycin decreased the release of exosome both in neuronal and glial cells.

Discussion

Parkinson's disease is typically characterized by the death of dopaminergic neurons in the substantia nigra part of the brain; however, it has been well established that visual impairments occur commonly in PD, along with loss of DA-producing retinal amacrine cells in the inner nuclear and ganglion cell layers and secondary depletion of the dopaminergic fiber plexus of the inner plexiform layer. Similarly, neuronal loss and Lewy body pathology has been observed in the anterior olfactory nucleus as well as the olfactory bulb [38]. The spread of the pathology to different cell types suggest the importance of inter-neuronal communication through exosomes. The exosomal release is a complex crosstalk of mitochondria, lysosome and MVBs to counter the cellular stress and cell may release the damaged organelle/proteins along with other cargo to protect the cells. In the current study, we studied the mitochondria-lysosomal crosstalk in the release of exosome in PD stress conditions.

We used neuronal and glial cell lines for the study since it is now well established that glial cells play a role in PD. Glial reaction occurs as a result of the neuronal cell death in neurodegenerative diseases, and it has been found that even after the initial insult to the neuron has disappeared, the glial reaction initiated further propagates the neuronal degeneration [39, 40]. Moreover, it is now known that the density of microglial cells is remarkably higher in the substantia nigra as compared to the other regions of the brain-like hippocampus and the midbrain regions, which also suggest that the substantia nigra



◀ **Fig. 4** Altered autophagic flux modulates exosome release in PD stress conditions: **a** Quantification of red and green puncta in mCherry-GFP-LC3 transfected cells in the presence and absence of 6-OHDA and Rotenone. The numbers of LC3 puncta per cell were counted, and graph was plotted for numbers of mCherry-LC3 puncta per cell in (i) SH-SY5Y, (ii) SK-N-SH and (iii) U-87 MG. Asterisk (*), (**), and (***) indicates number of LC3 puncta statistically significant from control; p value < 0.05, < 0.01 and < 0.001 (respectively), SEM of three independent experiments. **b** (i)(a) SH-SY5Y, (ii)(a) SK-N-SH and (iii)(a) U-87 MG cells were treated with Rotenone and 6-OHDA and western blot analysis of autophagy marker, LC3 was performed in presence and absence of Bafilomycin A1. Relative quantification of LC3 II/ LC3 I ratio in (i)(b) SH-SY5Y, (ii)(b) SK-N-SH and (iii)(b) U-87 MG cells treated with 6-OHDA and Rotenone in the presence and absence of Bafilomycin A1. Asterisk (*) and (**) indicates levels statistically significant from control; p value < 0.05 and < 0.01 (respectively), SEM of three independent experiments. **c** (i)(a) SH-SY5Y, (ii)(a) SK-N-SH and (iii)(a) U-87 MG cells were treated with Rotenone and 6-OHDA, and subsequent exosome release was monitored in the presence and absence of Bafilomycin A1 by performing western blot against the exosome marker, CD63. Relative quantification of CD63 as compared to untreated samples in (i)(b) SH-SY5Y, (ii)(b) SK-N-SH and (iii)(b) U-87 MG exosome lysates of cells treated with 6-OHDA and Rotenone in the presence and absence of Bafilomycin A1. Asterisk (*), (**) and (***) indicates levels statistically significant from control; p value < 0.05, < 0.01 and < 0.001 (respectively), SEM of three independent experiments

neurons are more susceptible to microglial-mediated injuries, supporting the implication of gliosis in PD pathogenesis [41].

We first isolated and characterized the exosomes released from both cell types. Isolation of exosomes was performed by an affinity purification-based method. The exosomes were subsequently characterized by Nanoparticle Tracking Analysis and western blotting against the well-characterized exosomal marker, CD63. We also checked the exosome release in the presence of 6-OHDA and Rotenone, which are the two chemicals used to mimic the Parkinson's disease conditions. All the evidences here strongly suggest the enhanced exosomal release in PD stress conditions in dopaminergic neuronal cells (SH-SY5Y and SK-N-SH) and glial cells (U-87 MG).

Previous reports have shown that mitochondria in the neurons are more susceptible to oxidative stress as compared to other cell types [42]. Fragmented mitochondria are usually followed by a decrease in respiration and eventual cell death and is observed in PD models [43]. In our study, we show that mitochondrial fragmentation occurs in the U-87 MG glial cells on treatment with 6-OHDA and Rotenone. Furthermore, consistent with previous reports [44–46], we showed that SH-SY5Y and SK-N-SH dopaminergic neuronal cells treated with 6-OHDA and Rotenone show impaired mitochondrial complex I activity and ATP level decline and oxidative stress which is the hallmark in PD pathogenesis [47, 48]. An association between PD and hindered complex I activity in the brain was reported by several groups [49, 50]. Chemicals and environmental toxins including Rotenone, 1-methyl-4-phenyl-1,2,3,6-tetrahydropyridine (MPTP), paraquat and

nitric oxide are all shown to inhibit mitochondrial functions which show Parkinson-type symptoms [51]. This impaired mitochondrial respiration leads to reduction of ATP levels [46] and is one of the major causes of neurodegeneration, including PD [52].

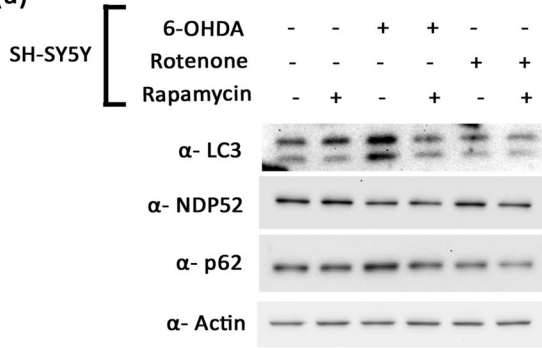
Mitochondrial OXPHOS activity is known to maintain NADH/NAD ratio which is also important for the maintenance of the lysosomal functions [30]. The crosstalk is further established by recent report where lysosomal dysfunction can lead to generation of a LIPL-4, a lipid signalling messenger which adjust the mitochondrial ETC activity and mitochondrial β -oxidation to reduce lipid storage and promote longevity in *Caenorhabditis elegans* [53]. Therefore, the evidence here and emerging reports strongly suggest the mitochondria and lysosomal crosstalk in regulation of neuronal homeostasis; however, its implication of this signalling in PD pathogenesis needs to be further understood.

Lysosome is now becoming one of the important organelles in cellular homeostasis. The dysfunction in lysosomes may lead to alteration of several pathways leading to cell death and progression of several chronic diseases. The dysfunction leads to decrease in autophagy flux and hence accumulation of autophagosomes. We showed the dysfunction in lysosomes in neuronal as well as glial cell lines by using LysoTracker Blue dye and counting average number of lysosomes per cell through confocal microscopy. Acid phosphatase activity was also hampered in all the three cell lines in PD stress conditions. TFEB is a major regulator in coordinating autophagy induction along with lysosomal biogenesis, and its activation has ameliorated various neurodegenerative disorders in mouse models [54]. By nuclear fractionation of the cells and western blot analysis, we showed that the nuclear translocation of TFEB is perturbed in 6-OHDA conditions, indicating defective lysosomal biogenesis and autophagy flux. This was further confirmed by monitoring the autophagy flux in all three cell lines in 6-OHDA and Rotenone conditions using the tandem construct mCherry-GFP-LC3. The number of yellow puncta considerably increased in 6-OHDA and Rotenone conditions indicating the reduced autophagic flux and impaired autophagy.

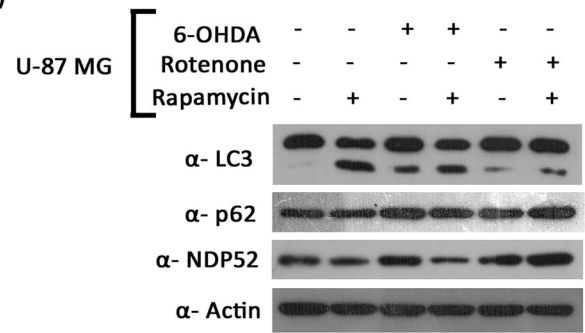
How the impairment of autophagy in PD stress conditions affects the exosome release is not well understood. Hence, we assessed the exosome release under the same conditions. The blocking of autophagy pathway by Bafilomycin A1 greatly enhances the exosome release in the dopaminergic neuronal and glial cells.

The class III PI3Ks are known to play a role in recruitment of specific effector proteins to promote endocytosis, endosome fusion, and maturation, as well as cargo sorting to lysosomes, and moreover are essential for the ILV formation [55]. We observed here that inhibition of class III PI3Ks with the help of wortmannin resulted in decreased release of exosomes

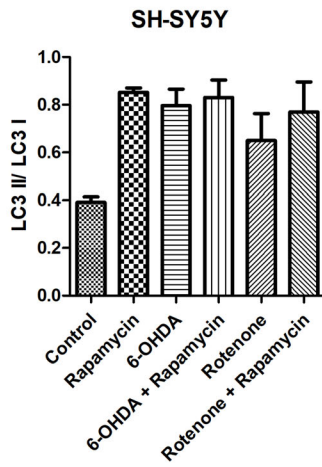
(a) (i)(a)



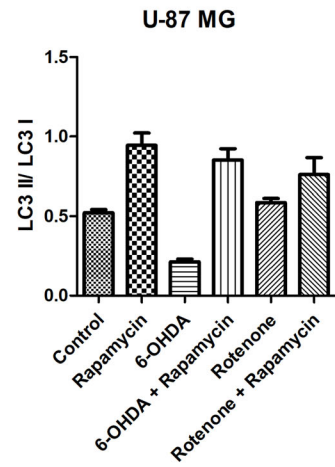
(ii)(a)



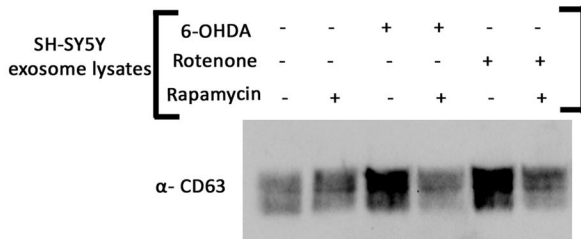
(i)(b)



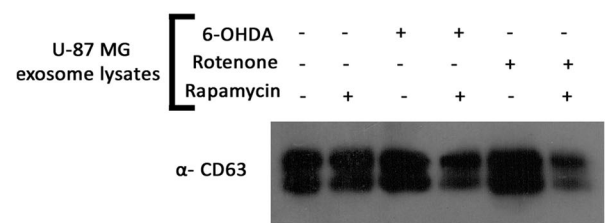
(ii)(b)



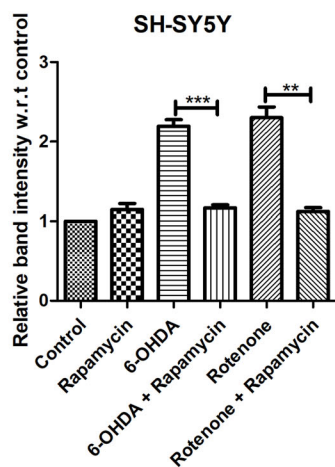
(b) (i)(a)



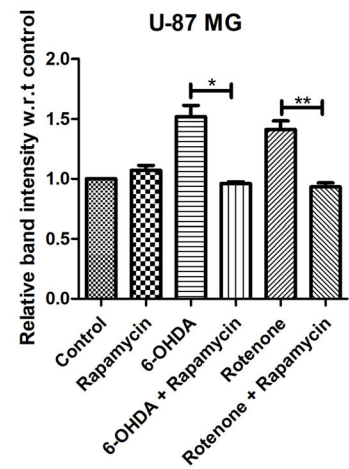
(ii)(a)



(i)(b)



(ii)(b)



◀ **Fig. 5** Enhancement of autophagy flux by rapamycin decreases the release of exosomes in PD stress conditions: **a** (i)(a) SH-SY5Y and (ii)(a) U-87 MG cells were treated with Rotenone and 6-OHDA, and western blot analysis of autophagy markers was performed in the presence and absence of rapamycin. Relative quantification of LC3 II/ LC3 I ratio in (i)(b) SH-SY5Y and (ii)(b) U-87 MG cells treated with 6-OHDA and Rotenone in the presence and absence of rapamycin, SEM of three independent experiments. **b** (i)(a) SH-SY5Y and (ii)(a) U-87 MG cells were treated with Rotenone and 6-OHDA, and subsequent exosome release was monitored in the presence and absence of rapamycin by performing western blot against the exosome marker, CD63. Relative quantification of CD63 as compared to untreated samples in (i)(b) SH-SY5Y and (ii)(b) U-87 MG exosome lysates of cells treated with 6-OHDA and Rotenone in the presence and absence of rapamycin. Asterisk (*), (**) and (***) indicates levels statistically significant from control; *p* value < 0.05, < 0.01 and < 0.001 (respectively), SEM of three independent experiments

in PD stress conditions. This indicates that the regulation of exosome release is largely dependent on the inhibition of the autophagy process at the terminal step of fusion of the autophagosome with the lysosome. The results here suggest that wortmannin, which blocks autophagy at the initiation stage, also may affect a number of other different pathways because of their broad-spectrum action, and hence the enhanced exosome release is not observed in these cases.

The enhancement of autophagy by rapamycin in PD stress conditions in both SH-SY5Y dopaminergic neuronal cells and U-87 MG glial cells showed a decrease in the release of exosomes. This is in consonance with previous reports where it has been observed that rapamycin plays a protective role against cell death in *in vitro* and *in vivo* models of PD [37], and this may be because of preventing the exosomal release by enhancing the autophagy flux. This suggests that enhancement of autophagy pathway by Rapamycin could lower the exosome release content by the cells in PD stress conditions, which could provide a therapeutic possibility to stop the spread of the pathogenesis of the disease through exosomes.

Conclusion

In conclusion, the study here demonstrates that inter-organellar crosstalk between mitochondria, lysosomes and MVB is now emerging important in PD pathogenesis. The mutation in several proteins regulating mitochondrial dysfunction may in turn inhibit the lysosomal function leading to decreased autophagy flux; hence, increased exosomal release is observed, containing several pathogenic cargo components which may intensify the pathogenesis of PD. The evidences here suggest that the understanding of the inter-organellar crosstalk may provide unique opportunity to modulate the combinatorial strategy to enhance the autophagy flux and prevent exosomal release hereby reducing the spread of PD and helping ameliorate the disease.

Supplementary Information The online version contains supplementary material available at <https://doi.org/10.1007/s12035-020-02243-3>.

Acknowledgements Authors acknowledge the DBT-MSUB-ILSPARE programme of the Department of Biochemistry, the M S University of Baroda sponsored by DBT, Government of India. Authors also acknowledge the FIST programme supported by DST, Government of India. This work is a part of the Ph.D. thesis of Fatema Currim. Fatema Currim received Junior Research Fellowship from DST-INSPIRE, Government of India. Dhruv Gohel received Senior Research Fellowship from the Indian Council of Medical Research (ICMR), Government of India. Minal Mane received Senior Research fellowship from the Council of Scientific and Industrial Research (CSIR), Government of India.

Authors Contribution Fatema Currim: Investigation, validation, writing—original draft

Jyoti Singh Anjali Shinde, Milton Roy, Dhruv Gohel, Kritarth Singh, Shatakshi Shukla, Minal Mane and Hitesh Vasiyani: Formal data analysis, methodology and resources

Rajesh Singh: Conceptualization, methodology, resources, writing—original draft, visualization, supervision and funding acquisition

Funding The current research work was financially supported by the Department of Biotechnology, Government of India grant (BT/PR19937/MED/122/17/2016) to RS.

Compliance with Ethical Standards

Conflict of Interest The authors declare that they have no competing interests.

References

1. Draoui A, El Hiba O, Aimrane A et al (2020) General review Parkinson's disease: from bench to bedside. *Rev Neurol (Paris)* 176:1–17. <https://doi.org/10.1016/j.neurol.2019.11.002>
2. Jellinger KA (2014) Neuropathology of Parkinson's disease. Springer, Inflammation in Parkinson's Disease, pp. 25–74. <https://doi.org/10.1007/978-3-319-08046-8>
3. Beyer K, Ariza A (2009) Molecular pathology of Lewy body diseases. *Int J Mol Sci*:724–745. <https://doi.org/10.3390/ijms10030724>
4. Henderson MX, Cornblath EJ, Darwich A, Zhang B, Brown H, Gathagan RJ, Sandler RM, Bassett DS et al (2019) Spread of α -synuclein pathology through the brain connectome is modulated by selective vulnerability and predicted by network analysis. *Nat Neurosci* 22:1248–1257. <https://doi.org/10.1038/s41593-019-0457-5>
5. Lill CM (2016) Genetics of Parkinson's disease. *Mol Cell Probes* 30:386–396. <https://doi.org/10.1016/j.mcp.2016.11.001>
6. Braak RH, Ghebremedhin E, Del Tredici K (2004) Stages in the development of Parkinson's disease-related pathology. *Cell Tissue Res*:121–134. <https://doi.org/10.1007/s00441-004-0956-9>
7. Frühbeis C, Fröhlich D, Kuo WP (2013) Extracellular vesicles as mediators of neuron – glia communication. *Front Cell Neurosci* 7: 1–6. <https://doi.org/10.3389/fncel.2013.00182>
8. Raposo G, Stoorvogel W (2013) Extracellular vesicles: exosomes, microvesicles, and friends. *J Cell Biol* 200:373–383. <https://doi.org/10.1083/jcb.201211138>
9. Hessvik NP, Llorente A (2018) Current knowledge on exosome biogenesis and release. *Cell Mol Life Sci* 75:193–208. <https://doi.org/10.1007/s00018-017-2595-9>

10. Desplats P, Lee H, Bae E et al (2009) Inclusion formation and neuronal cell death through neuron-to-neuron transmission of α -synuclein. *PNAS* 106(31):13010–13015. <https://doi.org/10.1073/pnas.0903691106>
11. Lee H, Suk J, Patrick C et al (2010) Direct transfer of α -synuclein from neuron to astroglia causes inflammatory responses in synucleinopathies. *J Biol Chem* 285:9262–9272. <https://doi.org/10.1074/jbc.M109.081125>
12. Perier C, Vila M (2012) Mitochondrial biology and Parkinson's disease. *Cold Spring Harbor Perspectives in medicine* 2:1–19. <https://doi.org/10.1101/cshperspect.a009332>
13. Vries D, Rosa LA, Przedborski S (2013) Mitophagy and Parkinson's disease: be eaten to stay healthy. *Mol Cell Neurosci* 55:37–43. <https://doi.org/10.1016/j.mcn.2012.07.008>
14. Narendra D, Tanaka A, Suen D, Youle RJ (2008) Parkin is recruited selectively to impaired mitochondria and promotes their autophagy. *J Cell Biol* 183:795–803. <https://doi.org/10.1083/jcb.200809125>
15. Matsuda N, Sato S, Shiba K, Okatsu K, Saisho K, Gautier CA, Sou YS, Saiki S et al (2010) PINK1 stabilized by mitochondrial depolarization recruits Parkin to damaged mitochondria and activates latent Parkin for mitophagy. *J Cell Biol* 189:211–221. <https://doi.org/10.1083/jcb.200910140>
16. He X, Yuan W, Li Z, Hou Y, Liu F, Feng J (2018) 6-Hydroxydopamine induces autophagic flux dysfunction by impairing transcription factor EB activation and lysosomal function in dopaminergic neurons and SH-SY5Y cells. *Toxicol Lett* 283:58–68. <https://doi.org/10.1016/j.toxlet.2017.11.017>
17. Ramirez A, Gru J, Stiller B et al (2006) Hereditary parkinsonism with dementia is caused by mutations in ATP13A2, encoding a lysosomal type 5 ATPase. *Neuron* 50:1184–1191. <https://doi.org/10.1038/ng1884>
18. Dehay B, Ramirez A, Martinez-vicente M et al (2012) Loss of P-type ATPase ATP13A2 / PARK9 function induces general lysosomal deficiency and leads to Parkinson disease neurodegeneration. *PNAS* 109(24):9611–9616. <https://doi.org/10.1073/pnas.1112368109>
19. Richaud-patin Y, Carballo-carbalaj I, Sa A et al (2012) Disease-specific phenotypes in dopamine neurons from human iPSC-based models of genetic and sporadic Parkinson's disease. *EMBO Mol Med*:380–395. <https://doi.org/10.1002/emmm.201200215>
20. Nguyen HN, Byers B, Cord B, Shcheglovitov A, Byrne J, Gujar P, Kee K, Schüle B et al (2011) LRRK2 mutant iPSC-derived DA neurons demonstrate increased susceptibility to oxidative stress. *Cell Stem Cell* 8:267–280. <https://doi.org/10.1016/j.stem.2011.01.013>
21. Baixauli F, López-otín C, Mittelbrunn M (2014) Exosomes and autophagy: coordinated mechanisms for the maintenance of cellular fitness. *Front Immunol* 5:1–6. <https://doi.org/10.3389/fimmu.2014.00403>
22. Huotari J, Helenius A (2011) Endosome maturation. *EMBO J* 30:3481–3500. <https://doi.org/10.1038/emboj.2011.286>
23. Colombo M (2014) Biogenesis, secretion, and intercellular interactions of exosomes and other extracellular vesicles. *Annu Rev Cell Dev Biol*:255–292. <https://doi.org/10.1146/annurev-cellbio-101512-122326>
24. Plotegher N, Duchen MR (2017) Crosstalk between lysosomes and mitochondria in Parkinson's disease. *Frontiers in cell and developmental biology* 5:2011–2018. <https://doi.org/10.3389/fcell.2017.00110>
25. Zhang H, Freitas D, Kim HS, Fabijanic K, Li Z, Chen H, Mark MT, Molina H et al (2018) Identification of distinct nanoparticles and subsets of extracellular vesicles by asymmetric flow field-flow fractionation. *Nat Cell Biol* 20:332–343. <https://doi.org/10.1038/s41556-018-0040-4>
26. Galindo F, Tomero D, Gonza C (2004) Bcl-x L blocks mitochondrial multiple conductance channel activation and inhibits 6-OHDA-induced death in SH-SY5Y cells. *J Neurochem*:124–133. <https://doi.org/10.1046/j.1471-4159.2003.02299.x>
27. Xiong N, Long X, Xiong J et al (2012) Mitochondrial complex I inhibitor rotenone-induced toxicity and its potential mechanisms in Parkinson's disease models. *Crit Rev Toxicol*:1–20. <https://doi.org/10.3109/10408444.2012.680431>
28. Savina A, Vidal M, Colombo MI (2002) The exosome pathway in K562 cells is regulated by Rab11. *J Cell Sci* 115(12):2505–2515
29. Li N, Ragheb K, Lawler G, Sturgis J, Rajwa B, Melendez JA, Robinson JP (2003) Mitochondrial complex I inhibitor rotenone induces apoptosis through enhancing mitochondrial reactive oxygen species production. *J Biol Chem* 278:8516–8525. <https://doi.org/10.1074/jbc.M210432200>
30. Baixauli F, Acín-pérez R, Villarroya-beltrí C et al (2015) Mitochondrial respiration controls lysosomal function during inflammatory T cell responses. *Cell Metab* 22:485–498. <https://doi.org/10.1016/j.cmet.2015.07.020>
31. Demers-lamarche J, Guillebaud G, Tlili M et al (2016) Loss of mitochondrial function impairs lysosomes. *J Biol Chem* 291:10263–10276. <https://doi.org/10.1074/jbc.M115.695825>
32. Cortes CJ, La Spada AR, Biology C (2019) TFEB dysregulation as a driver of autophagy dysfunction in neurodegenerative disease: Molecular mechanisms, cellular processes, and emerging therapeutic opportunities. *Neurobiol Dis* 122:83–93. <https://doi.org/10.1016/j.nbd.2018.05.012>
33. Cheung ZH, Ip NY (2009) The emerging role of autophagy in Parkinson's disease. *Molecular Brain* 6:1–6. <https://doi.org/10.1186/1756-6606-2-29>
34. Kimura S, TN & TY (2007) Dissection of the autophagosome maturation process by a novel reporter protein, tandem fluorescent-tagged LC3. *Autophagy*, 452–460. <https://doi.org/10.4161/auto.4451>
35. Chittaranjan S, Bortnik S, Gorski SM (2015) Monitoring autophagic flux by using lysosomal inhibitors and western blotting of endogenous MAP1LC3B:743–751. <https://doi.org/10.1101/pdb.prot086256>
36. Xu J, Camfield R, Gorski SM (2018) The interplay between exosomes and autophagy – partners in crime. *J Cell Sci* 131:1–11. <https://doi.org/10.1242/jcs.215210>
37. Malagelada C, Jin ZH, Jackson-lewis V et al (2010) Rapamycin protects against neuron death in in vitro and in vivo models of Parkinson's disease. *J Neurosci* 30:1166–1175. <https://doi.org/10.1523/JNEUROSCI.3944-09.2010>
38. Alexander GE (2004) Biology of Parkinson's disease: pathogenesis and pathophysiology of a multisystem neurodegenerative disorder. *Dialogues Clin Neurosci*:259–280
39. Langston JW, Forno LS, Tetud J, Reeves AG (1999) Evidence of active nerve cell degeneration in the Substantia Nigra of humans years after 1-methyl-4-phenyl, 1,2,3,6-tetrahydropyridine exposure. *Annals of Neurology: Official Journal of the American Neurological Association and the Child Neurology Society*:598–605
40. Bronstein DM, Sun V, Sawin SBM et al (1995) Glia-dependent neurotoxicity and neuroprotection in mesencephalic cultures. *Brain Res* 704:112–116
41. Kim W, Mohny RP, Wilson B et al (2000) Regional difference in susceptibility to lipopolysaccharide-induced neurotoxicity in the rat brain: role of microglia. *J Neurosci* 20:6309–6316
42. Schumacker S (2013) Calcium, bioenergetics, and neuronal vulnerability in Parkinson's disease. *J Biol Chem* 288:10736–10741. <https://doi.org/10.1074/jbc.R112.410530>
43. Nakamura K, Nemani VM, Azarbal F, Skibinski G, Levy JM, Egami K, Munishkina L, Zhang J et al (2011) Direct membrane association drives mitochondrial fission by the Parkinson disease-associated protein α -Synuclein. *J Biol Chem* 286:20710–20726. <https://doi.org/10.1074/jbc.M110.213538>
44. Devi L, Raghavendran V, Prabhu BM, Avadhani NG, Anandatheerthavarada HK (2008) Mitochondrial import and

- accumulation of α -Synuclein impair complex I in human dopaminergic neuronal cultures and Parkinson disease brain. *J Biol Chem* 283:9089–9100. <https://doi.org/10.1074/jbc.M710012200>
45. Parker J, Parks KRHS (2008) Complex I deficiency in Parkinson's disease frontal cortex. *Brain Res*:215–218
 46. Keeney PM, Xie J, Capaldi RA, Bennett JP Jr (2006) Parkinson's disease brain mitochondrial complex I has oxidatively damaged subunits and is functionally impaired and misassembled. *J Neurosci* 26:5256–5264. <https://doi.org/10.1523/JNEUROSCI.0984-06.2006>
 47. Chan P, Delanney LE, Irwin I et al (1991) Rapid ATP loss caused by 1-methyl-4-phenyl-1,2,3,6-tetrahydropyridine in mouse brain. *J Neurochem*:348–351. <https://doi.org/10.1111/j.1471-4159.1991.tb02134.x>
 48. Tretter L, Sipos I, Adam-vizi V (2004) Initiation of neuronal damage by complex I deficiency and oxidative stress in Parkinson's disease. *Neurochem Res* 29:569–577
 49. Parker WD, Boyson TSJ, Parks JK (1989) Abnormalities of the electron transport chain in idiopathic Parkinson's disease. *Annals of Neurology: Official Journal of the American Neurological Association and the Child Neurology Society* 26(6):719–723
 50. Schapira A, H. V, et al (1990) Mitochondrial complex I deficiency in Parkinson's disease. *J Neurochem*, 54(3):823–827
 51. Polito L, Greco A, Seripa D (2016) Genetic profile, environmental exposure, and their interaction in Parkinson's disease. *Parkinson's Disease*. <https://doi.org/10.1155/2016/6465793>
 52. Caspersen C, Jackson-lewis V, Carelli V et al (2005) Complex I deficiency primes Bax-dependent neuronal apoptosis through mitochondrial oxidative damage. *PNAS* 102(52):19126–19131. <https://doi.org/10.1073/pnas.0508215102>
 53. Ramachandran PV, Savini M, Follick AK, Hu K (2019) Lysosomal signaling promotes longevity through adjusting mitochondrial activity. *Dev Cell* 48:685–696. <https://doi.org/10.1016/j.devcel.2018.12.022>
 54. Martini-stoica H, Xu Y, Ballabio A et al (2017) The autophagy–lysosomal pathway in neurodegeneration: A TFEB perspective. *Trends Neurosci* 39:221–234. <https://doi.org/10.1016/j.tins.2016.02.002>
 55. Jaber N, Mohd-naim N, Wang Z et al (2016) Vps34 regulates Rab7 and late endocytic trafficking through recruitment of the GTPase activating protein Armus. *J Cell Sci* 129(23):4424–4435. <https://doi.org/10.1242/jcs.192260>

Publisher's Note Springer Nature remains neutral with regard to jurisdictional claims in published maps and institutional affiliations.

RESEARCH

Open Access



TNF- α differentially modulates subunit levels of respiratory electron transport complexes of ER/PR +ve/–ve breast cancer cells to regulate mitochondrial complex activity and tumorigenic potential

Anjali Shinde^{1†}, Hyeryeon Jung^{2†}, Hayun Lee^{2†}, Kritarth Singh^{3†}, Milton Roy¹, Dhruv Gohel¹, Han Byeol Kim², Minal Mane¹, Hitesh Vasiyani¹, Fatema Currim¹, Yu Ri Seo², Seojin Yang², Ara Cho², Eugene C. Yi^{2*} and Rajesh Singh^{1*} 

Abstract

Background: Tumor necrosis factor- α (TNF- α) is an immunostimulatory cytokine that is consistently high in the breast tumor microenvironment (TME); however, its differential role in mitochondrial functions and cell survival in ER/PR +ve and ER/PR –ve breast cancer cells is not well understood.

Methods: In the current study, we investigated TNF- α modulated mitochondrial proteome using high-resolution mass spectrometry and identified the differentially expressed proteins in two different breast cancer cell lines, ER/PR positive cell line; luminal, MCF-7 and ER/PR negative cell line; basal-like, MDA-MB-231 and explored its implication in regulating the tumorigenic potential of breast cancer cells. We also compared the activity of mitochondrial complexes, ATP, and ROS levels between MCF-7 and MDA-MB-231 in the presence of TNF- α . We used Tumor Immune Estimation Resource (TIMER) webserver to analyze the correlation between TNF- α and mitochondrial proteins in basal and luminal breast cancer patients. Kaplan-Meier method was used to analyze the correlation between mitochondrial protein expression and survival of breast cancer patients.

(Continued on next page)

* Correspondence: euyi@snu.ac.kr; singhraj1975@gmail.com

[†]Anjali Shinde, Hyeryeon Jung, Hayun Lee and Kritarth Singh contributed equally to this work.

²Department of Molecular Medicine and Biopharmaceutical Sciences, Graduate School of Convergence Science and Technology, Seoul National University, Seoul 03080, South Korea

¹Department of Bio-Chemistry, Faculty of Science, The Maharaja Sayajirao University of Baroda, Sayajigunj, Vadodara, Gujarat 390002, India
Full list of author information is available at the end of the article



© The Author(s). 2021 **Open Access** This article is licensed under a Creative Commons Attribution 4.0 International License, which permits use, sharing, adaptation, distribution and reproduction in any medium or format, as long as you give appropriate credit to the original author(s) and the source, provide a link to the Creative Commons licence, and indicate if changes were made. The images or other third party material in this article are included in the article's Creative Commons licence, unless indicated otherwise in a credit line to the material. If material is not included in the article's Creative Commons licence and your intended use is not permitted by statutory regulation or exceeds the permitted use, you will need to obtain permission directly from the copyright holder. To view a copy of this licence, visit <http://creativecommons.org/licenses/by/4.0/>. The Creative Commons Public Domain Dedication waiver (<http://creativecommons.org/publicdomain/zero/1.0/>) applies to the data made available in this article, unless otherwise stated in a credit line to the data.

(Continued from previous page)

Results: The proteome analysis revealed that TNF- α differentially altered the level of critical proteins of mitochondrial respiratory chain complexes both in MCF-7 and MDA-MB-231, which correlated with differential assembly and activity of mitochondrial ETC complexes. The inhibition of the glycolytic pathway in the presence of TNF- α showed that glycolysis is indispensable for the proliferation and clonogenic ability of MDA-MB-231 cells (ER/PR -ve) as compared to MCF-7 cells (ER/PR +ve). The TIMER database showed a negative correlation between the expressions of TNF- α and key regulators of mitochondrial OXPHOS complexes in basal breast vs lobular carcinoma. Conversely, patient survival analysis showed an improved relapse-free survival with increased expression of identified proteins of ETC complexes and survival of the breast cancer patients.

Conclusion: The evidence presented in our study convincingly demonstrates that TNF- α regulates the survival and proliferation of aggressive tumor cells by modulating the levels of critical assembly factors and subunits involved in mitochondrial respiratory chain supercomplexes organization and function. This favors the rewiring of mitochondrial metabolism towards anaplerosis to support the survival and proliferation of breast cancer cells. Collectively, the results strongly suggest that TNF- α differentially regulates metabolic adaptation in ER/PR +ve (MCF-7) and ER/PR -ve (MDA-MB-231) cells by modulating the mitochondrial supercomplex assembly and activity.

Keywords: Breast cancer heterogeneity, TNF- α , Mitochondria, Metabolism, Inflammation

Introduction

Breast cancer is still a leading cause of death in women worldwide [1], hence it requires a further understanding of metabolic adaptations of different breast cancer subtypes, for the identification of alternative or novel drug targets. Broadly, breast cancer has been categorized as hormone-responsive ER/PR +ve representing an early benign tumor condition, whereas ER/PR -ve as aggressive and metastasis at a late stage. The tumor microenvironment (TME) of a solid tumor is complex and constitutes many different cell types including the recruitment of circulating monocytes and its differentiation to tumor-associated macrophage (TAM) [2]. The interaction of TAMs and breast cancer cells lead to an inflammatory milieu in TME which reprograms the genetic expression landscape of tumor cells leading to immune evasion and tumor progression. The mechanisms regulating these processes are emerging, however not well understood.

Inflammation in TME enhances tumor growth and metastasis in cancers of different origin like pancreatic, lung, and gastric [3–6] including breast cancer. Inflammation affects all phases of malignancy, including proliferation at the early stage, angiogenesis, progression, and tumor metastasis [7, 8]. The increased levels of several pro-inflammatory cytokines like TNF- α , IL-8, IL-10, and growth factors like TGF- β have been observed in the tumor microenvironment [8–10]. Despite the close association between inflammation and tumorigenesis, the mechanisms underlying the cytokine-mediated metabolic adaptation and its impact on regulating the tumorigenic potential of breast cancer cells is not well understood.

TNF- α is a pleiotropic cytokine and acts as pro- or anti-tumorigenic depending on the type and stage of specific cancer. TNF- α level is high in tumors of

different origin including breast cancer. Moreover, studies in the last decade had shown that mitochondria are emerging as a platform for assembly of the complexes regulating the NF- κ B and IFN pathways, hence innate immunity during viral infections. Previously, we have reported that adaptor proteins like STING and NLRX1 localize to mitochondria and its contact site, which beyond their role in innate immunity, can act as tumor suppressor and modulate mitochondrial functions in the presence of TNF- α [11, 12]. This evidences suggest that mitochondria act as a signaling hub for integrating inflammatory and metabolic cues; however, their role in maintaining cancer cell metabolism and regulating the overall tumor growth within the altered cytokine milieu of a TME, needs to be further investigated. In the current study, we systematically investigated the TNF- α modulated mitochondrial proteome by employing quantitative mass spectrometry. We observed that TNF- α differentially modulate the subunits of oxidative phosphorylation (OXPHOS) complexes and mitochondrial functions to regulate the clonogenic and migration abilities of the breast cancer cells.

Materials and methods

Cell Lines used and the reagents

MCF-7 and MDA-MB-231 cells were cultured in Dulbecco's modified Eagle's medium (DMEM, Life Technologies, Carlsbad, CA, USA) media were supplemented with 10% v/v heat-inactivated fetal bovine serum (Life Technologies) 1% penicillin, streptomycin, and neomycin (PSN) antibiotic mixture (Life Technologies). Human TNF- α (premium grade) was purchased from MiltenylBiotec GmbH, Germany. 2-deoxy-glucose, NAC (N-Acetyl Cysteine) were purchased from Sigma-Aldrich, USA. CM-H₂DCFDA and MitoSOXTM Red were purchased from Molecular Probes Inc., USA.

Mitochondria isolation and quality control

Cells were seeded at 3×10^6 density and after overnight incubation cells were treated as indicated. The cells were collected and passed through 24-G \times 1" syringe 50–60 times using Sucrose-Tris mitochondria isolation buffer (0.25 M Sucrose, 10 mM Tris HCl, and 1X protease inhibitor). After centrifugation at $600\times g$ for 10 min, the supernatant was collected and centrifuged at $8000\times g$. The obtained pellet (mitochondrial fraction) was washed thrice with the isolation buffer and lysed in RIPA lysis buffer. Purity of mitochondrial fraction was checked by western blotting using antibodies against Actin, Tom20, SDHA, and UQCRC2.

Sample preparation and digestion

Isolated mitochondrial fractions were lysed in RIPA lysis buffer (Thermo Scientific, Rockford, IL, USA) with protease inhibitor (Roche Diagnostics, Mannheim, Germany) and phosphatase inhibitor cocktail (Roche Diagnostics), followed by a brief sonication on ice. The cells were sonicated and centrifuged for 15 min at $24,000\times g$ at 4 °C and the supernatant was transferred to a new tube. Protein concentration was determined using BCA assay kit (Thermo Scientific). Protein samples were fractionated on 4–12% Bis-Tris Gels (Invitrogen, Carlsbad, CA, USA) and stained with Coomassie Brilliant Blue (Sigma-Aldrich, St. Louis, MO, USA). Each gel lane was cut into ten pieces and subjected to in-gel tryptic digestion following the general protocol [13]. Briefly, protein bands were excised, destained, washed, and further reduced with 20 mM DTT and alkylated with 55 mM iodoacetamide. After dehydration, the proteins were digested with 13 ng/ml sequencing-grade modified porcine trypsin (Promega, Madison, WI, USA) in 50 mM ammonium bicarbonate overnight at 37 °C. Peptides were extracted from the gel slices in 50% (v/v) ACN and 5% (v/v) formic acid and dried under vacuum.

Mass spectrometry analysis

Peptides were resuspended in 25 μ L Solvent A (0.1% formic acid in water, pH 2.0) and 5 μ L sample was loaded onto an analytic column (PepMap, 75 μ m ID \times 50 cm 3 μ m, ES803, Thermo Fisher Scientific, San Jose, CA, USA) interfaced with a nano-ultra-HPLC system (EasynLC, Thermo Fisher Scientific) and separated with a linear gradient of 5–32% Solvent B (0.1% formic acid in ACN), time (B%) 0~12 min (5% solvent B), 97 (40%), 105 (70%), 117 (70%), and 120 (2%), for 120 min at a flow rate 300 nL/min. MS spectra were recorded on a Q-Exactive Orbitrap mass spectrometer (Thermo Fisher Scientific). The standard mass spectrometric condition of the spray voltage was set to 2.2 kV and the temperature of the heated capillary was set to 250 °C. The full MS scans were acquired in the mass analyzer at

400–1400 m/z with a resolution of 70,000 and the MS/MS scans were obtained with a resolution of 17,500 by normalized collision energy of 27 eV for high-energy collisional dissociation fragmentation. The automatic gain control target was 1×10^5 , the maximum injection time was 120 ms, and the isolation window was set to 2.0 m/z. The Q-Exactive was operated in a data-dependent mode with one survey MS scan followed by ten MS/MS scans, and the duration time of dynamic exclusion was 20 s.

Database search

Collected MS/MS data were searched against the decoy UniProt human database (version 3.83, 186 578 entries) by Proteome Discoverer 2.2 (PD 2.2, Thermo Scientific) software. Precursor and fragment ion tolerance were set to 10 ppm and 0.5 Da, respectively. Trypsin was chosen as the enzyme with a maximum allowance of up to two missed cleavages. Carbamidomethyl (+ 57.02) of cysteine was considered as the fixed modification, while the variable modification was set for methionine oxidation (+ 15.99). The result filtration parameters of PD 2.2 were set as follows: peptide and protein identifications were accepted if they could be established at greater than 95% and 99% probability, respectively, as specified by the Peptide and Protein Prophet algorithm and if the protein identification contained at least two identified peptides with a false discovery rate \leq 0.1%.

Relative protein quantification and bioinformatics analysis

Relative protein quantitation was accomplished using spectral counting. The MS/MS data were normalized to compare the abundances of proteins between samples using PD 2.2 software. The normalized spectral counts from triplicate analyses of the MCF-7 and MDA-MB-231 cells treated or untreated with TNF- α were compared using the R program [14] with power-law global error model (PLGEM; version 1.50.0) software used to determine signal-to-noise ratio and *P*-value [15, 16]. We filtered statistically significant differentially expressed proteins (DEPs) using 0.01 as a *p*-value threshold. Then we refined spectral count readouts for the proteins within the range of $0.01 \leq p\text{-value} \leq 0.05$ using the Moment Adjusted Imputation (MAI) equation [17] to identify DEPs with statistical significance with more sensitivity. After the MAI refinements, we have determined the *p*-value with PLGEM and filtered statistically significant DEPs using 0.01 as a *p*-value threshold. The subcellular localization and functional annotation of the identified proteins were classified using Ingenuity Pathway Analysis (IPA, QIAGEN Inc., Valencia, CA, US) and Protein Analysis through Evolutionary Relationships Classification System (PANTHER, version 7.2.) [18].

Kaplan-Meier survival analysis was used to estimate the association of the gene's expression with survival of patients.

BN-PAGE

MCF7 and MDA-MB231 cells were seeded at density $3 \times 10^6/100$ mm dish. After overnight incubation cells were treated as required. Mitochondria from MCF-7 and MDA-MB231 cells were isolated in Tris-Sucrose buffer as described above and 50 μ g pellets were solubilized as per manufacturer's protocol (Thermo Fisher Scientific) and BN-PAGE was performed on Native PAGE Novex3%–12% Bis-Tris Protein Gels (ThermoFisher Scientific). In-gel enzyme activity of different OXPHOS complexes was analyzed on gradient Bis-Tris gel.

Substrate: for complex I, 1 mg NADH and 25 mg NTB was prepared in 2 mM Tris-HCl (pH 7.4), and for complex IV, 5 mg DAB and 10 mg cytochrome C in 50 mM potassium phosphate buffer (pH 7.4) was used for in-gel activity. For complex III and complex IV combined, 10 mg 3,3'-diaminobenzidine tetrachloride (DAB) and 25 mg cytochrome C in 25 ml of 50 mM sodium phosphate buffer (pH 7.2) was used.

Spectrophotometric analysis of mitochondrial complex I and complex II assays

MCF-7 and MDA-MB-231 cells were seeded at the density of 5×10^5 cells/well in the 6-well plate. The cells were treated as indicated, harvested, and washed with cold DPBS. The cells were subjected to 2–3 freeze-thaw cycles in a freeze-thaw complete solution (0.25 M sucrose, 20 mM Tris-HCl (pH 7.4), 40 mM KCl, 2 mM EDTA supplemented with 1 mg/ml fatty acid-free BSA, 0.01% Digitonin and 10% Percoll). The cells were washed again with the freeze-thaw solution devoid of digitonin and resuspended in complex I assay buffer (35 mM potassium phosphate (pH 7.4), 1 mM EDTA, 2.5 mM NaN_3 , 1 mg/ml BSA, 2 μ g/ml antimycin A, 5 mM NADH). Complex I activity was measured by monitoring the decrease in absorbance at 340 nm after the addition of 2.5 mM acceptor decylubiquinone indicating the oxidation of NADH.

Similarly, for complex II activity, cells were seeded at a density of $1.5 \times 10^6/60$ mm dish. The cells were harvested and washed with cold DPBS. The cells were suspended in 0.5 ml of 20 mM hypotonic potassium phosphate buffer (pH 7.5) and lysed using a 24-G sterile syringe and subjected to freeze-thaw cycle. The cell lysate (80 μ g) was added to the 1 ml of complex II assay buffer (0.1 M potassium phosphate (pH 7.5), 50 mg/ml BSA, 100 mM NaN_3 , 200 mM succinate) and incubated at 37 °C. Complex II activity was measured for 6 min by monitoring the decrease in absorbance at 600 nm after the addition of 2.5 mM acceptor decylubiquinone and DCPIP.

ATP assay

MCF-7 and MDA-MB-231 cells were seeded in a density of 5×10^4 in 24 well plates. ATP levels were measured in control and treatment conditions by an ATP dependent luciferase assay using an ATP determination kit (Molecular Probes/Life Technologies, ON, Canada).

Assay of intracellular and mitochondrial ROS

ROS levels and mitochondrial ROS were measured by CM-H₂DCFDA (10 μ M) and MitoSOXTM Red (5 μ M) staining, respectively. Briefly, MCF-7 and MDA-MB-231 cells were plated at the density of 1.5×10^5 cells/well in 24-well plates. The cells were treated and stained with indicated reagent and monitored under a fluorescence microscope (Olympus IX81 microscope; Olympus, Tokyo, Japan). A minimum of 5 images and 80–100 cells were used for analysis.

ROS levels were also quantified by fluorometry. Briefly, MCF-7 and MDA-MB231 cells were treated and stained with CM-H₂DCFDA (12.5 μ M) in DPBS for intracellular ROS quantification and MitoSOX Red (2.5 μ M) in DMEM for mitochondrial ROS quantification. The cells were washed with DPBS and normalized to 1×10^6 cells/ml. Fluorescence intensity was quantified by a fluorometer (Hitachi High-Technologies Corp., Japan) with excitation/emission at 495/520–540 nm and 510/570–600 nm, respectively.

MTT assay

MCF-7 and MDA-MB-231 cells were seeded (5000 cells/well) in 96-well plate. The cells were treated as indicated and cell viability was determined using the standard MTT [3-(4,5-dimethylthiazol-2-yl)-2,5-diphenyltetrazoliumbromide] assay. The purple formazan crystals were dissolved in DMSO, transferred in a 96-well plate (100 μ L/well) and the absorbance was recorded on a microplate reader at a wavelength of 570 nm.

Clonogenic assay

MCF-7 and MDA-MB-231 cells (2000 cells/well) were seeded in 6 well plates and treated as per requirements. Cells were incubated till single clones were visible and later were fixed using methanol and stained using 0.2% crystal violet as described earlier [19].

Survival analysis

BRCA patients in The Cancer Genome Atlas (TCGA) database were ranked by the level of NDUFB1, SDHA, and COX7C expression and divided into two groups: top quarter and low quarter in expression level. These groups were analyzed in Kaplan-Meier survival plot to estimate the correlation between the gene's expression level and survival of patients using OncoLnc [20].

Scratch assay

Scratch assay was performed in MCF-7 and MDA-MB-231 cells. Cells were seeded at a density of 2.5×10^5 cells per well in 12 well plates. After overnight incubation cells were treated and a vertical wound was created using a sterile P200 micropipette tip. At zero time point, images of each scratch were taken using Nikon Ti-2 eclipse inverted fluorescent microscope at $\times 10$ and were analyzed after 24 h of treatment. Migration rate was measured using ImageJ software which measures open area at a different time interval. The percentage of open area in each condition was plotted.

Statistical analysis

Data are expressed as mean \pm SEM of two or three independent experiments. Unpaired two-tailed Student's

t-test was performed. GraphPad Prism was used to perform all statistical analyses.

Results

TNF- α differentially modulates mitochondrial proteome in ER/PR +ve (MCF-7) and ER/PR -ve (MDA-MB-231) breast cancer cells

To identify TNF- α modulated differentially expressed mitochondrial proteins in MCF-7 (ER/PR +ve) and MDA-MB-231 (ER/PR -ve) cells, we performed quantitative proteomic analysis of mitochondrial proteins of both cell lines in the absence and presence of TNF- α . Mitochondrial fractions were prepared from MCF-7 and MDA-MB-231 cells and the purity was assessed by western blotting using selected mitochondrial marker proteins (Tom20, UQCRC2, and SDHA) including nuclei (PARP), cytosol (β -actin) (Fig. 1a). The mitochondrial

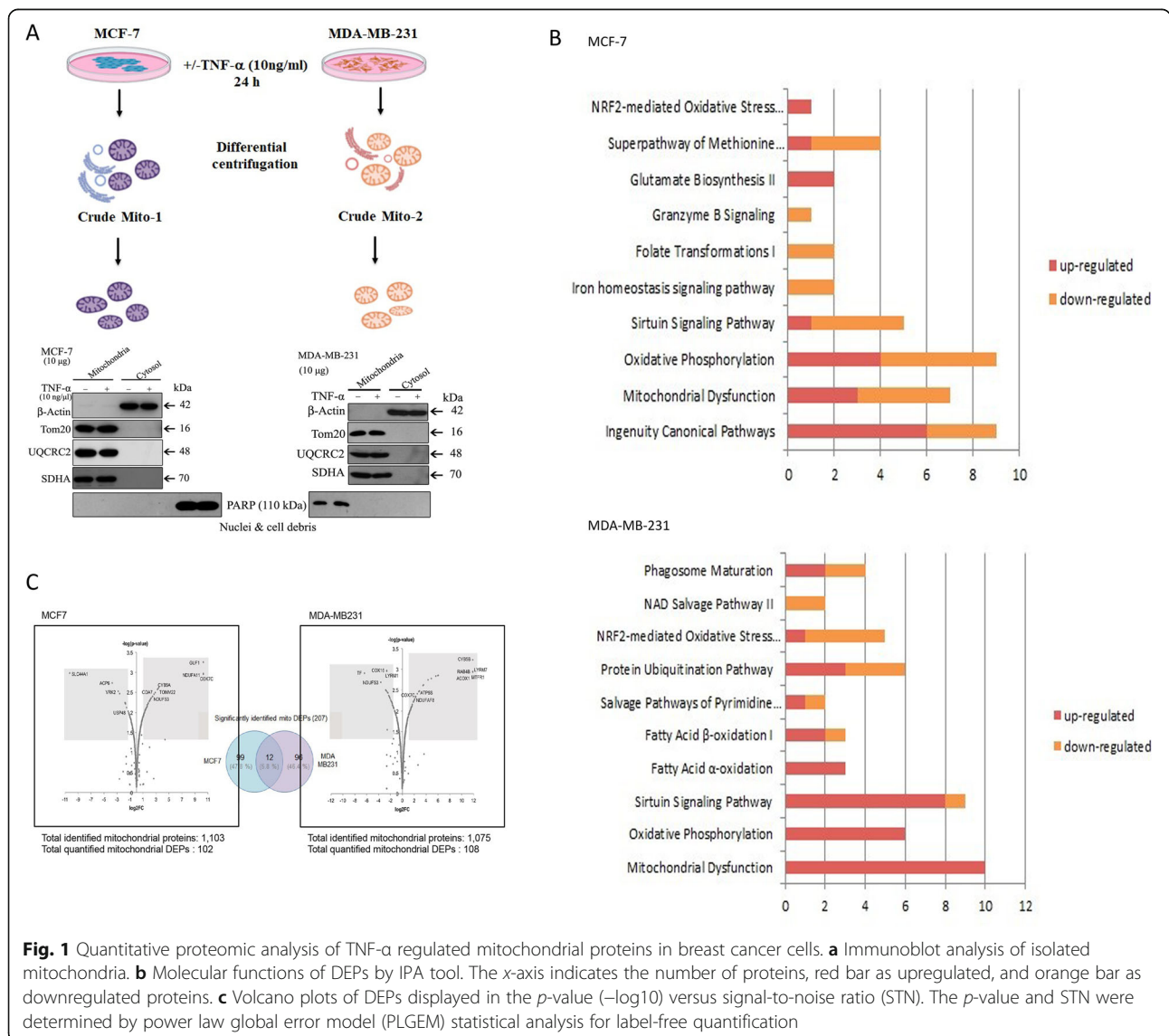


Fig. 1 Quantitative proteomic analysis of TNF- α regulated mitochondrial proteins in breast cancer cells. **a** Immunoblot analysis of isolated mitochondria. **b** Molecular functions of DEPs by IPA tool. The x-axis indicates the number of proteins, red bar as upregulated, and orange bar as downregulated proteins. **c** Volcano plots of DEPs displayed in the *p*-value ($-\log_{10}$) versus signal-to-noise ratio (STN). The *p*-value and STN were determined by power law global error model (PLGEM) statistical analysis for label-free quantification

fraction of both MCF-7 and MDA-MB-231 showed a high level of mitochondrial proteins of TOM20, UQCRC2, and SDHA, whereas PARP, a marker of nuclei, was not detected. LC-MS/MS data of MCF-7 +/- TNF- α and MDA-MB-231 +/- TNF- α were searched against the decoy UniProt human database and identified 1077 and 1150 mitochondrial proteins (peptide probability > 95%; protein probability > 99%) for MCF-7 and MDA-MB-231 cells, respectively. The list of identified mitochondrial proteins were further compared with mitochondrial protein databases; MitoCarta [21] and Gene Ontology [22]. It was observed that 57.5% of proteins overlapped between MDA-MB-231 and MCF-7 cells (Fig. 1c).

The quantitative statistical analysis by integrated PLGE M-STNMAI proteomics of triplicate LC-MS/MS data with the *p*-value threshold 0.01, identified 108 (62 upregulated and 49 downregulated proteins) and 111 (81 upregulated and 27 downregulated proteins) differentially expressed proteins (DEPs) in MCF-7 and MDA-MB-231, respectively (Fig. 1c), in the presence of TNF- α . Ingenuity pathway analysis (IPA) indicated that DEPs were involved in mitochondrial function (20%), Sirtuin Signaling Pathway (18%), oxidative phosphorylation (12%), protein ubiquitination (12%), and NRF2-mediated oxidative stress (10%) in MCF-7 cells. Interestingly, IPA analysis of DEPs in MDA-MB-231, ER/PR (-ve) cell line showed that proteins involved in mitochondrial dysfunction, oxidative phosphorylation, sirtuin signaling, and fatty acid β -oxidation were enriched in the presence of TNF- α as compared to MCF-7 cell lines (Fig. 1b).

The functional annotation of the DEPs of MCF-7 and MDA-MB-231 cell lines using IPA and hierarchical clustering analysis (Mev software) (Supplementary Figure 1A) showed a distinct cluster of genes regulating specific pathways were modulated in the presence of TNF- α . Cluster 1 shows DEPs between MCF-7 and MDA-MB-231 cells in the presence of TNF- α , associated with PPAR α /RXR α activation, pyrimidine deoxyribonucleotides de novo biosynthesis, and salvage pathways of pyrimidine ribonucleotides. Cluster 2 shows that proteins downregulated in MCF-7 and upregulated in MDA-MB-231 cells in the presence of TNF- α , are associated with mitochondrial function, sirtuin signaling pathway, oxidative phosphorylation, oxidative ethanol degradation, fatty acid α -oxidation, TCA cycle, and glutamate biosynthesis. The results here suggest that the TNF- α differentially modulates mitochondrial proteome in both ER/PR +ve (MCF-7) and ER/PR -ve (MDA-MB-231) cells.

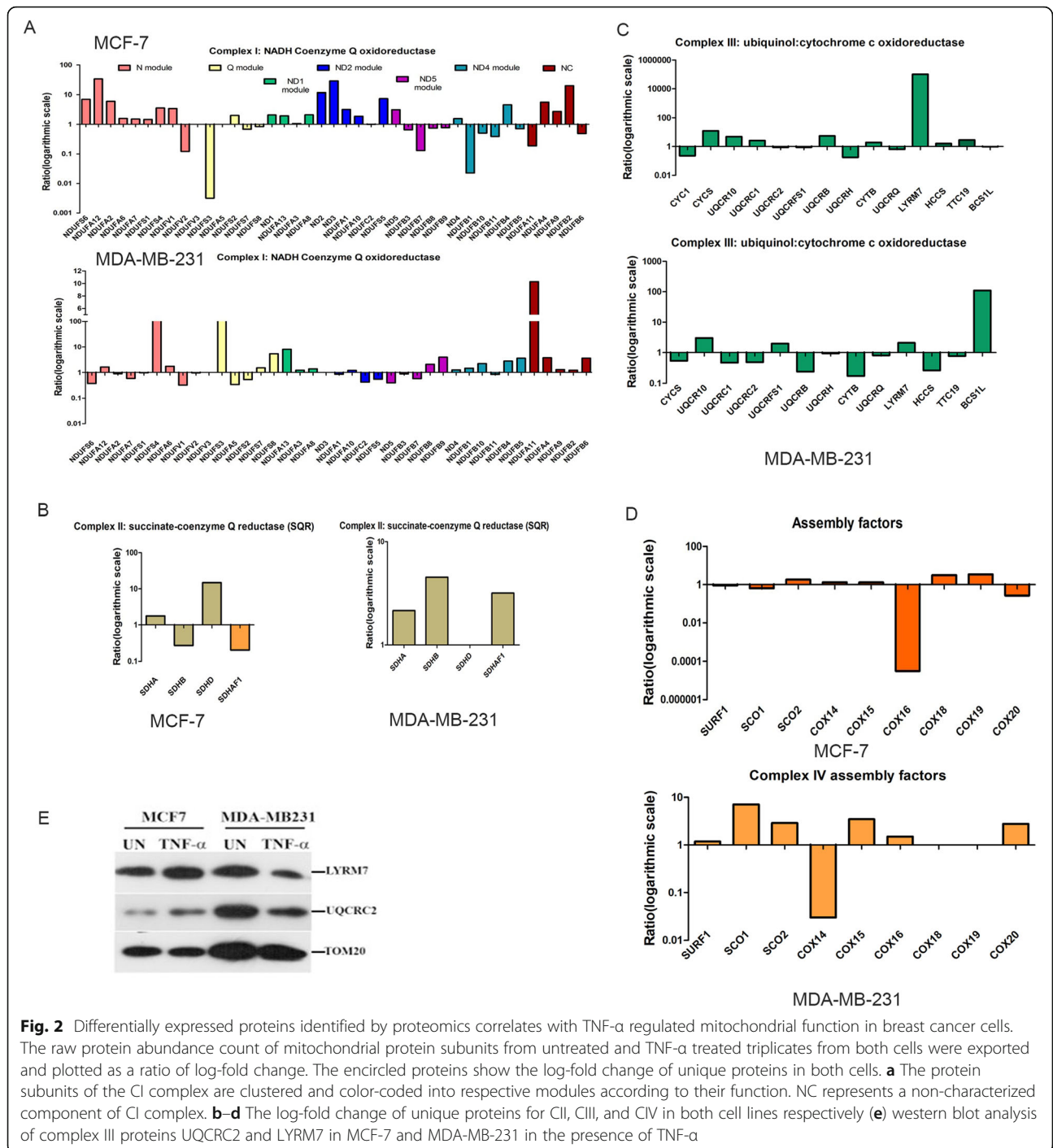
TNF- α differentially regulates the level of critical proteins involved in mitochondrial ETC complex assembly

The remodeling of electron transport chain complexes assembly and/or activity is important for the bioenergetic

adaptation in cancer cells; hence, we focused specifically on the individual protein constituents of each respiratory complex. All the known subunits of electron transport chain (ETC) complexes including complex I, II, III, and IV were analyzed both in MCF-7 and MDA-MB-231 in the presence of TNF- α . The levels of NDUFS3 (a N module component) and NDUFBI (the component of ND4 module) significantly decreased in MCF-7 cells in the presence of TNF- α and, however, increased in MDA-MB-231 (Fig. 2a). The levels of NDUFA11, the matrix-facing subunit of CI increased several folds in MDA-MB-231 cells and decreased in MCF-7 in the presence of TNF- α . This suggests that the levels of mitochondrial complex I proteins are differentially altered in ER/PR +ve(MCF-7) and ER/PR -ve(MDA-MB-231) cells in the presence of TNF- α .

Complex II is the smallest mitochondrial complex and unique as it forms a part of the TCA cycle as well as a part of ETC hence directly linking metabolism and oxidative phosphorylation; we, therefore, analyzed the levels of complex II subunits in MCF-7 and MDA-MB-231 cells in the presence of TNF- α . MCF-7 showed increased levels of SDHD subunit whereas other subunits SDHA and the assembly factor, SDHAF1, decreased in the presence of TNF- α (Fig. 2b). MDA-MB-231 cells treated with TNF- α showed no change in SDHD level whereas the level of SDHA and SDHB increased in mitochondria. The level of SDHAF1 was significantly high in mitochondria of TNF- α treated MDA-MB-231 cells as compared to MCF-7.

Mitochondrial complex III is an important complex as it accepts electrons both from complex I and complex II via the acceptor, ubiquinone. The alteration of complex III may lead to oxidative stress and accumulation of oncometabolite leading to increased cell proliferation [23]. We further analyzed the level of complex III subunits from the mitochondrial proteome of both MCF-7 and MDA-MB-231 cells in the presence of TNF- α . Levels of most subunits of complex III remained same both in MCF-7 and MDA-MB-231 in the presence of TNF- α . Interestingly, LYRM7, a protein having the LYR (Leucine, Tyrosine, Arginine) consensus sequence binds to HSC20 and facilitate incorporation of Fe-S cluster into UQCRC1 in complex III [24, 25] during assembly of the respiratory chain showed altered levels in both cell lines. The level of LYRM7 significantly increased in MCF-7 in the presence of TNF- α as compared to MDA-MB-231 (Fig. 2c). To confirm this, the expression levels of LYRM7 levels were also analyzed by western blotting. LYRM7 protein levels also increased in mitochondrial fraction of TNF- α treated MCF-7 cells whereas decreased in MDA-MB-231 cells (Fig. 2e). UQCRC2, a complex III subunit also decreased in TNF- α treated MDA-MB-231 mitochondrial fraction and correlated



with proteomics data (Fig. 2e). Similarly, BCS1L, a 419-amino-acid chaperone protein, is a member of the family called AAA; is localized in the inner membrane of the mitochondria; and is presumed to facilitate the insertion of Rieske Fe/S protein into precursors to complex III [26]. We also analyzed the level BCS1L in mitochondrial proteome and observed increased levels in mitochondria

of MDA-MB-231 cells in the presence of TNF- α whereas remained unchanged in MCF-7 cells.

Complex IV subunit levels were also analyzed in mitochondrial fraction of both MCF-7 and MDA-MB-231. We did not observe any significant changes in the levels of different cytochrome-c oxidase (COX) complex subunits. However, interestingly the assembly factors

required for the complex IV biogenesis were differentially regulated in the presence of TNF- α in the breast cancer cells. COX14 assembly factor plays an important role in the translation of the COX1, the main constituent of complex IV [27]. Its abundance decreased significantly in the mitochondria of MDA-MB-231 as compared to MCF-7 in the presence of TNF- α (Fig. 2d). Similarly, another assembly factor, COX16, was downregulated in MCF-7 cells as compared to MDA-MB-231. Altogether, the above evidence from quantitative mitochondrial proteomics and immunoblotting suggests that protein levels of specific subunits of mitochondrial ETC complexes are differentially regulated (Supplementary figure 2) which may, in turn, modulate the assembly and/or activity in the presence of TNF- α .

TNF- α differentially regulates mitochondrial supercomplex assembly and activity in ER/PR +ve (MCF-7) and ER/PR -ve (MDA-MB-231) breast cancer cells

To understand the implication of TNF- α modulated subunits of mitochondrial ETC complexes, we analyzed the organization and activity of ETC complexes from both MCF-7 and MDA-MB-231 cells in the presence/absence of TNF- α using Blue native-PAGE. We observed that TNF- α decreased the levels, as well as the activity of supercomplex (SC) containing complex I and complex IV in both the cell line; however, this decrease was significantly higher in MDA-MB-231 cells in the presence of TNF- α (Fig. 3a). A significant decrease in individual complex III activity was observed in MDA-MB-231 in the presence of TNF- α compared to MCF-7 (Fig. 3b). To further quantify the enzyme kinetics of individual ETC complexes, we monitored the specific activity of complex I and complex II using the spectrophotometric assay in MCF-7 and MDA-MB-231 cells in the presence of TNF- α either alone or combination with 2-deoxyglucose (2-DG). 2-DG, the glucose analog, inhibits glycolysis and decreases the growth of tumor cells, which are primarily dependent on the glycolytic pathway. Complex I activity significantly decreased in the presence of TNF- α in MDA-MB-231 as compared to MCF-7 cells. The inhibition of glycolysis with either 2DG alone or in combination with TNF- α increased complex I activity in MCF-7 cells. On the other hand, the activity of complex I decreased significantly upon inhibition of glycolysis by 2-DG in MDA-MB-231 but remained unchanged in the presence of both 2-DG and TNF- α (Fig. 3b). These results suggest that TNF- α negatively regulates complex I activity in MDA-MB-231 cells which depends on glycolysis to maintain its activity in contrast to MCF-7.

The measurement of complex II activity revealed no significant changes either in MCF-7 or MDA-MB-231 in the presence of TNF- α . However, treatment with 2-DG alone or in combination with TNF- α significantly

increased complex II activity in MDA-MB-231 suggesting a compensatory response by complex II to maintain the overall ETC function during glycolytic inhibition. Altogether, these results indicate that TNF- α modulates the levels of critical components of complex I, complex III, and complex IV, hence differentially regulate the organization and activity of ETC complexes in MDA-MB-231 cells (ER/PR -ve) and MCF-7 cells (ER/PR +ve) in the presence of TNF- α .

TNF- α downregulates ATP levels and enhances ROS generation in triple-negative MDA-MB-231 cells

To investigate the effect of TNF- α regulated ETC complexes assembly/activity on the mitochondrial bioenergetic status of both the cells, we analyzed the level of ATP and ROS in the presence/absence of TNF- α . In accordance with the above results, TNF- α treatment significantly decreased both total cellular and mitochondrial ATP level in MDA-MB-231 cells but not in MCF-7 cells. MCF-7 cells cultured in the presence of 2-DG in the presence/absence of TNF- α showed a significant decrease in total ATP levels; however, the mitochondrial ATP levels increased significantly under all treatment conditions suggesting an upregulated ETC function (Fig. 4a, b). In contrast, MDA-MB-231 cells displayed increased sensitivity to a decrease in both mitochondrial and total cellular ATP levels in the presence of TNF- α with or without 2-DG (Fig. 4a, b). This result suggested that MDA-MB-231 cells are strongly dependent on the glucose-pyruvate axis for substrate oxidation and ATP generation by OXPHOS, which is altered in the presence of TNF- α . Similarly, both intracellular and mitochondrial ROS levels significantly increased in both cell lines however MDA-MB-231 cells displayed an enhanced ROS generation in the presence of TNF- α (Fig. 4c) as compared to MCF-7. Altogether, these results strongly suggest that TNF- α alters the mitochondrial bioenergetic status of MDA-MB-231 cells by negatively regulating the ETC complexes activity leading to a decrease in ATP levels and increased ROS generation.

TNF- α modulated mitochondrial functions differentially regulate migration and clonogenic ability of breast cancer cells

To further investigate the role of TNF- α modulated mitochondrial OXPHOS complex activity in regulating tumorigenic potential of ER/PR +ve: MCF-7 and ER/PR-ve: MDA-MB-231 cells, we analyzed the clonogenic ability in the presence/absence of TNF- α . Interestingly, TNF- α inhibits the clonogenic ability of MCF-7 cells whereas enhances clonogenicity of MDA-MB-231 cells (Fig. 5b). The addition of 2DG in the presence of TNF- α further reduced clonogenic ability of the MDA-MB-231 cells suggesting the glycolysis is essential for MDA-MB-

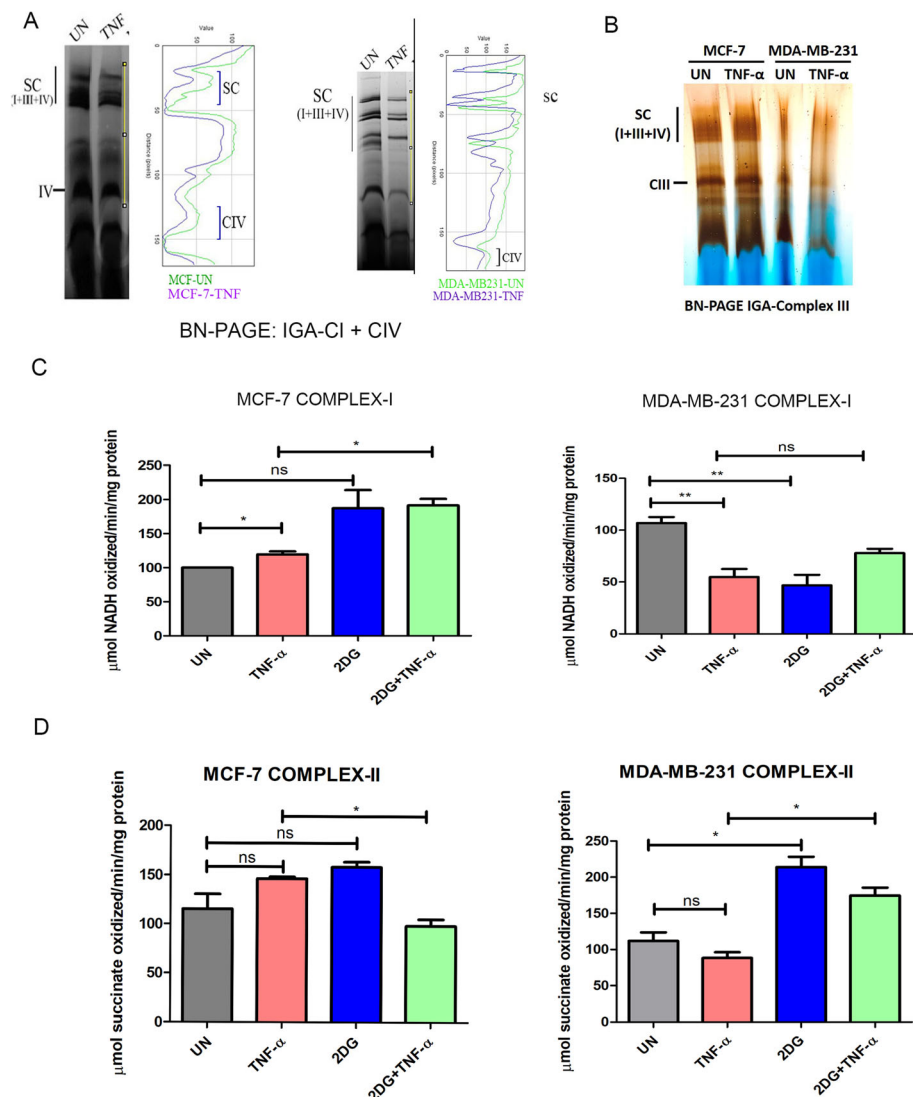


Fig. 3 TNF- α alters the OXPHOS assembly and activity in breast cancer cells. **a** MCF-7 and MDA-MB-231 cells were treated with TNF- α (10 ng/ μ l) for 24 h. After treatment, the mitochondrial fraction was isolated and further analyzed by BN-PAGE, and in-gel enzyme staining for CI and CIV was performed. **b** Complex III in-gel activity was analyzed by BN-PAGE and enzyme staining. **c, d** MCF-7 and MDA-MB-231 cells were treated with TNF- α (10 ng/ μ l) and 2-DG (10 mM) either alone or in combination for 24 h and complex I and complex II activity was measured spectrophotometrically

231 cells. The rescue of clonogenicity was observed in the presence of NAC (N-Acetyl cysteine), a ROS scavenger in MDA-MB-231 cells, whereas it was not observed in the MCF-7 cells. Previously, it had been observed that electron acceptors are limited to drive ETC and other anaplerotic reactions in cancer cells (TCA in cancer); hence, we monitored the clonogenic ability in the presence of pyruvate. The presence of pyruvate can rescue clonogenic ability in the presence of TNF- α in MCF-7 (Fig. 5c). Interestingly, there was no major change in pyruvate stimulated clonogenic ability of MDA-MB-231 cells in the presence of TNF- α . We also checked the migration ability of both cells in the presence of TNF- α

and observed that TNF- α enhanced the migration ability of MDA-MB-231 cells as compared to MCF-7 (Fig. 5a). This is further supported by the increase in the number of colony-forming units in culture medium supplemented with pyruvate. This suggests that it is not ROS but electron acceptor ability that maintains the ratio of NAD/NADH in the cell to drive the TCA cycle and glycolysis in MCF-7, whereas pyruvate, the electron acceptor, is not the limiting factor [28, 29].

Hemin is known to degrade BTB and CNC homology1 (BACH1), a haem binding transcription factor that is increased in TNBC tumors and enhance mitochondrial respiratory activity[30]. To further confirm the reliance of

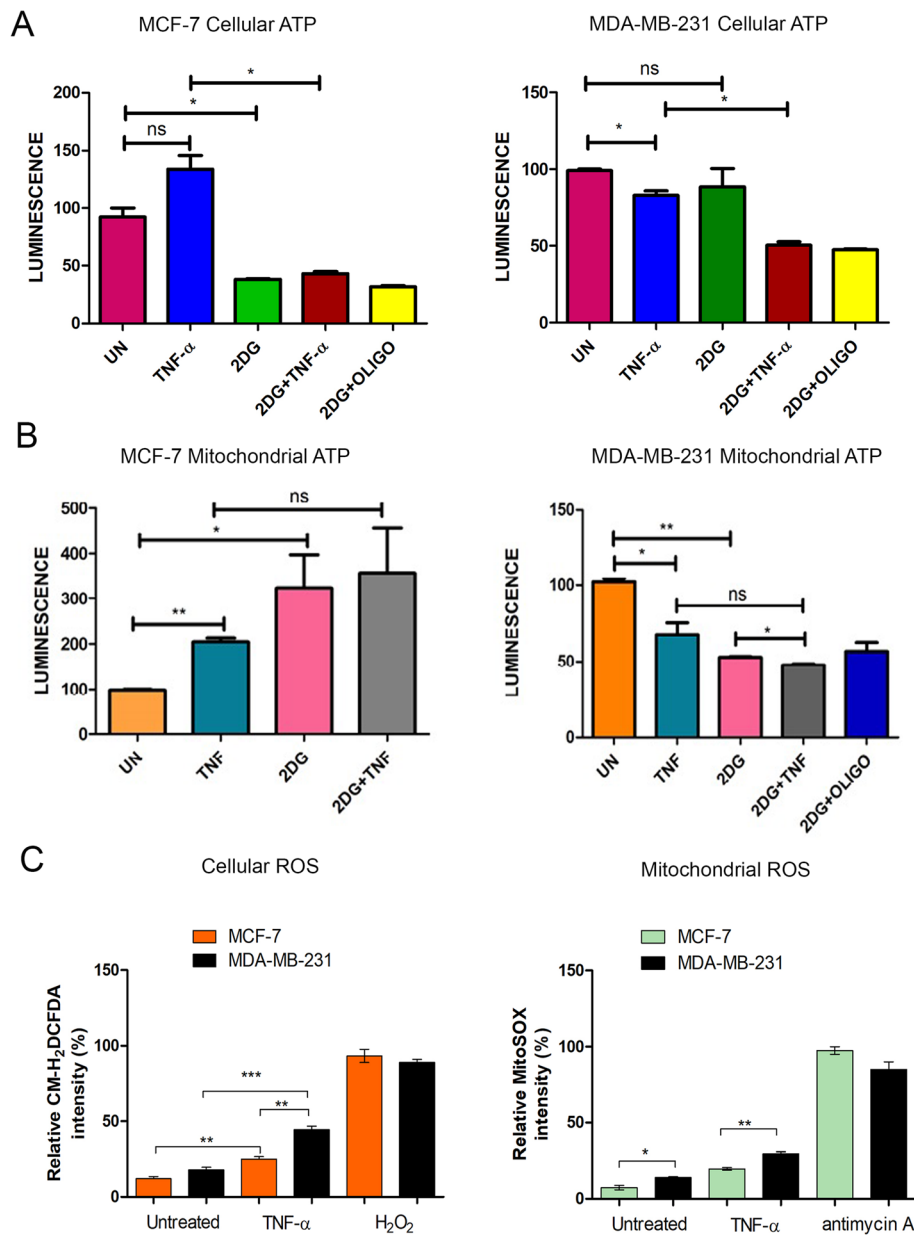


Fig. 4 TNF- α decreases ATP levels and increases ROS generation in MDA-MB-231 cells. **a** MCF-7 and MDA-MB-231 cells were treated with TNF- α either alone or in combination with 2-DG (10 mM) and the total steady-state ATP levels were determined by the luciferase-based assay as described in methodology. **b** As in **a**, mitochondria from respective cells were isolated upon treatment and ATP levels were measured. Oligomycin (5 μ g) treatment for 20 min was used as a positive control. **c** MCF-7 and MDA-MB-231 cells were treated with TNF- α . After treatment, the cells were stained with fluorogenic ROS-sensitive dye and relative fluorescence was monitored as described in methodology. H₂O₂ (100 μ M) and antimycin A (10 μ g) treatment for 2 h were used as a positive control

MDA-MB-231 on OXPHOS activity, we checked for cell viability of MDA-MB-231 in the presence of TNF- α in combination with Hemin. We observed that the cell viability of MDA-MB-231 cells significantly decreased in the presence of TNF- α and Hemin (Fig. 5d). This suggests that enhancing the mitochondrial proteins and functions in MDA-MB-231 cells in the presence of

TNF- α can inhibit the triple-negative breast cancer cell survival.

Subunit of mitochondrial complexes negatively correlates with survival of the breast cancer patients

The TIMER database is a web resource used for systemic analysis and evaluation of clinical impacts of

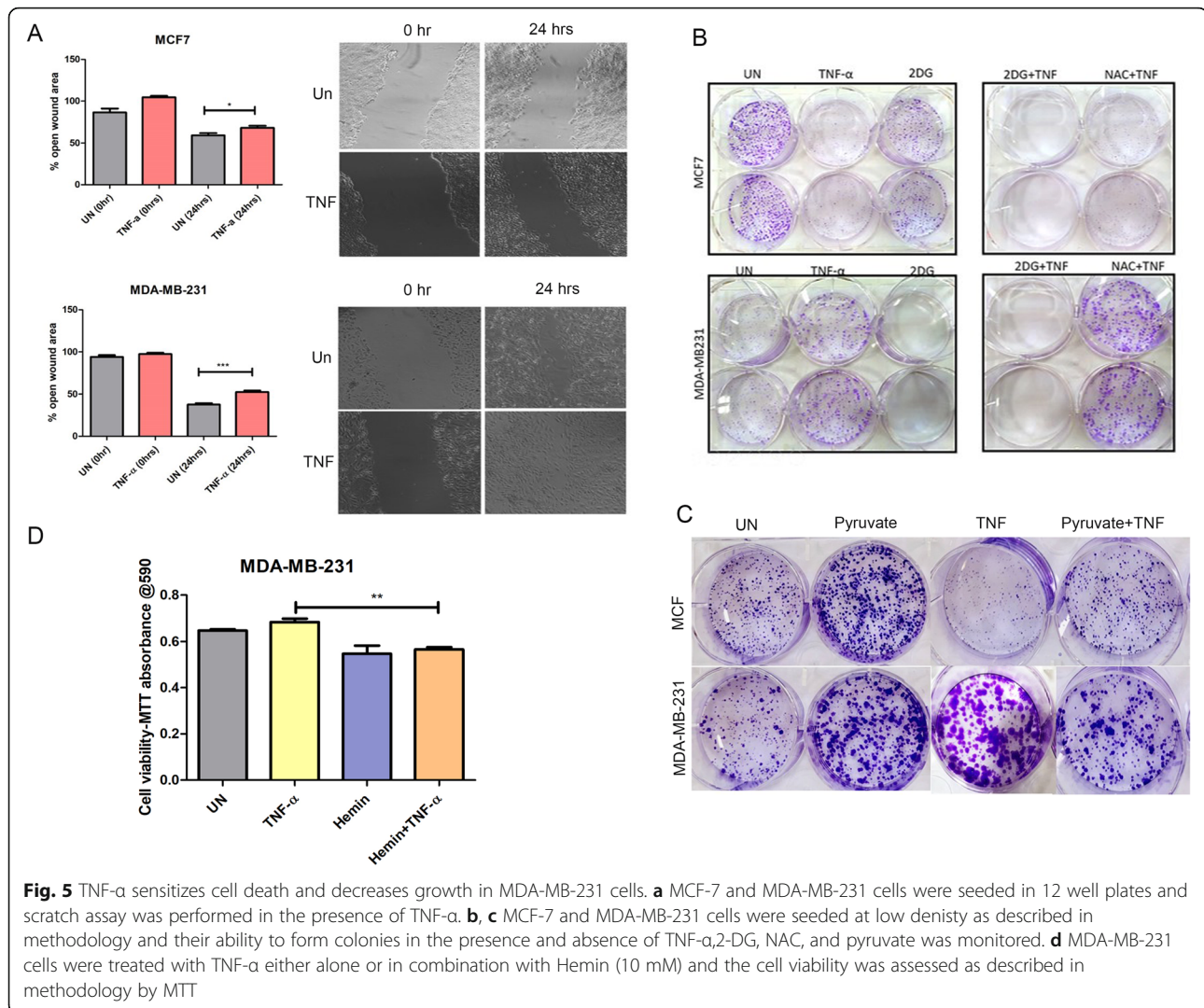


Fig. 5 TNF- α sensitizes cell death and decreases growth in MDA-MB-231 cells. **a** MCF-7 and MDA-MB-231 cells were seeded in 12 well plates and scratch assay was performed in the presence of TNF- α . **b, c** MCF-7 and MDA-MB-231 cells were seeded at low density as described in methodology and their ability to form colonies in the presence and absence of TNF- α , 2-DG, NAC, and pyruvate was monitored. **d** MDA-MB-231 cells were treated with TNF- α either alone or in combination with Hemin (10 mM) and the cell viability was assessed as described in methodology by MTT

different immune factors in diverse cancer types hence we analyzed the correlation between TNF- α and the expression level of identified DEPs. The TIMER data showed that increased expression of TNF- α in basal breast cancer patients is associated with decreased gene expression of subunits of mitochondrial complex I. This negative correlation between TNF- α and complex I subunits is significantly higher in basal breast cancer patients (Fig. 6a) and no significant correlation in luminal breast cancer patients was observed. CIII subunits like UQCR10, UQCRB, and UQCRQ expression were also altered in basal breast cancer patients which showed a significant negative correlation with TNF- α expression as compared to luminal breast cancer patients (Fig. 6b).

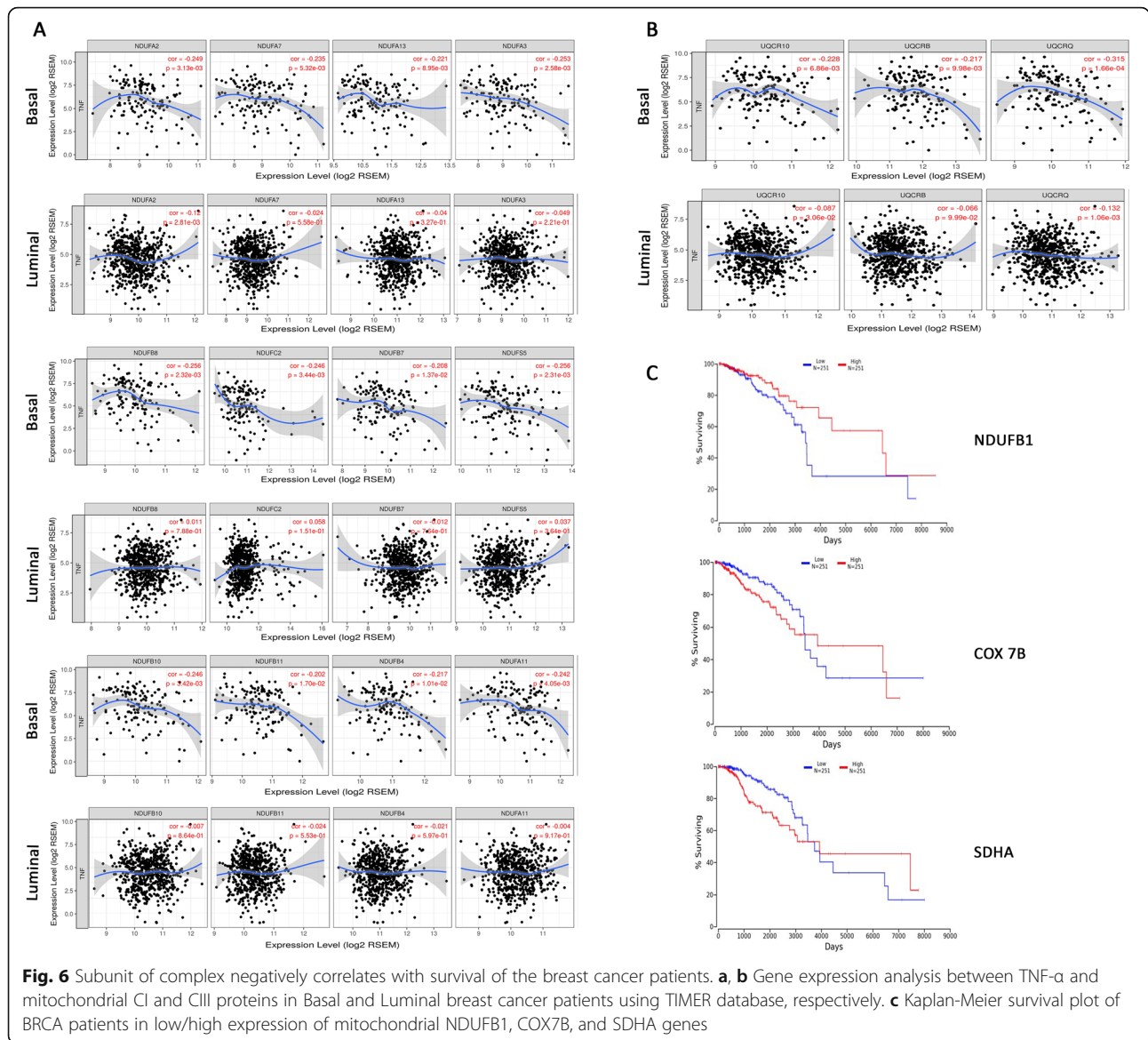
We also checked the survivability of breast cancer patients using the Kaplan-Meier survival plot analysis. The high expression of subunits of mitochondrial complexes like NDUFB1 ($p = 0.052$), SDHA ($p = 0.011$), and COX7B

($p = 0.064$) showed an increased percentage of survival and an increased number of survival days (Fig. 6c).

These evidence strongly suggest that TNF- α differentially regulates the mitochondrial subunits in luminal and basal breast cancer patients and determine the survival rate and span of the breast cancer patients.

Discussion

Increased level of cytokines in TME of solid tumors may modulate mitochondrial function for metabolic adaptation; however, its systemic role in the regulation of mitochondrial proteome and OXPHOS assembly is not well understood. The regulation of TNF- α mediated mitochondrial complex assembly and its role in the regulation of tumorigenic potential of different breast cancer cell types had not been systemically investigated. To understand the differential regulation, we here systemically characterized mitochondrial proteome of



two different cell types MCF-7: ER/PR +ve, responsive representing early tumor conditions, and MDA-MB-231 cells: ER/PR -ve representing aggressive and metastatic conditions tumor cell types. There is no systemic study monitoring the mitochondrial proteome in different breast cancer cells which determines differential metabolic adaptations in TME. There are some previous reports where TRAIL, a member of the TNF- α family, modulated total cellular proteome had been analyzed [31]; however, total cellular proteome truly does not reflect mitochondrial proteins [32]. Hence, it is important to understand the TNF- α modulated mitochondrial proteome to understand the differential mitochondrial role in driving the tumor characteristic and heterogeneity.

The high-resolution proteomics clearly showed that TNF- α differentially modulates mitochondrial proteome of MDA-MB-231 and MCF-7 cells leading to differential mitochondrial function and OXPHOS capacity. Other pathways that are differentially regulated in the presence of TNF- α like sirtuin pathways and iron homeostasis in MCF-7 and MDA-MB-231 cells also regulate mitochondrial functions; however, this can be a topic of further investigation. The study further focused on the assembly of mitochondrial respiratory chain complexes which are differentially regulated in MCF-7 and MDA-MB-231 cells. The level of mitochondrial DNA encoded transcripts specifically ND2 and ND3 which form part of the core unit of the complex I, increased in MCF-7, whereas

remaining unaltered in MDA-MB-231 cells. The levels of NDUFS3 (N module component) and NDUFB1 (the component of ND4 module) were significantly decreased in MCF-7 cells in the presence of TNF- α but, however, increased in MDA-MB-231 suggesting that TNF- α can differentially modulate the complex I activity which is in consonance with in-gel activity and super complex assembly.

Similarly, mitochondrial complex III, which can accept electrons from both complex I and complex II through ubiquinone is critical for mitochondrial function. The study here showed a decrease in complex III activity which correlates with mitochondrial proteomics data. The level of assembly factor LYRM7 decreased in MDA-MB-231 cells compared to MCF-7 cells. Emerging reports suggest that binding of HSC20 (co-chaperone) to the LYR motif of LYRM7 in a pre-assembled UQCRCF1-LYRM7 intermediate in the mitochondrial matrix facilitates Fe-S cluster transfer to UQCRCF1, hence assembly of complex III (Chaperon CI-III). This decrease in LYRM7 in mitochondria of MDA-MB-231 cells strongly suggests that incorporation of Fe-S complexes in mitochondrial electron transport chain may be modulated in mitochondrial complex III. Hence, TNF- α modulates flux of NADH which will shift the TCA cycle intermediates towards anaplerotic reactions in aggressive breast tumor cells (MDA-MB-231). This is further supported by the analysis of clonogenic abilities of the cells in the presence of TNF- α . Interestingly, we observed that TNF- α inhibited the clonogenic ability of MCF-7 cells which is rescued in the presence of pyruvate suggesting that electron acceptors are limiting factor. Pyruvate level can be differentially regulated in MCF-7/MDA-MB-231 cells, which is known to act as an electron acceptor and can determine the cell proliferation. Interestingly, in MDA-MB-231, highly metastatic cells, pyruvate is not a limiting factor as TNF- α reprogrammed the activity of OXPHOS for anaplerotic reaction, as we observed pyruvate supplementation showed no major effect on cell proliferation or clonogenic abilities of the cells. This observation further supported as we observed a high level of pyruvate in MDA-MB-231 cells as compared to MCF-7 cells (unpublished observation).

The decrease in complex I/III activity may increase the level of ROS in triple-negative aggressive breast cancer cells which may act as mitohormetic response rather than cell death. This observation is in consonance with a recent report where it had been observed that an increased level of ROS in selected aggressive breast cancer cells from TNBC patients can induce mitohormetic response in modulating nuclear genes which help to survive in the hostile tumor microenvironment.

The overall decrease in the mitochondrial proteins and complex activity in MDA-MB-231 is supported by a

recent study where BTB and CNC homology1 (BACH1), a haem binding transcription factor increased in tumors from patients with TNBC which negatively regulates transcription of electron transport chain (ETC) genes [30]. It was observed that enhancing the reliance of breast cancer cells to mitochondrial functions by modulating the transcription factor BACH1 using hemin which initiates degradation of BACH1, sensitizes the cancer cells to metformin. In our study, the TIMER webserver showed a negative correlation of CI and CIII subunits with TNF- α in basal breast cancer patients. This correlates with the decrease in complex assembly and activity in MDA-MB-231 in the presence of TNF- α . Further, the survivability of breast cancer patients also correlates with the expression of mitochondrial complexes.

Conclusion

In conclusion, the subcellular proteomics identifies the differential behavior of the ER/PR +ve and ER/PR -ve breast cancer cells in response to TNF- α . The evidences here clearly suggest that TNF- α modulates metabolism differentially in ER/PR +ve and ER/PR -ve breast cancer cells by modulating the levels of critical assembly factors and subunits involved in mitochondrial respiratory chain supercomplexes. TNF- α modulated metabolic reprogramming favors survival and proliferation of more aggressive ER/PR -ve breast cancer cells. This study identified novel assembly factors as possible therapeutic target to prevent the progression of aggressive breast cancer cells hence the survival of the breast cancer patients.

Abbreviations

TME: Tumor microenvironment; TNF- α : Tumor necrosis factor alpha; ER: Estrogen receptor; PR: Progesterone receptor; TAM: Tumor-associated macrophages; OXPHOS: Oxidative phosphorylation; ETC: Electron transport chain; TIMER: Tumor Immune Estimation Resource; ATP: Adenosine triphosphate; ROS: Reactive oxygen species; NAC: N-acetylcysteine; TNBC: Triple-negative breast cancer

Supplementary Information

The online version contains supplementary material available at <https://doi.org/10.1186/s40170-021-00254-9>.

Additional file 1: Figure S1. Proteomic profiling of mitochondrial proteins in MCF-7 and MDA-MB-231 under TNF- α stimulation. (A) Heat map of a hierarchical clustering showing the expression patterns of proteins of the mitochondria. The fold change scale represents a sample of the mean-subtracted average of the regularized log-transformed read counts in each sample. The up-regulated proteins are in red and down-regulated proteins are in green(B) Cellular processes of DEPs by IPA tool. **Figure S2.** Biological network analysis of DEPs. Associations among DEPs are shown by gray lines, which represent direct or indirect interactions. Upregulated proteins are shown in red, and downregulated proteins are shown in green. (A)& (B) DEPs in MCF-7 and MDA-MB-231 in presence of TNF- α respectively.

Acknowledgements

Authors acknowledge the instrumentation facility at the Department of Biochemistry, the M. S. University of Baroda, Vadodara. Kritarth Singh

received a Senior Research Fellowship from the University Grants Commission (UGC), Govt. of India. Dhruv Gohel received Senior Research Fellowship from ICMR, India. Minal Mane received Senior Research Fellowship from CSIR, India. Fatema Currim received fellowship from INSPIRE. We also acknowledge DST FIST for providing an instrumentation facility for the work.

Authors' contributions

R.S. and E.C.Y. conceptualized and designed the experiments, analyzed proteomics data, and wrote the manuscript. A.S., H.L., and K.S. performed the experiments and wrote the manuscript. M.R. helped with data analysis and TIMER data correlation. D.G. helped with mitochondrial experiments. M.M., H.V., and F.C. assisted with in vitro experiments. H.R.J. and Y.S. performed the metabolite extraction, H.B.K., A.C., and S.J.Y. performed targeted metabolomics and analyzed the data. The authors read and approved the final manuscript.

Funding

This work was supported by the Department of Science and Technology, Govt. of India, grant number INT/Korea/P-39 to Prof. Rajesh Singh. Global Infrastructure Program through the NRF funded by the Ministry of Science and ICT (NRF-2017K1A3A1A19071651 to ECY) and National Research Foundation of Korea (NRF) grant funded by the Korean Government (MSIP) (NRF-2016R1A5A1010764 and NRF-2015M3A9B6073835 to ECY) to Prof. Eugene C. Yi.

Availability of data and materials

The datasets used and/or analyzed during the current study are available from the corresponding author on reasonable request.

Declarations

Ethics approval and consent to participate

Not applicable.

Consent for publication

Consent to publish this paper from all the participants is obtained.

Competing interests

The authors declare that they have no competing interests.

Author details

¹Department of Bio-Chemistry, Faculty of Science, The Maharaja Sayajirao University of Baroda, Sayajigunj, Vadodra, Gujarat 390002, India.

²Department of Molecular Medicine and Biopharmaceutical Sciences, Graduate School of Convergence Science and Technology, Seoul National University, Seoul 03080, South Korea. ³Department of Cell and Developmental Biology, University College London, Gower Street, London WC1E 6BT, UK.

Received: 30 September 2020 Accepted: 1 April 2021

Published online: 29 April 2021

References

- Coughlin SS, Ekwueme DU. Breast cancer as a global health concern. *Cancer Epidemiol.* 2009;33(5):315–18.
- Vitale I, Manic G, Coussens LM, Kroemer G, Galluzzi L. Macrophages and metabolism in the tumor microenvironment. *Cell Metab.* 2019;30(1):36–50.
- Padoan A, Plebani M, Basso D. Inflammation and pancreatic cancer: focus on metabolism, cytokines, and immunity. *Int J Mol Sci.* 2019;20(3):676.
- Pierce BL, Ballard-Barbash R, Bernstein L, Baumgartner RN, Neuhaus ML, Wener MH, Ulrich CM. Elevated biomarkers of inflammation are associated with reduced survival among breast cancer patients. *J Clin Oncol.* 2009; 27(21):3437.
- Pullamsetti SS, Kojonazarov B, Storn S, Gall H, Salazar Y, Wolf J, Savai R. Lung cancer-associated pulmonary hypertension: Role of microenvironmental inflammation based on tumor cell-immune cell cross-talk. *Sci Transl Med.* 2017;9(416).
- Qu X, Tang Y, Hua S. "Immunological approaches towards cancer and inflammation: a cross talk," *Front Immunol.* 2018;9:563. <https://doi.org/10.3389/fimmu.2018.00563>.
- Bachelot T, Ray-Coquard I, Menetrier-Caux C, Rastkha M, Duc A, Blay JY. Prognostic value of serum levels of interleukin 6 and of serum and plasma levels of vascular endothelial growth factor in hormone-refractory metastatic breast cancer patients. *British J cancer.* 2003;88(11): 1721–6.
- Ma Y, Ren Y, Dai ZJ, Wu CJ, Ji YH, Xu J. IL-6, IL-8 and TNF- α levels correlate with disease stage in breast cancer patients. *Adv Clin Exp Med.* 2017;26(3): 421–6.
- Mocellin S, Rossi CR, Pilati P, Nitti D. Tumor necrosis factor, cancer and anticancer therapy. *Cytokine Growth Factor Rev.* 2005;16(1):35–53.
- Yu M, Zhou X, Niu L, Lin G, Huang J, Zhou W, Li Z. Targeting transmembrane TNF- α suppresses breast cancer growth. *Cancer Res.* 2013; 73(13):4061–74.
- Bhatelia K, Singh K, Prajapati P, Sripada L, Roy M, Singh R. "MITA modulated autophagy flux promotes cell death in breast cancer cells," *Cell Signal.* 2017; 35:73–83. <https://doi.org/10.1016/j.cellsig.2017.03.024>.
- Singh K, Roy M, Prajapati P, Lipatova A, Sripada L, Gohel D, Singh R. NLRX1 regulates TNF- α -induced mitochondria-lysosomal crosstalk to maintain the invasive and metastatic potential of breast cancer cells. *Biochim Biophys Acta (BBA)-Mol Basis Dis.* 2019;1865(6):1460–76. <https://doi.org/10.1016/j.bbdis.2019.02.018>.
- Rosenfeld J, Capdevielle J, Guillemot JC, Ferrara P. In-gel digestion of proteins for internal sequence analysis after one- or two-dimensional gel electrophoresis. *Anal Biochem.* 1992;203(1):173–9.
- "R: a language and environment for statistical computing." <https://www.gbif.org/tool/81287/r-a-language-and-environment-for-statistical-computing>. Accessed 28 Dec 2020.
- Keller A, Nesvizhskii AI, Kolker E, Aebersold R. Empirical statistical model to estimate the accuracy of peptide identifications made by MS/MS and database search. *Analytical chemistry.* 2002;74(20):5383–92.
- Pavelka N, Fournier ML, Swanson SK, Pelizzola M, Ricciardi-Castagnoli P, Florens L, Washburn MP. Statistical similarities between transcriptomics and quantitative shotgun proteomics data. *Mol Cell Proteomic.* 2008;7(4):631–44.
- Thomas L, Stefanski L, Davidian M. A moment-adjusted imputation method for measurement error models. *Biometrics.* 2011;67(4):1461–70.
- Thomas PD, Campbell MJ, Kejariwal A, Mi H, Karlak B, Daverman R, Narechania A. PANTHER: a library of protein families and subfamilies indexed by function. *Genome Res.* 2003;13(9):2129–41.
- Singh K, Poteryakhina A, Zheltukhin A, Bhatelia K, Prajapati P, Sripada L, Singh R. NLRX1 acts as tumor suppressor by regulating TNF- α induced apoptosis and metabolism in cancer cells. *Biochim Biophys Acta (BBA)-Mol Cell Res.* 2015;1853(5):1073–86. <https://doi.org/10.1016/j.bbamcr.2015.01.016>.
- Anaya J. "OncoLnc: linking TCGA survival data to mRNAs, miRNAs, and lncRNAs," *PeerJ Comp Sci.* 2:e67. <https://doi.org/10.7717/peerj-cs.67>.
- Calvo SE, Clauser KR, Mootha VK. MitoCarta 2: an updated inventory of mammalian mitochondrial proteins. *Nucleic Acid Res.* 2016;44(D1):D1251–7.
- Pagliarini DJ, Calvo SE, Chang B, Sheth SA, Vafai SB, Ong SE, Mootha VK. A mitochondrial protein compendium elucidates complex I disease biology. *Cell.* 2018;134(1):112–23.
- Weinberg SE, Singer BD, Steinert EM, Martinez CA, Mehta MM, Martínez-Reyes I, Chandel NS. Mitochondrial complex III is essential for suppressive function of regulatory T cells. *Nature.* 2019;565(7740):495–9.
- Maio N, Kim KS, Singh A, Rouault TA. A single adaptable cochaperone-scaffold complex delivers nascent iron-sulfur clusters to mammalian respiratory chain complexes I–III. *Cell Metab.* 2014;25(4):945–53.
- Maio N, Singh A, Uhrigshardt H, Saxena N, Tong WH, Rouault TA. Cochaperone binding to LYR motifs confers specificity of iron sulfur cluster delivery. *Cell Metab.* 2014;19(3):445–57.
- Cruciani CM, Hell K, Fölsch H, Neupert W, Stuart RA. Bcs1p, an AAA-family member, is a chaperone for the assembly of the cytochrome bc1 complex. *EMBO J.* 1999;18(19):5226–33.
- Mick DU, Vukotic M, Piechura H, Meyer HE, Warscheid B, Deckers M, Rehling P. Coa3 and Cox14 are essential for negative feedback regulation of COX1 translation in mitochondria. *J Cell Biol.* 2010;191(1):141–54.
- Sullivan LB, Gui DY, Hosios AM, Bush LN, Freinkman E, Vander Heiden MG. Supporting aspartate biosynthesis is an essential function of respiration in proliferating cells. *Cell.* 2015;162(3):552–63.
- Gui DY, Sullivan LB, Luengo A, Hosios AM, Bush LN, Gitego N, Vander Heiden MG. Environment dictates dependence on mitochondrial complex I for NAD⁺ and aspartate production and determines cancer cell sensitivity to metformin. *Cell Metab.* 2016;24(5):716–27.

30. Lee J, Yesilkamal AE, Wynne JP, Frankenberger C, Liu J, Yan J, Rosner MR. Effective breast cancer combination therapy targeting BACH1 and mitochondrial metabolism. *Nature*. 2019;568(7751):254–8.
31. Leong S, et al. "iTRAQ-based proteomic profiling of breast cancer cell response to doxorubicin and TRAIL". *J Proteome Res.*2012;11(7):3561–72. <https://doi.org/10.1021/pr2012335>.
32. Chen A, et al. "Proteomics analysis of myocardial tissues in a mouse model of coronary microembolization,". *Front Physiol*. 2018;9:1–10. <https://doi.org/10.3389/fphys.2018.01318>.

Publisher's Note

Springer Nature remains neutral with regard to jurisdictional claims in published maps and institutional affiliations.

Ready to submit your research? Choose BMC and benefit from:

- fast, convenient online submission
- thorough peer review by experienced researchers in your field
- rapid publication on acceptance
- support for research data, including large and complex data types
- gold Open Access which fosters wider collaboration and increased citations
- maximum visibility for your research: over 100M website views per year

At BMC, research is always in progress.

Learn more biomedcentral.com/submissions



Terms and Conditions

Springer Nature journal content, brought to you courtesy of Springer Nature Customer Service Center GmbH (“Springer Nature”).

Springer Nature supports a reasonable amount of sharing of research papers by authors, subscribers and authorised users (“Users”), for small-scale personal, non-commercial use provided that all copyright, trade and service marks and other proprietary notices are maintained. By accessing, sharing, receiving or otherwise using the Springer Nature journal content you agree to these terms of use (“Terms”). For these purposes, Springer Nature considers academic use (by researchers and students) to be non-commercial.

These Terms are supplementary and will apply in addition to any applicable website terms and conditions, a relevant site licence or a personal subscription. These Terms will prevail over any conflict or ambiguity with regards to the relevant terms, a site licence or a personal subscription (to the extent of the conflict or ambiguity only). For Creative Commons-licensed articles, the terms of the Creative Commons license used will apply.

We collect and use personal data to provide access to the Springer Nature journal content. We may also use these personal data internally within ResearchGate and Springer Nature and as agreed share it, in an anonymised way, for purposes of tracking, analysis and reporting. We will not otherwise disclose your personal data outside the ResearchGate or the Springer Nature group of companies unless we have your permission as detailed in the Privacy Policy.

While Users may use the Springer Nature journal content for small scale, personal non-commercial use, it is important to note that Users may not:

1. use such content for the purpose of providing other users with access on a regular or large scale basis or as a means to circumvent access control;
2. use such content where to do so would be considered a criminal or statutory offence in any jurisdiction, or gives rise to civil liability, or is otherwise unlawful;
3. falsely or misleadingly imply or suggest endorsement, approval, sponsorship, or association unless explicitly agreed to by Springer Nature in writing;
4. use bots or other automated methods to access the content or redirect messages
5. override any security feature or exclusionary protocol; or
6. share the content in order to create substitute for Springer Nature products or services or a systematic database of Springer Nature journal content.

In line with the restriction against commercial use, Springer Nature does not permit the creation of a product or service that creates revenue, royalties, rent or income from our content or its inclusion as part of a paid for service or for other commercial gain. Springer Nature journal content cannot be used for inter-library loans and librarians may not upload Springer Nature journal content on a large scale into their, or any other, institutional repository.

These terms of use are reviewed regularly and may be amended at any time. Springer Nature is not obligated to publish any information or content on this website and may remove it or features or functionality at our sole discretion, at any time with or without notice. Springer Nature may revoke this licence to you at any time and remove access to any copies of the Springer Nature journal content which have been saved.

To the fullest extent permitted by law, Springer Nature makes no warranties, representations or guarantees to Users, either express or implied with respect to the Springer nature journal content and all parties disclaim and waive any implied warranties or warranties imposed by law, including merchantability or fitness for any particular purpose.

Please note that these rights do not automatically extend to content, data or other material published by Springer Nature that may be licensed from third parties.

If you would like to use or distribute our Springer Nature journal content to a wider audience or on a regular basis or in any other manner not expressly permitted by these Terms, please contact Springer Nature at

onlineservice@springernature.com



TNF- α -induced E3 ligase, TRIM15 inhibits TNF- α -regulated NF- κ B pathway by promoting turnover of K63 linked ubiquitination of TAK1

Milton Roy, Kritarth Singh¹, Anjali Shinde, Jyoti Singh, Minal Mane, Sawani Bedekar, Yamini Tailor, Dhruv Gohel, Hitesh Vasiyani, Fatema Currim, Rajesh Singh^{*}

Department of Biochemistry, Faculty of Science, The MS University of Baroda, Vadodara, Gujarat 390002, India

ARTICLE INFO

Keywords:

TNF- α
NF- κ B
TRIM15
TRIM8
Ubiquitination
Functional antagonism

ABSTRACT

Ubiquitin E3-ligases are recruited at different steps of TNF- α -induced NF- κ B activation; however, their role in temporal regulation of the pathway remains elusive. The study systematically identified TRIMs as potential feedback regulators of the TNF- α -induced NF- κ B pathway. We further observed that TRIM15 is “late” response TNF- α -induced gene and inhibits the TNF- α -induced NF- κ B pathway in several human cell lines. TRIM15 promotes turnover of K63-linked ubiquitin chains in a PRY/SPRY domain-dependent manner. TRIM15 interacts with TAK1 and inhibits its K63-linked ubiquitination, thus NF- κ B activity. Further, TRIM15 interacts with TRIM8 and inhibits cytosolic translocation to antagonize TRIM8 modulated NF- κ B. TRIM8 and TRIM15 also show functionally inverse correlation in psoriasis condition. In conclusion, TRIM15 is TNF- α -induced late response gene and inhibits TNF- α induced NF- κ B pathway hence a feedback modulator to keep the proinflammatory NF- κ B pathway under control.

1. Introduction

The NF- κ B family of transcription factors are activated by a range of pathophysiological stimuli including viral and bacterial factors (LPS, dsRNA), antigen receptors, DNA damage, reactive oxygen species (ROS), and cytokines (TNF- α , IL-1), [1–3]. Activated NF- κ B promotes transcription of a several target genes that include growth factors, chemokines, cytokines, immune modulators, regulators of apoptosis, acute response genes, cell adhesion molecules [1,3]. NF- κ B pathway is tightly regulated by post-transcriptional and post-translational regulatory mechanisms, however, its dysregulation leads to prolonged activation of NF- κ B and chronic inflammatory conditions hence critical for organismal survival and fitness [4].

Pleiotropic cytokine TNF- α is an activator of the NF- κ B pathway and inflammation [1,5]. The increased level of TNF- α and persistent activation of proinflammatory NF- κ B is observed in many pathological conditions including cancer [6–9]. TNF- α activated NF- κ B target genes have been classified in ‘early’ ‘mid’ and ‘late’ response genes based on their temporal expression pattern [10]. Some of the early response genes

like NFKBIA (κ B α) and TNFIP3 (A20) act as negative feedback regulators of the pathway and dynamics of gene expression by controlling NF- κ B oscillations [10–12]. The modulation of the NF- κ B pathway by late responsive genes and its implication in feedback regulation to restrict inflammation had not yet been explored.

Ubiquitination plays a critical role in the regulation of TNF- α mediated NF- κ B pathway. cIAP1/2 mediated Lys-63-linked polyubiquitination of RIP1, recruits TAK1 [5,13]. After recruiting TAK1 to the complex, TAK1 is K(Lysine)-63-linked polyubiquitinated and activated to recruit κ B kinase (IKK) complex. Dual phosphorylation of κ B α by IKK complex leads its K48-linked polyubiquitination by SCF ^{β TRCP} ubiquitin ligase complex [5,13] which is degraded through ubiquitin proteasome system (UPS). Removal of K63-linked ubiquitin chains by deubiquitinase (DUB) like A20 and CYLD negatively regulates NF- κ B activation and plays a pivotal role in modulating NF- κ B pathway [4,5,13]. TNF- α stimulation also promotes the expression of several E3 ligases including various TRAFs, cIAPs, and XIAP and most of these modifiers positively regulate the pathway [1]. Surprisingly to date, no TNF- α -induced E3 ligase had been shown regulating the pathway in a

Abbreviations: TNF- α , Tumor necrosis facotr-alpha; TRIMs, Tripartite motif containing proteins; CCLE, Cancer Cell Line Encyclopedia; TRIM8, Tripartite motif containing protein 8; TRIM15, Tripartite motif containing protein 15; Baf-A1, Bafilomycin-A1; UPS, Ubiquitin proteasome system; GEO, Gene Expression Omnibus.

^{*} Corresponding author.

E-mail address: singhraj1975@gmail.com (R. Singh).

¹ Current Affiliation: Department of Cell and Developmental Biology, University College London, Gower Street, London, UK, WC1E 6BT.

<https://doi.org/10.1016/j.cellsig.2021.110210>

Received 19 April 2021; Received in revised form 25 November 2021; Accepted 30 November 2021

Available online 3 December 2021

0898-6568/© 2021 Elsevier Inc. All rights reserved.

negative feedback mechanism.

Ubiquitin E3 ligases identify unique substrates and promote their ubiquitination and topology of the ubiquitin chain assembled on the substrate determines their fate. *Tripartite Motif containing* (TRIM) proteins are RING E3 ligases characterized by the signature motif composed of RING, B-Box, and Coiled-coil domain. They are further subclassified based on the presence of the variable C-terminal domain [14,15]. The roles of these proteins are emerging in innate immune regulation, viral restriction, and autophagy [16,17]. The reports from our group and others had shown that TRIM8 and TRIM38 acts as positive and negative (respectively) regulators of the TNF- α and IL1 β activated NF- κ B pathway [18–20]. Besides, TRIMs have also been identified as regulators of NF- κ B in response to diverse stimuli, however, TRIM mediated negative feedback modulation of TNF- α regulated- κ B is not well understood [16,17].

In this study, we systemically identified potential feedback regulators of the TNF- α -induced NF- κ B pathway and further characterized the role of TRIM15 in negative regulation of TNF- α -induced NF- κ B pathway.

2. Results

2.1. Late response TNF- α induced TRIM15, inhibits TNF- α -induced NF- κ B pathway

TNF- α -induced temporal expression of NF- κ B target genes are crucial for optimal inflammatory response and resolution of inflammation. We performed a two-step screening strategy to identify possible feedback regulators of the TNF- α -induced NF- κ B pathway. Firstly, we analyzed expression of TRIMs in TNF- α treated HEK293 at 10 h to identify late expressing genes. The mRNA expression of several TRIMs (TRIM1, 2, 3, 8, 9, 15, 16, 21, 31, 37, 38, 39, 41, 44, 46, 47 and 55) increased >2 folds in TNF- α treated cells (Supplementary Fig. 1A). We reconfirmed the expression of TRIM1, 2, 15, and 16 using a different set of primers in HEK293 cells (Supplementary Fig. 1B).

The early response genes TNFAIP3 and I κ B α are the only NF- κ B activated genes known to negatively regulate NF- κ B [3,4]. We hypothesized that TRIMs transcribed during 'Late' response may regulate NF- κ Bn pathway in feedback manner. Therefore, we analyzed the role of

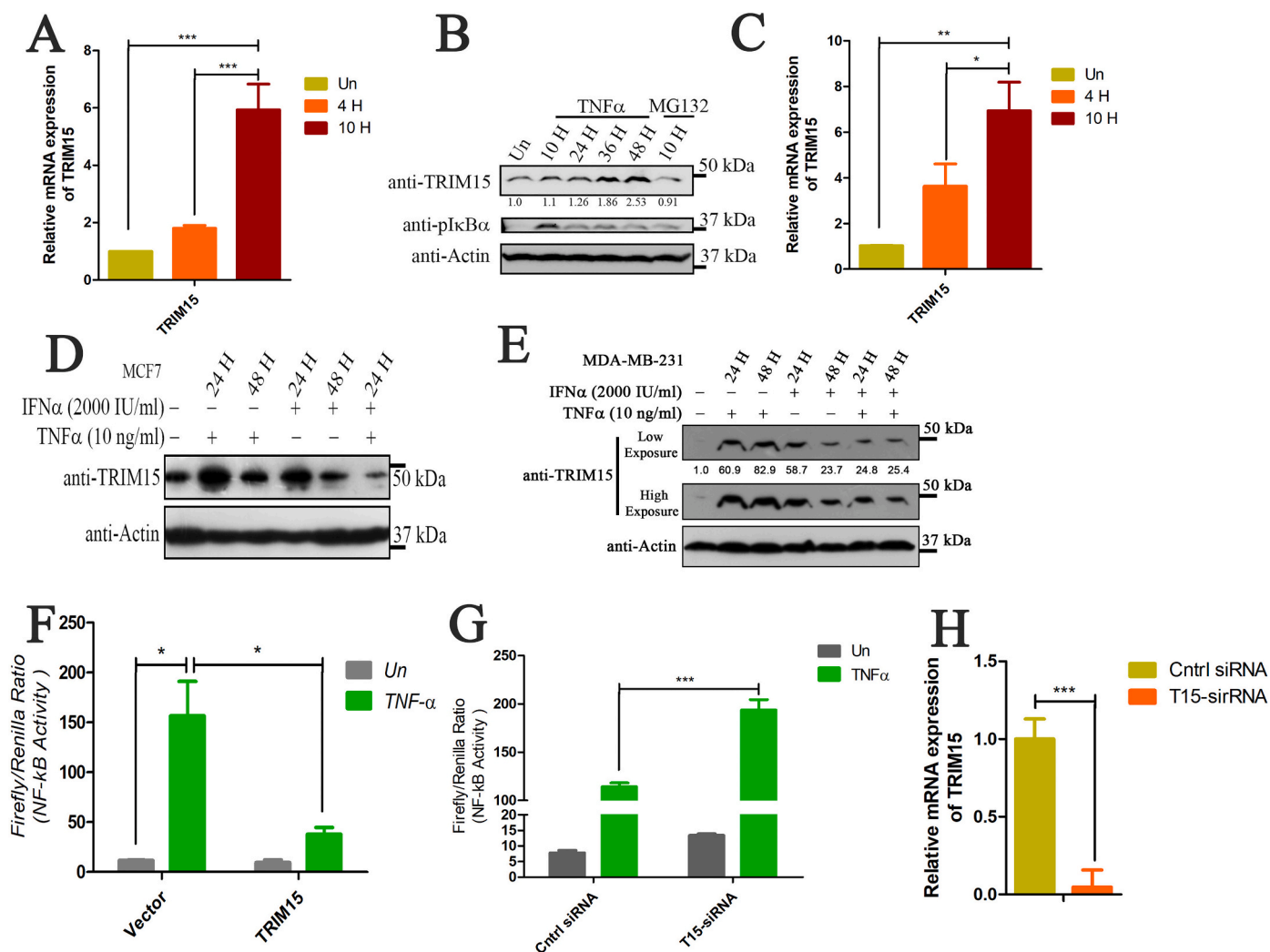


Fig. 1. TRIM15 is a late response TNF- α induced gene and inhibits TNF- α -induced NF- κ B activation. TNF- α induces expression of TRIM15. (A) HEK293 & (C) MCF-7 cells were treated with TNF- α for indicated time and mRNA expression of TRIM15 was analyzed using qRT-PCR. (B) HEK293, (D) MCF-7, and (E) MDA-MB-231 cells were treated as indicated and western blotting was performed to check TRIM15 protein levels. (F) TRIM15 inhibits TNF- α -induced NF- κ B activation. HEK293 cells were co-transfected with control vector or TRIM15 and NF- κ B reporter constructs. After 24 h of transfection, cells were treated with TNF- α for 10 h, and NF- κ B activity was measured by Dual glow luciferase reporter assay. (G) Control siRNA or TRIM15-siRNA was co-transfected with NF- κ B reporter constructs and 24 h post-transfection, cells were treated with TNF- α for 10 h and NF- κ B activity was measured. (H) Control siRNA or TRIM15-siRNA was transfected in HEK293 and mRNA expression of TRIM15 was analyzed using qRT-PCR. Asterisk (*), (**), and (***) indicates fold change or NF- κ B activity statistically significant from control; p -value < 0.05, < 0.01 and < 0.001 (respectively), SEM of minimum three independent experiments.

TNF- α -induced TRIMs in the regulation of NF- κ B pathway. In the second step, we knocked down TNF- α upregulated TRIMs using siRNA and monitored NF- κ B reporter activity in the presence/absence of TNF- α . The knockdown of TRIM1, 2, 15, 46, 47, 48, and 55 enhanced TNF- α -induced NF- κ B activation, whereas TRIM37 knockdown reduced the activity (Supplementary Fig. 1C). These results indicate that TNF- α -induced late response TRIMs act as negative regulators of the TNF- α -induced NF- κ B pathway.

A previous study exploring DNA methylation patterns associated with gastric cancer had identified TRIM15 as a hyper-methylated gene [21], hence we analyzed its methylation pattern and its correlation with expression. Firstly, we checked the expression and methylation of TRIM15 in various cancer cell lines using Cancer Cell Line Encyclopedia (CCLE) database [22]. Interestingly, the TRIM15 promoter region was highly methylated in most cancer cell lines except colorectal, pancreatic, and stomach cancer cell lines (Supplementary Fig. 2A, B, C & D). In consonance, TRIM15 mRNA expression was only observed in the colorectal, pancreatic, and stomach cancer cell lines (Supplementary Fig. 2A, B & C). Therefore, we reanalyzed the expression of TRIM15 during the “Mid” (4 h) and “Late” (10h) response using qRT-PCR in HEK293 (Fig. 1A) and MCF-7 (Fig. 1C) cells. TRIM15 mRNA transcript levels increased 6-fold after 10 h of TNF- α treatment in both the cell lines (Fig. 1A & C). Besides, while exploring GEO datasets, we also found that cultured aortic smooth muscle cells (SMCs) stimulated with TNF- α show increased expression of TRIM15 at 2 h, and the highest expression was observed at 6 h (Supplementary Fig. 2E) [23]. These results suggest that TRIM15 is primarily a late response TNF- α -induced gene.

Next, we checked protein levels of TRIM15 in TNF- α treated cells. We observed a temporal increase in TRIM15 protein levels in HEK293 (Fig. 1B). In MCF7 cells (Fig. 1D) TNF- α induced TRIM15 at 24 h which reduced at 48 h, whereas MDA-MB-231 (Fig. 1E) cells treated with TNF- α increased TRIM15 protein levels at both 24 and 48 h. Besides TNF- α treatment, we observed increased TRIM15 protein levels in MCF-7 and MDA-MB-231 cells in presence of Interferon- α (IFN α) (Fig. 1D & E).

Further, we validated the role of TRIM15 on NF- κ B activation by Dual Glow Luciferase Reporter assay. The expression of TRIM15 decreased TNF- α -induced NF- κ B activation as compared to control (Fig. 1F), whereas its knockdown by siRNA increased TNF- α -induced NF- κ B activation (Fig. 1G & H). We also analyzed its effect on NF- κ B inhibition at different time points and found that ectopic expression of TRIM15 inhibited TNF- α -induced NF- κ B activity at both 4 h and 24 h (Supplementary Fig. 2F).

2.2. TRIM15 form foci in the cytoplasm and nucleus and stabilizes in the presence of TNF- α

TRIMs are known to dynamically localize in different subcellular compartments [15,19,24]. Therefore, we monitored the subcellular localization of TRIM15. Western blotting showed the presence of TRIM15 in both cytosolic and nuclear fractions Treated with TNF- α , MG132 (Proteasome inhibitor), and Bafilomycin-A1 (Baf-A1; Autophagy inhibitor) (Fig. 2A). The level of 50 kDa band corresponding to TRIM15 was higher in nuclear fraction compared to the untreated cells in TNF- α treated condition. Additionally, TRIM15 levels in cytosolic fraction increased in MG132 (Proteasome inhibitor), Baf-A1 and co-treated cells (Fig. 2A). Further, we monitored subcellular localization using YFP tagged TRIM15. Confocal microscopy showed TRIM15 is present as discrete foci as well as large protein aggregates distributed in the cytosol (Fig. 2B). We also observed the presence of TRIM15 foci in the nucleus (Fig. 2C, Supplementary Fig. 3B).

TRIMs are known to dynamically localize to different subcellular compartments under specific stimuli [15,24]. Therefore, we checked the effect of TNF- α on dynamic localization of TRIM15. Interestingly, we observed that both mean fluorescence intensity (MFI) and binary area of TRIM15-YFP increased in TNF- α treated cells compared to control (Fig. 2D, E & F). We further monitored the TRIM15 foci in TNF- α ,

MG132 and Baf-A1 treated cells. Interestingly, the puncta size of TRIM15-YFP having $\geq 10 \mu\text{m}$ increased in TNF- α , MG132 and Baf-A1 treated cells compared to untreated control (Supplementary Fig. 3C). We also observed a corresponding decrease in puncta size ranging up to $\leq 2 \mu\text{m}$ in TNF- α , MG132, and Baf-A1 treated cells compared to control (Supplementary Fig. 3C). The increase in TRIM15 puncta size in presence of MG132 and Baf-A1 suggests its possible turnover through proteasome and autophagy pathway, whereas its increase in TNF- α treatment is possibly due to enhanced transcription of TRIM15 or stabilization at protein levels and formation of higher-order structure.

2.3. TRIM15 acts downstream of TRAF2 and inhibits I κ B α phosphorylation

TNF- α -induced NF- κ B pathway is broadly regulated at three major levels; TRADD-TRAF2 complex at TNF receptor, TAB-TAK complex, and IKK complex respectively [3,5]. To further investigate the mechanism of TRIM15 mediated inhibition of NF- κ B activity we analyzed the step regulated by TRIM15. We co-transfected TRAF2 with TRIM15 in HEK293 cells and analyzed NF- κ B activation in the presence/absence of TNF- α . The expression of TRAF2 was sufficient to enhance NF- κ B activation (Fig. 3A) and TRIM15 co-transfection significantly reduced the activity in untreated cells (Fig. 3A). Similar inhibition of TRAF2 induced NF- κ B activation was observed in TRIM15 co-transfected cells treated with TNF- α (Fig. 3A).

Further, we monitored the effect of TRIM15 on the TAK1 induced NF- κ B pathway. TAK1 expression did not affect NF- κ B activity in untreated cells but enhanced NF- κ B activity in TNF- α treated cells compared to vector (Fig. 3B). We also observed that co-transfection of TRIM15 with TAK1 inhibited NF- κ B activity (Fig. 3B) in presence of TNF- α . The co-expression of TRIM15 with TAK1 reduced the levels of p-I κ B α in both untreated and TNF- α treated cells compared to vector co-transfected cells (data not shown). Many regulators of TNF- α -induced NF- κ B pathway act on the NF- κ B heterodimers to regulate the activation of the pathway [3–5]. Therefore, we further checked the effect of TRIM15 on p65 induced NF- κ B activation. We observed that p65 expression increased NF- κ B activity in untreated cells and co-transfection of TRIM15 failed to inhibit NF- κ B activation (Fig. 3C). These results confirm that TRIM15 acts upstream of p65 and downstream of the TRADD-TRAF complex.

Phosphorylated (p) I κ B α is ubiquitinated and degraded by the Ubiquitin-Proteasome System (UPS) [2,3,5]. We argued that TRIM15 may affect I κ B α phosphorylation, therefore, we analyzed p-I κ B α levels by western blotting. Cells were transfected with indicated TRIMs and cells were treated with a combination of TNF- α and MG132. Western blotting showed the 40 kDa band corresponding to p-I κ B α was significantly reduced in TRIM15 transfected cells compared to control, suggesting inhibition of I κ B α phosphorylation (Fig. 3D). Similarly, we also analyzed the p-I κ B α levels in MCF-7 cells transfected with control vector or TRIM15 and treated with TNF- α , MG132, Baf-A1 (Inhibitor of autophagy) or in combination. Western blotting showed a significant reduction in the level of 40 kDa band corresponding to p-I κ B α in TRIM15 transfected cells compared to control, TNF- α , MG132, Baf-A1, and TNF- α -Baf-A1 co-treated cells (Fig. 3E). Interestingly, we did not observe any significant difference in p-I κ B α levels between TRIM15-YFP and control transfected cells co-treated with TNF- α and MG132. These results clearly show that TRIM15 inhibits the NF- κ B pathway by inhibiting I κ B α phosphorylation.

2.4. TRIM15 enhances turnover of TNF- α -induced K63-linked ubiquitin chains

Recruitment of different ubiquitin ligases brings stringency and specificity to the pathway by identifying specific substrates and the addition of ubiquitin in specific topologies [25]. Therefore, we analyzed the effect of TRIM15 on various ubiquitin chain topologies to further

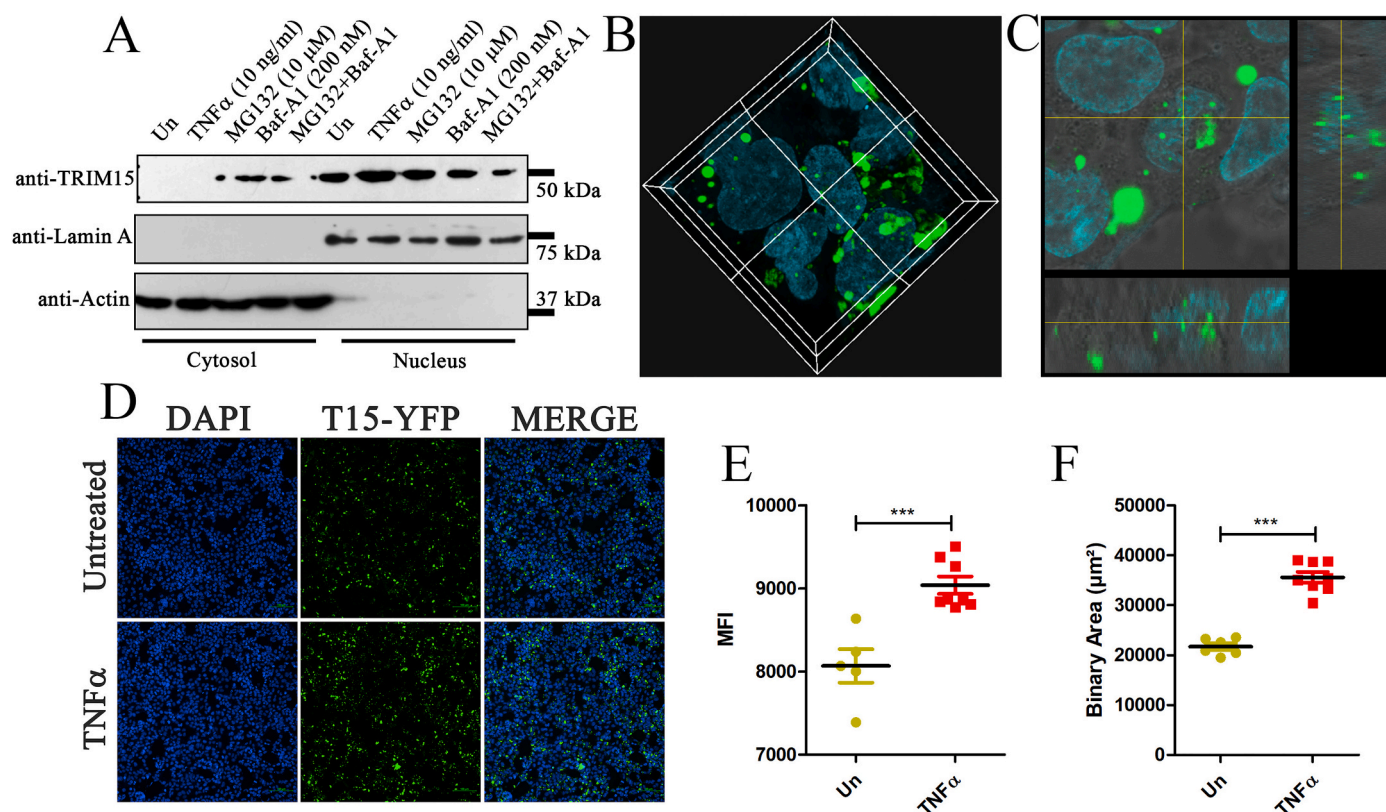


Fig. 2. TRIM15 forms foci in the cytoplasm and nucleus and stabilizes in the presence of TNF- α . (A) HEK293 cells were treated with TNF- α , MG132, and Baf-A1 as indicated for 10 h. Nuclear and cytosolic fractions were prepared and indicated specific antibodies were used to detect protein levels. (B & C) HEK293 cells were transfected with TRIM15-YFP and 24 h post-transfection cells were stained with Hoechst nuclear stain and monitored under a confocal microscope. (D) TRIM15-YFP transfected cells were grown on a coverslip and treated with TNF- α for 10 h. Cells were fixed and stained with DAPI and monitored under a fluorescent microscope for DAPI and YFP fluorescence. (E&F) The binary area and mean fluorescence intensity of TRIM15-YFP was measured from the captured images using the automated measurement feature of Nikon Elements AR software. Asterisk (**) and (***) indicates statistically significant difference in MFI and binary area from control; p-value <0.01 and < 0.001 (respectively), SEM of minimum six different fields.

understand its E3 ligase function. We co-transfected HEK293 cells with HA-Ub-K6, K11, K27, K29, K48, K63, and either vector control or TRIM15 and treated them with TNF- α . Interestingly we found that TRIM15 co-transfection significantly reduced K6, K11, K27, K29, K48, and K63 linked polyubiquitination of proteins and reflected the most pronounced effect on K6 and K63 linked polyubiquitination (Fig. 4A).

Therefore, we further checked the effect of TRIM15 on cellular ubiquitination by co-transfecting vector or TRIM15 with HA-Ub-K63 and monitored K63 linked ubiquitination. We observed higher molecular weight adducts of HA-Ub-K63 linked proteins were increased in presence of TNF- α in vector-transfected cells (Fig. 4B). TRIM15 co-transfection significantly reduced the level of K63 linked ubiquitination in TNF- α treated cells (Fig. 4B). Interestingly, we found that levels of HA-Ub-K63 linked protein adducts increased in TRIM15 transfected cells in presence of MG132 as compared to untreated and TNF- α (Fig. 4B). Further, we monitored total cellular ubiquitination in the same blot using a ubiquitin-specific antibody, however, no difference was observed in ubiquitination between control or TRIM15 transfected cells in different treatment conditions (Fig. 4B).

To reconfirm, we co-transfected HA-Ub-K63 with control or TRIM15-siRNA and monitored the levels of K63-linked ubiquitination of proteins using HA-specific antibody. We observed a significant increase in levels of higher molecular weight K63-linked protein adducts in TRIM15-siRNA transfected cells compared to control transfected cells both in the absence and presence of TNF- α (Fig. 4C). We also observed an increase in total cellular ubiquitination in TRIM15-siRNA transfected cells both in the absence and presence of TNF- α as compared to control (Fig. 4C). Interestingly, a similar increase in K63-linked ubiquitination

was also observed in TRIM15 knockdown cells treated with MG132 and in combined treatment of TNF- α and MG132 (Fig. 4C), whereas we observed no difference in total ubiquitination in these conditions, suggesting decreased turnover of K63 linked proteins in absence of TRIM15.

As observed earlier that TRIM15 is present in both cytosol and nucleus (Fig. 2A, B & C), we monitored its effect on nuclear and cytosolic protein ubiquitination levels. We co-transfected HA-Ub-K63 either with control or TRIM15-YFP in HEK293 cells and treated with TNF- α or MG132. Western blotting of cytosolic and nuclear fractions showed that TRIM15 significantly reduced K63-linked ubiquitination in the cytosol and nucleus of both untreated and TNF- α treated cells (Fig. 4D), whereas, its effect on total ubiquitination was less pronounced (Fig. 4D). Consistent with the previous blot (Fig. 4B) we observed increased K63-linked ubiquitination in TRIM15 transfected cells treated with MG132 as compared to untreated and TNF- α treated cells (Fig. 4D). These results suggest that E3 ligase TRIM15 enhances UPS mediated turnover of K63-linked ubiquitination in both nucleus and cytoplasm.

2.5. PRY/SPRY domain deletion of TRIM15 rescues inhibitor of TNF- α -induced K63-linked ubiquitination and NF- κ B activity

We further analyzed the effect of TRIM15-mediated inhibition of K63-linked ubiquitination on NF- κ B activation. Different domain deletion constructs of TRIM15 were co-transfected with HA-Ub-K63 and K63 linked ubiquitination and NF- κ B activation was monitored. Surprisingly, transfection of TRIM15 with RING and RING-B-Box deletion showed less rescue of K63-linked ubiquitinated adducts as compared to full-length TRIM15 (Fig. 5A), and strongly inhibited TNF- α -induced NF- κ B

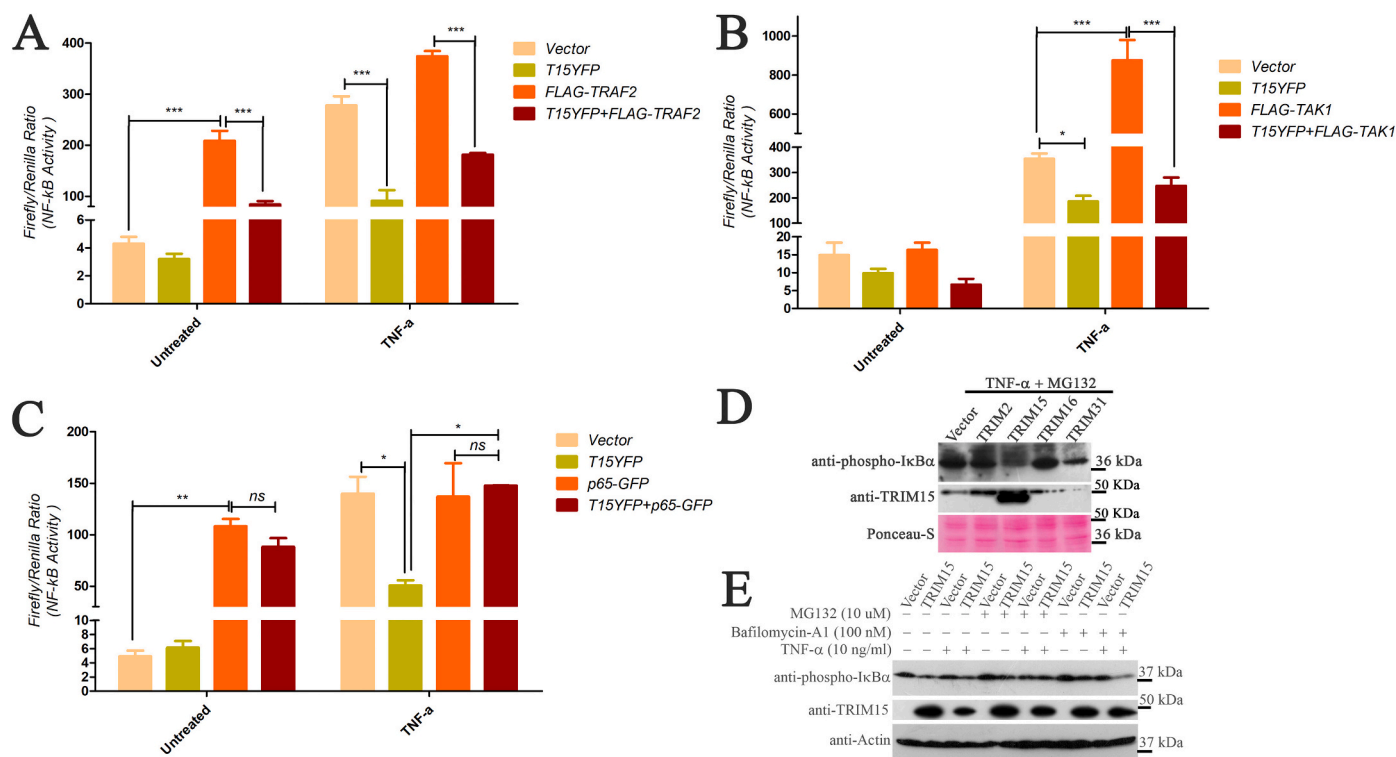


Fig. 3. TRIM15 acts downstream of TRAF2 and inhibits $\text{I}\kappa\text{B}\alpha$ phosphorylation. (A, B & C) TRIM15 acts upstream of p65 and downstream of TRAF2 in the NF- κB pathway. Vector or TRIM15 was co-transfected as indicated with TRAF2 (A), TAK1 (B), or p65 (C) in HEK293 cells along with NF- κB reporter constructs. 24 h post-transfection cells were treated with TNF- α for 10 h and NF- κB activity was measured. (D) TRIM15 inhibits $\text{I}\kappa\text{B}\alpha$ phosphorylation. HEK293 cells were transfected with indicated constructs and treated with TNF- α and MG132 for 10 h. Western blotting was performed to check the levels of p- $\text{I}\kappa\text{B}\alpha$ levels using a specific antibody. (E) MCF-7 cells were transfected with control vector or TRIM15 and TNF- α , MG132, and Bafilomycin-A1 as indicated, for 10 h. Western blotting was performed to check the levels of p- $\text{I}\kappa\text{B}\alpha$. Asterisk (*), (**), and (***) indicates NF- κB activity statistically significant from control; p -value < 0.05, < 0.01 and < 0.001 (respectively), SEM of minimum three independent experiments.

activity (Fig. 5B). Interestingly, we observed that deletion of SPRY and PRY/SPRY domain of TRIM15 rescued K63-linked ubiquitination and TNF- α -induced NF- κB activity (Fig. 5C). Additionally, transfection of CC domain deleted TRIM15 and CC domain mutant (T15Cm) showed less rescue of K63 linked ubiquitination compared to PRY/SPRY domain deleted TRIM15 (Fig. 5C) and NF- κB activity (Fig. 5D). These results suggest that the PRY/SPRY domain of TRIM15 is essential for the turnover of K63-linked ubiquitination and TNF- α -induced NF- κB activity. Interestingly, these results also confirmed that a significant correlation exists between cellular TRIM15-mediated K63-linked ubiquitination and NF- κB activity.

2.6. TRIM15 inhibits NF- κB activation by turnover of K63-linked ubiquitination of TAK1

TAK1 is modified by K63-linked ubiquitin chains in presence of TNF- α and IL-1 β [20] and we observed that TRIM15 enhances turnover of K63-linked ubiquitin adducts (Fig. 5C). Therefore, we analyzed whether TRIM15 had any effect on the K63-linked ubiquitination of TAK1. We co-transfected cells with Flag-TAK1 and control vector, TRIM15-YFP or tagless-TRIM15, and treated them with MG132 and TNF- α . TAK1 was pulled down using anti-Flag affinity beads and immunoprecipitation (IP) showed that 75 kDa band corresponding to TRIM15-YFP appeared in the Flag-TAK1 pull-down confirming interaction of TRIM15 and TAK1 (Fig. 6A). Blotting with ubiquitin antibody showed increased higher molecular weight adducts of polyubiquitinated proteins in Flag-TAK1 pull-down, whereas it was reduced in TRIM15 co-transfected cells (Fig. 6A). A similar reduction of TAK1 ubiquitination was observed in Flag-TAK1 co-transfected with tag-less TRIM15 (Fig. 6A).

TRIM15 had been identified as an E3 ligase [26] and it showed

interaction with TAK1, therefore we analyzed if TRIM15 affects the turnover of TAK1. To address this, we co-transfected Flag-tagged TAK1 with a control vector or TRIM15 and treated the cells with TNF- α , MG132, or in combination. We observed that the 50 kDa band corresponding to TAK1 remained unchanged in control and TRIM15 transfected cells (Fig. 6B) and no significant difference was observed in the TAK1 levels in control and treated conditions (Fig. 6B).

K63-linked ubiquitination of TAK1 at Lysine 158 is required for TNF- α induced NF- κB activation [2,20,27] and TRIM15 showed reduced levels of K63-linked ubiquitination. Therefore, we checked whether TRIM15 modulates the K63-linked ubiquitination of TAK1. Flag-TAK1 and HA-Ub-K63 were co-transfected with TRIM15 and treated with TNF- α and IP were performed using anti-Flag affinity beads. Western blotting reconfirmed the interaction of TRIM15 and TAK1 and reduction of TAK1 ubiquitination in presence of TRIM15 (Fig. 6C). Detection of K63-linked ubiquitination using HA-specific antibody showed that TNF- α treatment promotes K63-linked ubiquitination of TAK1 whereas TRIM15 co-transfection completely diminished K63-linked ubiquitination of TAK1 (Fig. 6C). Besides, we performed a similar IP and pulled down K63-linked ubiquitin chains using HA-affinity beads. Increased level of ubiquitinated TAK1 was observed in the presence of TNF- α , whereas the transfection of TRIM15 enhanced the turnover of K63-linked TAK1 in presence of TNF- α (Fig. 6D). Together these results suggest that TRIM15 interacts with ubiquitinated K63-linked TAK1 and reduced its level by enhancing the turnover through UPS.

2.7. TRIM15 interacts with TRIM8, inhibits its cytoplasmic translocation and TNF- α -induced NF- κB activity

The previous report from our group had shown that nucleo-

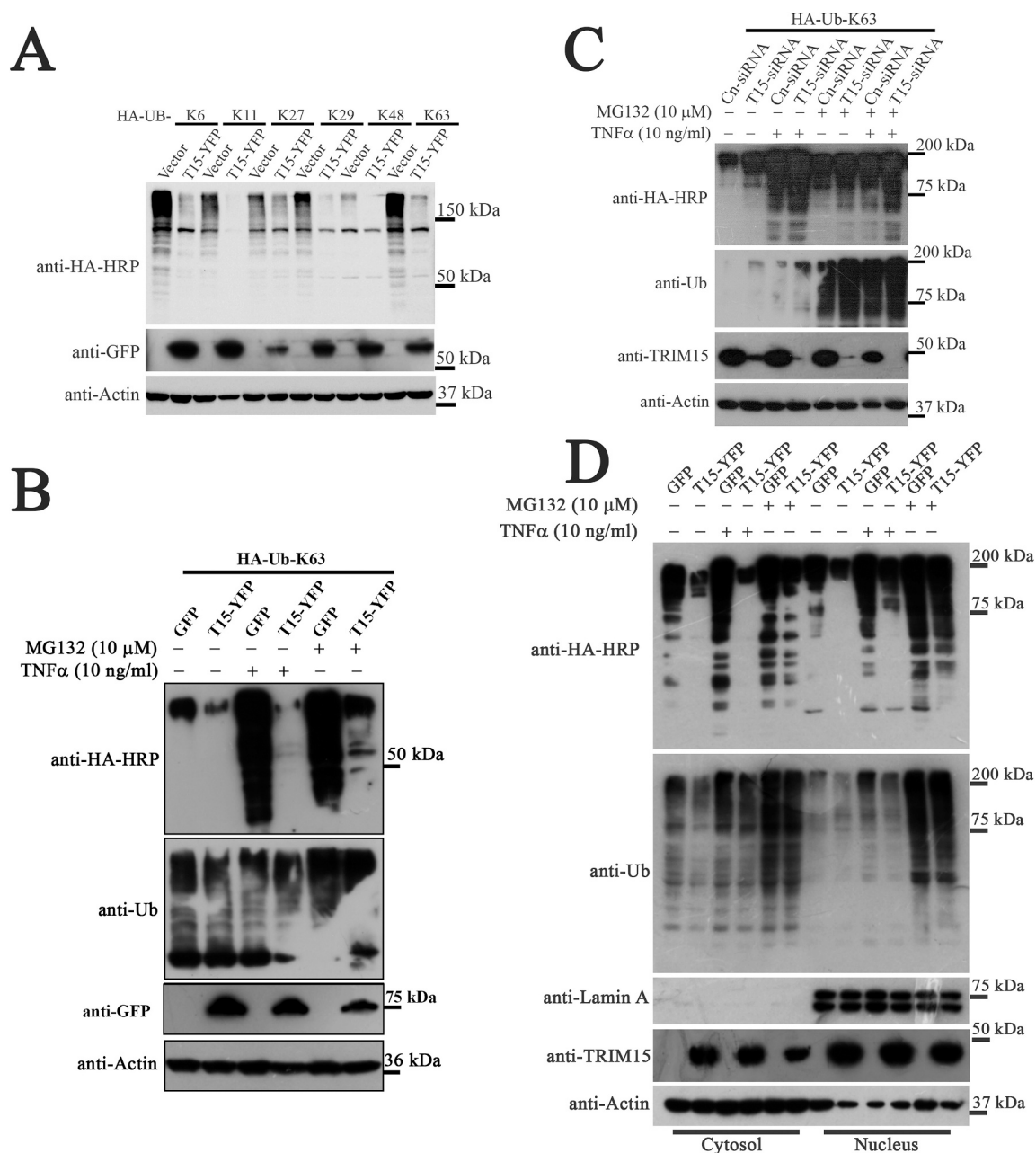


Fig. 4. TRIM15 enhances turnover of TNF- α -induced K63-linked ubiquitin chains. (A) HA-tagged Ub-K6, K11, K27, K29, K48, and K63 were co-transfected with either vector or TRIM15-YFP. Cells were treated with TNF- α for 10 h after transfection and western blotting was performed. (B) Vector or TRIM15-YFP constructs were co-transfected with HA-Ub-K63 in HEK293 cells. 24 h post-transfection cells were treated with TNF- α and MG132 as indicated for 10 h. Western blotting was performed to check total ubiquitination and K63 linked polyubiquitinated proteins using indicated antibodies. (C) HA-Ub-K63 was co-transfected with control or TRIM15-siRNA in HEK293 cells and treated with TNF- α and MG132 as indicated for 10 h. Western blotting was performed to check protein levels using indicated antibodies. (D) Vector or TRIM15-YFP constructs were co-transfected with HA-Ub-K63 in HEK293 cells and treated as indicated. After 10 h of treatment nuclear-cytoplasmic fractions were prepared and levels of indicated proteins were detected using specific antibodies.

cytoplasmic translocation of TRIM8 is required for TNF- α -induced NF- κ B activation [19], additionally TRIM8 promotes K63-linked polyubiquitination of TAK1 in cytoplasm to induce NF- κ B activation [20]. TRIMs are known to homo and heterodimerize for target identification and assembly of signalosomes [28,29]. While exploring interaction partners of TRIM15, the literature survey showed possible interaction between TRIM8 and TRIM15 [30] therefore, we performed co-immunoprecipitation (Co-IP) to confirm their interaction. HA-tagged TRIM8 was transfected with either vector or TRIM15-YFP and treated with TNF- α and MG132 or MG132 alone. TRIM8 was pulled down using anti-HA affinity beads and western blotting showed that the 75 kDa

band corresponding to TRIM15-YFP was observed in TRIM15 and HA-TRIM8 co-transfected cells co-treated TNF- α and MG132 (Fig. 7A).

TRIM8's nucleo-cytoplasmic translocation in TNF- α is required for activation of NF- κ B [19], therefore we further analyzed the effect of TRIM15 on TRIM8 dynamics. We transfected HA-tagged TRIM8 with TRIM15-YFP or vector control in HEK293 cells and treated with TNF- α and monitored TRIM8 and TRIM15 in nucleo-cytoplasmic fractions. The level of 75 kDa band corresponding to TRIM15-YFP was higher in nuclear fraction as compared to the cytosol, whereas its cytosolic levels increased in presence of TNF- α (Fig. 7B). The 62 kDa band corresponding to HA-TRIM8 was high in nuclear fraction compared to the

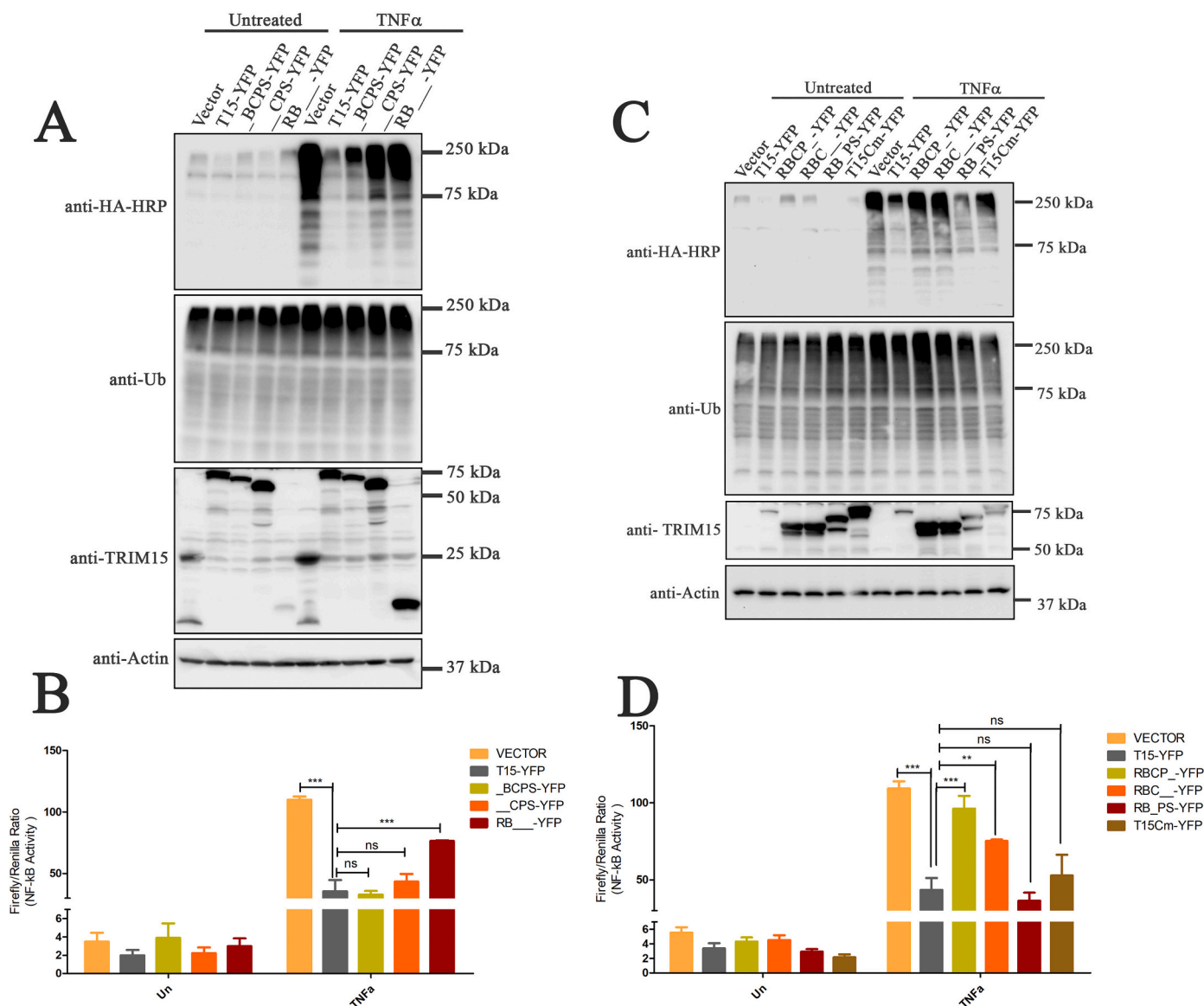


Fig. 5. PRY/SPRY domain deletion of TRIM15 rescues TNF- α -induced K63-linked ubiquitination and NF- κ B activity. (A & C) HA-Ub-K63 was co-transfected with either vector or indicated TRIM15 construct in HEK293 and treated with TNF- α for 10 h. Western blotting was performed to check total ubiquitination and K63-linked polyubiquitinated proteins using indicated antibodies. PRY/SPRY domain of TRIM15 is essential for inhibition of TNF- α -induced NF- κ B activity. (B & D) Vector or indicated TRIM15 construct were co-transfected with NF- κ B reporter constructs and cells were treated with TNF- α for 10 h, later NF- κ B activity was measured using dual glow luciferase assay. Asterisk (**) and (***) indicates NF- κ B activity statistically significant from control; p -value < 0.01 and < 0.001 (respectively), SEM of minimum three independent experiments.

cytosol (Fig. 7B) and interestingly, the level of TRIM8 was higher in the nuclear fraction of TRIM8-TRIM15 co-transfected cells (Fig. 7B). We also observed a corresponding decrease in TRIM8 levels in the cytoplasm in TRIM15 co-transfected cells (Fig. 7B).

To further check the functional effect of TRIM15 on TRIM8-enhanced TNF- α -induced NF- κ B activity we checked the effect of TRIM15 on TRIM8-regulated TNF- α -induced NF- κ B activity. We observed ectopic expression of TRIM8 enhanced NF- κ B activity compared to vector-transfected TNF- α treated cells (Fig. 7C) as observed previously [19,20]. Interestingly, we observed that co-expression of TRIM15 with TRIM8 significantly reduced TRIM8-regulated NF- κ B activation (Fig. 7C). Since we observed functional antagonism between these proteins in the regulation of the NF- κ B pathway, we further explored their physiological significance in inflammatory conditions. We analyzed the GEO databases for disease progression related to inflammatory conditions, specifically Psoriasis. Interestingly gene expression analysis of microarray dataset comparing expression

between normal, non-lesional, and lesional psoriasis tissue showed a marked increase in TRIM15 mRNA expression in lesional psoriasis tissue compared to normal control and non-lesional (psoriasis) tissue (Supplementary Fig. 4A, B & C). We also observed that TRIM8 expression was decreased in lesional psoriasis tissue compared to normal control and non-lesional (Supplementary Fig. 4D, & E). Together these results confirm functional and physiological antagonism between TRIM8 and TRIM15 and indicate its implication in the regulation of inflammation and chronic inflammatory condition like psoriasis.

3. Discussion

Increased levels of TNF- α ; a prototypic activator of the pro-inflammatory NF- κ B pathway, had been observed in several pathophysiological conditions [6–9]. This pathway had been intensively studied, however, the resolution TNF- α -induced inflammatory pathway is still not well understood in pathophysiological conditions. Majority

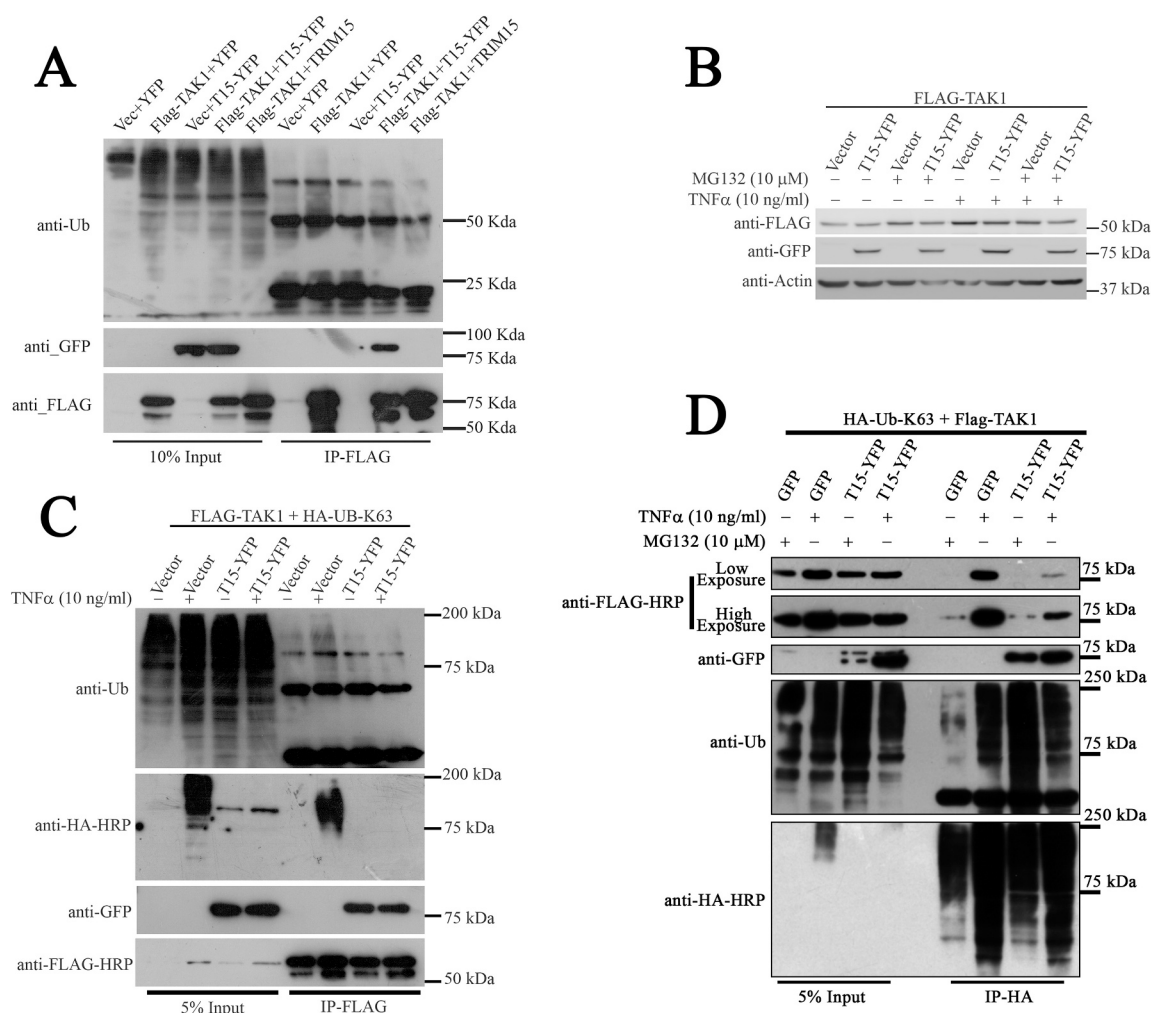


Fig. 6. TRIM15 inhibits NF- κ B activation by turnover of K63-linked ubiquitination of TAK1. (A) TRIM15 interacts with TAK1 and inhibits its ubiquitination. HEK293 cells were transfected with the control vector, TRIM15-YFP, tagless-TRIM15, and Flag-TAK1 as indicated. Cells were co-treated with TNF- α and MG132 for 10 h and TAK1 was pulled down using Flag affinity beads. Western blotting was performed and indicated antibodies were used to check the interaction. (B) HEK293 cells were co-transfected with Flag-TAK1 and vector control or TRIM15-YFP and treated as indicated. Western blotting was performed to check the levels of indicated proteins using specific antibodies. (C & D) HA-Ub-K63 and Flag-TAK1 were co-transfected with either control vector or TRIM15-YFP and treated with or without TNF- α for 10 h. TAK1 was pulled using Flag affinity beads (C), whereas K63-linked chains were pulled down using HA affinity beads (D), from lysates and western blotting was performed to detect interaction and ubiquitination using indicated antibodies.

of the studies focused on early response genes however dysregulation of physiological equilibrium in chronic disease conditions is not well understood. The selective ubiquitination of proteins implicated in presence of TNF- α either leads to its degradation or its recruitment to assemble signaling complexes defining the unique outcome of the TNF- α -pathophysiological responses. In this study, we systematically identified late response TNF- α activated E3 ligases and their role in the regulation of TNF- α -induced NF- κ B activation and further characterized TRIM15 in negative feedback regulator of TNF- α -induced NF- κ B pathway.

We and others have previously observed that turnover of TRIMs is high and stabilized during specific pathophysiological conditions [31,32]. Cells keep inflammatory pathways under stringent control and hence it can be inferred that late response genes may have important regulatory functions, hence, we systematically planned to identify late response TNF- α induced TRIMs regulating the NF- κ B pathway. In this study we performed screening and identified several TRIM genes (TRIM1, 2, 3, 8, 9, 15, 16, 21, 31, 37, 38, 39, 41, 44, 46, 47 and 55) which are late response TNF- α activated genes. Interestingly, most of the late response TRIMs: TRIM1, 2, 15, 46, 47, 48, and 55 inhibit TNF- α -induced NF- κ B pathway, suggesting that TRIMs may act as feedback regulator of the TNF- α -induced NF- κ B pathway. These results further warrant a more

focused investigation of late response genes and their role in feedback regulation of TNF- α induced NF- κ B pathway in different pathophysiological conditions.

Isolated reports from different groups including our group had shown that TRIMs, a family of RING E3 ligases regulates cellular pathways by identification and modification of their target substrates [16–18,20,33,34]. Stimuli-specific expression of TRIMs brings precision and specificity to the pathways and determines the physiological outcome [24,31,35,36]. Previously upregulation of TRIM15 was observed in THP1-derived macrophages stimulated with ligands of TLR3 and TLR4 [37] but its expression was found unaffected by type-I IFNs in various immune cells [35]. In this study, we suggest that TRIM15 is a TNF- α -induced late response gene and strongly inhibits NF- κ B activation in different cell types. TRIM15 has restricted tissue expression and data from cancer cell line encyclopedia (CCLE) suggest that DNA methylation of TRIM15 promoter regions restricts its mRNA expression. Our observation of TRIM15 gene expression in response to TNF- α is supported by recent reports suggesting that infection [38] and TNF- α promotes [39] DNA demethylation of genes and promote their transcription. This also suggests that hypermethylated genes may also contribute to the regulation of cellular pathways in response to specific

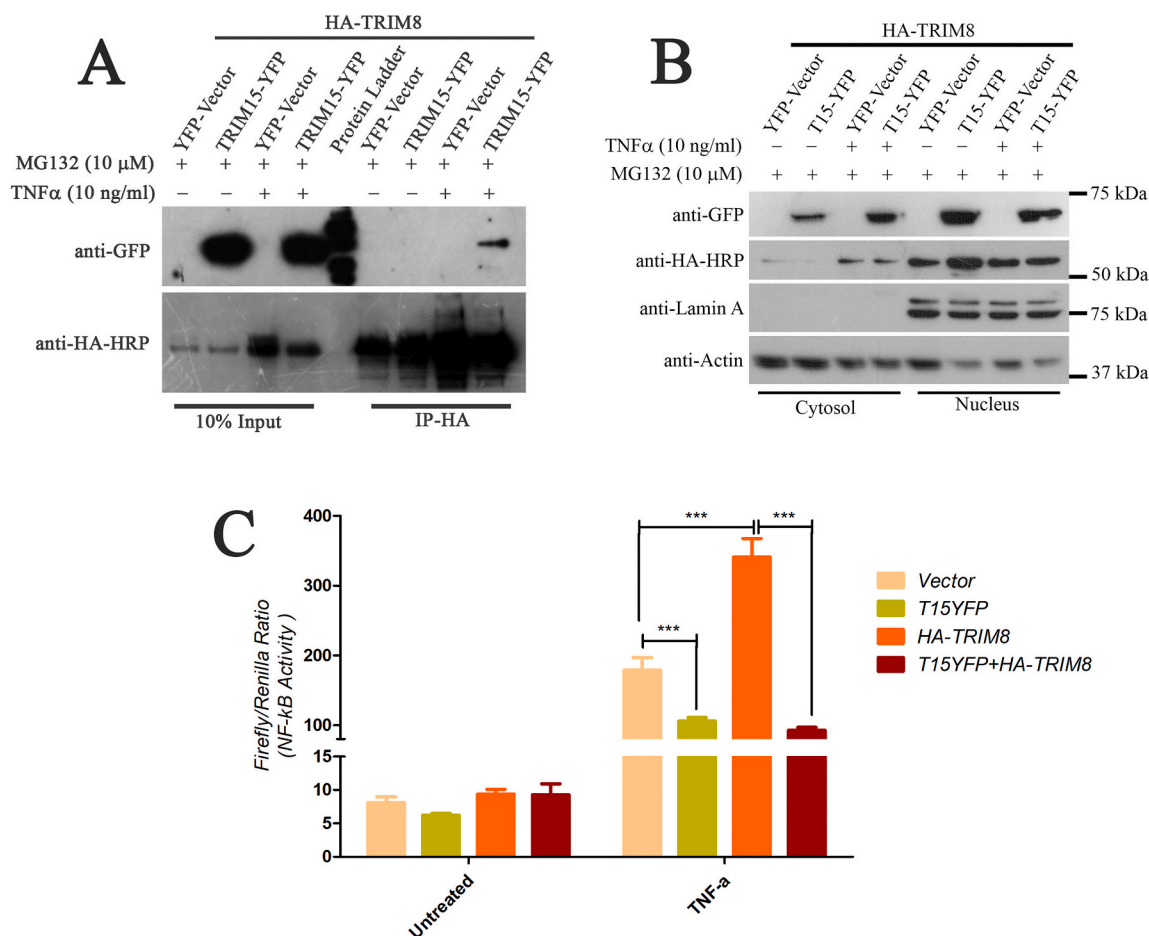


Fig. 7. TRIM15 interacts with TRIM8, inhibits its cytoplasmic translocation and TNF- α -induced NF- κ B activity. (A) TRIM15 interacts with TRIM8 in TNF- α treated cells. HA-TRIM8 was co-transfected with a control vector or TRIM15-YFP and treated as indicated for 10 h. Cells were collected and TRIM8 was pulled down using HA affinity gel. Western blotting was performed and indicated antibodies were used to check the interaction. (B) TRIM15 inhibits cytosolic translocation of TRIM8. HA-TRIM8 was co-transfected with vector or TRIM15-YFP in HEK293 cells and treated with TNF- α and MG132 as indicated. After 10 h of treatment, nuclear-cytosolic fractions were prepared and levels of indicated proteins were detected using specific antibodies. (C) TRIM15 inhibits TRIM8 enhanced NF- κ B activation. HEK293 cells were co-transfected with vector, TRIM15, and TRIM8 as indicated. After 24 h of transfection cells were treated with TNF- α for 10 h and NF- κ B activity was measured. Asterisk (***) indicates NF- κ B activity statistically significant from control; p-value <0.001, SEM of minimum three independent experiments.

stimuli [38,39]. Previous studies from our lab and others have demonstrated that TRIMs have high turnover and stabilizes only specified pathophysiological conditions [16,24,31,32]. Interestingly, unlike other TRIMs, TRIM15 protein is stable and turnover is not high as it had been observed to play an essential role in focal adhesion involved in cell migration, an essential cellular process [26]. TNF- α induced expression of highly methylated gene TRIM15 indicates existence of an additional layer regulation of NF- κ B, which is via demethylation of their regulatory genes, however, this concept requires further validation.

Ubiquitin E3 ligases are known to modify substrates by adding specific ubiquitin chains and regulate their stability and degradation. Several NF- κ B target genes are E3 ligases and found to regulate the pathway positively by modifying specific targets and regulating their turnover [3,5,40–42]. Surprisingly we observed that TRIM15 enhances turnover of K63-linked ubiquitin chains and further characterization revealed the involvement of the PRY/SPRY domain for turnover of K63-linked ubiquitination and inhibition of TNF- α -induced NF- κ B activity. K63-linked ubiquitination had been suggested to promote the stability of proteins and function generally independent of UPS, however, emerging evidence suggests that some targets modified by K63-linked ubiquitin chains are degraded by UPS [43]. Further, it had been found that K63-linked chains act as seeds for the formation of K48/K63 branched chains and associates with the proteasome [44]. Furthermore, assembly of K48/K63 branched ubiquitin chains assembled on TRAF6 by E3 ligase

HUWE1 protects deubiquitination of K63-linked chains of TRAF6 to positively regulate IL-1 β mediated NF- κ B pathway [45]. Therefore, it will be interesting to explore if TRIM15 mediated degradation of K63-linked ubiquitination requires the similar deployment of K48/K63-linked branched ubiquitin chains to enhance the turnover of K63-linked substrate to negatively regulate the NF- κ B pathway.

Previous studies have shown that activation of the TAB-TAK complex is critical for activation of the TNF- α -induced NF- κ B pathway and K63 linked ubiquitination of TAK1 is critical for activation [3–5,46]. Our study shows that TRIM15 interacts with TAK1 and strongly inhibits NF- κ B activation by enhancing the turnover of K63-linked ubiquitin chain [3–5,20,27]. This is one of the first reports elucidating the role of TNF- α -induced late response genes in negative regulation of the NF- κ B pathway.

Homo/heteromeric interactions of TRIM proteins had been previously observed [15,30] however their physiological implication had not yet been studied. Cooperation between TRIMs has been observed and reports show antagonistic effect on the same substrate or pathway. Previous reports from our group and others have shown that TRIM8's nucleo-cytoplasmic trafficking is important for NF- κ B activation by promoting TAK1 ubiquitination [19,20]. Here we observed that TRIM15 mediated restriction of cytosolic translocation of TRIM8 which may further inhibit TRIM8 mediated K63 linked cytosolic ubiquitination of TAK1 as reported previously. More interestingly the observed functional

antagonism between these proteins is also relevant in the chronic inflammatory condition, Psoriasis. Besides its role in regulation of TNF- α -induced NF- κ B pathway and virus-induced IFN response [47] TRIM8 is also known to regulate different aspects of cancer signaling including estrogen signaling [48], genotoxic stress induced cell death [32] and chromosome stability [32]. Therefore, it will be interesting to check the relevance of TRIM8-TRIM15 functional antagonism in cancers.

In summary, the current study identified TRIMs as novel regulators of the TNF- α -induced NF- κ B pathway and further report TRIM15's role in negatively regulating TNF- α -induced NF- κ B activity. Interestingly, TNF- α may induce the expression of several TRIMs which may be selectively stabilized in different subcellular compartments hence different TRIMs may be recruited at the different regulatory steps of TNF- α -induced NF- κ B activation. These proteins are developing modulators of inflammatory pathways and chronic pathological conditions and further study may provide a novel way of targeting specific TRIMs for therapeutic intervention in given pathophysiological conditions.

4. Materials & methods

4.1. Cells and reagent

HEK293, MCF-7 and MDA-MB-231 cells were grown at 37 °C, 5% CO₂ in Dulbecco's Modified Eagle's Medium (DMEM, Cyclone, GE, USA) and Minimal Essential Media (MEM, HyClone, GE, USA) supplemented with 10% (v/v) heat-inactivated fetal bovine serum (Gibco, Thermo Fisher Scientific, USA) and 1% penicillin, streptomycin, and neomycin (PSN) antibiotic mixture (Gibco, Thermo Fisher Scientific, USA). TRIM15 in pCDNA-3 and all TRIM15-YFP constructs in pZsYellow1-N1 was provided by Dr. Walther H. Mothes and Dr. Pradeep Uchil (Section of Microbial Pathogenesis, Yale School of Medicine, USA) [26]. HA-TRIM8 in pCGN-HA was gifted by Dr. S. Hatakeyama (Department of Biochemistry, Hokkaido University Graduate School of Medicine) [34]. Flag-TAK1 was provided by Dr. Yan-Yi Wang [49]. Control and TRIM15-siRNA were purchased from Qiagen.

Primary antibodies Anti-HA-HRP, Anti-FLAG-HRP were purchased from Sigma, USA. Mouse polyclonal against β -Actin and Ubiquitin was from SantaCruz, USA, Rabbit polyclonal against GFP from Abclonal (Woburn, MA, United States) and p-I κ B α was from Cell signaling technology, USA. TRIM15 was purchased from St John's Laboratory (United Kingdom). HRP-conjugated secondary antibodies; anti-rabbit and anti-mouse were purchased from Jackson ImmunoResearch, USA. Recombinant Human TNF- α was purchased from Milteny Biotech, Germany, and PeproTech, USA. MG132, Bafilomycin A1, EZview™ Red Anti-HA Affinity Gel, and M2 FLAG-Affinity Gel were purchased from Sigma-Aldrich, USA. Lipofectamine® 3000 (Invitrogen, USA) was used for siRNA transfection. Dual Glow Luciferase Reporter Kits were purchased from Promega, USA.

4.2. Gene expression analysis of TRIM family proteins

HEK293 cells were treated with TNF- α (10 ng/ml) for 10 h and collected in RNA ISO plus reagent (Takara, Japan). Total RNA was isolated using RNAiso Plus Reagent and was reverse transcribed to synthesize cDNA using PrimeScript 1st strand cDNA Synthesis Kit (Takara, Japan) according to the manufacturer's protocol. The expression of TRIMs were analyzed by quantitative Real-Time PCR using TaqMan probes specific for the indicated TRIM gene (Applied Biosystems, Inc., USA). Data were processed using DataAssist v3.01 (Applied Biosystems, Inc., USA). 18S rRNA was used as endogenous control and fold change values ($2^{-\Delta\Delta Ct}$) were plotted.

Similarly, mRNA expression of various TRIMs was reconfirmed using Real-time PCR by SYBR Premix Ex Taq II (Tli RNase H Plus) (Takara, Japan) as per the manufacturer's instruction. β -Actin and GAPDH genes were used as multiple endogenous control and expression of indicated genes were calculated using QuantStudio 3 and 5 system's Design and

Analysis Software v1.5.1. fold change values ($2^{-\Delta\Delta Ct}$) of a minimum of three independent biological replicates were plotted.

Specific primers for the genes are listed in Supplementary Table 1.

4.3. NF- κ B luciferase reporter assay

Dual-Glo luciferase assay system was used for detecting NF- κ B activity (Promega, USA) as described previously [19]. HEK293 cells were seeded at a density of 2.5×10^5 cells per well in 12 well plates. siRNA targeting specific TRIMs or indicated vectors were co-transfected with NF- κ B firefly and Renilla luciferase reporter constructs. siRNA and vector co-transfection was done using Lipofectamine 3000 following the manufacturer's protocol. Transfected cells were treated with TNF- α for 10 h or indicated time points and Firefly/Renilla activity was measured by following the manufacturer's protocol using BioTek Synergy HTX multimode plate reader. The Firefly/Renilla ratio was plotted to show the activation of the NF- κ B pathway.

4.4. Fluorescence/confocal microscopy

HEK293 cells were seeded at a density of 1.5×10^5 cells on coverslips in 24 well plates. Cells were transfected with TRIM15-YFP or TRIM15-RFP. After 24 h of transfection, cells were treated with indicated chemicals and fixed with 4% Paraformaldehyde (PFA). Coverslips were removed from 24 well plates and slides were prepared using SlowFade™ Gold Antifade Mountant (Thermo, USA). Images were acquired using Nikon Eclipse Ti2 Inverted Microscope and processed using NIS-Elements Advanced Research software (Nikon, Japan). Similarly, slides were prepared, and images were acquired using Nikon Confocal Microscope A1R HD25 (Nikon, Japan).

Automated image analysis was performed using NIS-Elements Advanced Research software. For measurement of mean fluorescent intensity (MFI) and binary area "field measurement" feature of the "Automated image analysis" tool was used. Acquisition and measurement parameters for all YFP images were kept the same for all the images. Similarly, the "object count" feature of the "Automated image analysis" tool was used for counting the YFP puncta of TRIM15.

4.5. Nuclear-cytoplasmic fractionation

The nuclear and cytosolic fractions were prepared as described previously [19] with minor modifications. HEK293 cells were plated at a density of 1×10^6 in a 60-mm² dish and transfected with indicated vectors. After 24 h of transfection, the cells were treated with indicated chemicals. Cells were washed with DPBS (Hyclone, GE, USA) and resuspended in 300 μ l of buffer-A (10 mM HEPES buffer, pH 7.9, 0.1 mM EDTA, 10 mM KCl, 0.4% (v/v) NP40, 0.5 mM dithiothreitol (DTT), and 1 \times protease inhibitor cocktail (Roche, Germany) and incubated on ice for 30 min and lysed. Lysates were centrifuged at 15,000g for 15 min at 4 °C and the supernatant was collected as the cytosolic fraction. Pellets were washed three times with buffer-A and resuspended in 70 μ l of ice-cold buffer-B (20 mM HEPES buffer, pH 7.9, 400 mM NaCl, 1 mM EDTA, 1 mM DTT, and 1 \times protease inhibitor cocktail). The resuspended pellet was subjected to a high-speed vortex twice at an interval of 30 min. The nuclear lysate was centrifuged at 15000g for 15 min at 4 °C and the supernatant was collected as the nuclear fraction. Protein concentration was measured by Bradford assay (Bio-Rad Protein Assay Dye Reagent Concentrate, Bio-Rad, USA) and an equal amount of proteins (for both cytosol and nuclear fraction) were resolved on 10.5% SDS-PAGE. Protein expressions in nuclear and cytosolic fractions were analyzed by western blotting using specified antibodies.

4.6. Western blotting

To detect the levels of HA/FLAG/GFP tagged proteins, p-I κ B α , and ubiquitin western blotting was performed. HEK293 and MCF-7 cells

were seeded at a density of 2.5×10^5 per well in 12 well plates and indicated vectors were transfected using the standard calcium phosphate transfection method [50]. After 24 h of transfection cells were treated as indicated and harvested in ice-cold PBS. Cells were lysed in lysis buffer (100 mM NaCl, 50 mM Tris-HCl, 1% Triton-X 100, and $1 \times$ protease inhibitor cocktail). Protein concentration was determined by Bradford assay (Bio-Rad Protein Assay Dye Reagent Concentrate, Bio-Rad, USA) and an equal amount of proteins were resolved on 10.5% SDS-PAGE. Proteins were electro-blotted on PVDF membrane (Immun-Blot® PVDF Membrane, Bio-Rad, USA) at 110 V for 1 h at 4 °C. The membrane was blocked with 5% blocking buffer (5% non-fat dried milk and 0.1% Tween-20 in TBS) for 1 h at room temperature and incubated with primary antibody overnight at 4 °C. After incubation membrane was washed three times with TBS-T (TBS containing 0.1% Tween-20) and incubated with a secondary antibody at room temperature for 1 h and proteins were detected by using Clarity Western ECL Substrates (Bio-Rad, USA) and exposing to X-ray film or using ChemiDoc MP Imaging System (Bio-Rad, USA).

4.7. Co-immunoprecipitation

To study the protein interaction and ubiquitin conjugation of Flag-tagged proteins, co-immunoprecipitation experiments were performed. HEK293 cells were plated at a density of 2×10^6 per 90-mm-diameter dish and transfected with Flag-TAK1 or HA-TRIM8 in combination with indicated vectors using the calcium phosphate transfection method [50]. After 36 h of transfection, cells were treated with specified chemicals and incubated for 10 h. After treatment, cells were harvested, washed with ice-cold PBS (Hyclone, GE, USA), and lysed in immunoprecipitation buffer (100 mM NaCl, 50 mM Tris-HCl, 1% Triton-X 100, and $1 \times$ protease inhibitor cocktail). The cell lysates were incubated with HA or FLAG-Affinity Gel (Sigma, USA) on a roller shaker overnight at 4 °C. The gel beads were washed four times with IP buffer, resuspended in $5 \times$ SDS-PAGE sample buffers and separated on 10.5% SDS-PAGE, and analyzed by western blotting using specific antibodies.

4.8. Gene expression analysis from GEO datasets, CCLE database, and Methylation profile of cancer cell lines

We explored the Gene Expression Omnibus dataset (GEO) GDS3809 for TRIM15 expression (probe set: 1451916_s_at). The microarray expression values of TRIM15 were plotted as mRNA expression for indicated time points [23]. Similarly, we explored the GDS4062 dataset for expression of TRIM15 (probe set: 36742_at, 210885_at, and 210177_at) and TRIM8 in normal, psoriasis lesional, and non-lesional dataset. Microarray transformed counts were plotted for mRNA expression for each probe set separately. We retrieved mRNA expression data of TRIM15 (both microarray and RNAseq) across various cancer cell lines from the CCLE database [22]. The expression data scatter plots were retrieved for methylation status (X-axis) vs mRNA expression (Y-axis).

The methylation status of TRIM15 as bubble plots for breast cancer cell lines was retrieved using the ‘‘CpG Methylation Viewer’’ module of the CCLE database and presented as it is.

4.9. Statistical analysis

Data are shown as mean \pm SEM for n observations. Comparisons of groups were performed using one-way ANOVA (Newman-Keuls post-test) to determine the levels of significance for each group. The experiments have been repeated a minimum of three times independently and probability values of $p < 0.05$ were considered as statistically significant. The data were normalized as the maximum value was considered as 100% and 0 as 0% for all data set.

Supplementary data to this article can be found online at <https://doi.org/10.1016/j.cellsig.2021.110210>.

Author contribution

MR designed and performed experiments, analyzed/interpreted data, and co-wrote the manuscript. KS and AS provided reagents and provided critical revision of the manuscript. SB and YT provided reagents and helped with experiments. DG, HV, MM, and FC analyzed data and provided critical revision of the manuscript. RS conceptualized and supervised the research, co-wrote the manuscript, and acquired funding.

Declaration of Competing Interest

The authors declare that they have no conflict of interest.

Acknowledgments

This work was supported by the grant (BT/PR20692/BRB/10/1538/2016) from the Department of Biotechnology, Govt. of India, to Prof. Rajesh Singh. The author also acknowledges the facilities under DST-FIST program (SR/FST/LS-11/2017/87) at Department of Biochemistry, The Maharaja Sayajirao University of Baroda. Kritarth Singh, Minal Mane, and Dhruv Gohel received Senior Research Fellowship from University Grant Commission (UGC), Council of Scientific & Industrial Research (CSIR), and Indian Council of Medical Research (ICMR), Govt. of India, respectively. Fatema Currim received INSPIRE fellowship from the Department of Science and Technology (DST), Govt. of India. This work constitutes a part of the Ph.D. thesis of Milton Roy.

References

- [1] H.L. Pahl, Activators and target genes of Rel/NF-kappaB transcription factors, *Oncogene* 18 (49) (1999) 6853–6866.
- [2] A. Oeckinghaus, S. Ghosh, The NF-kappaB family of transcription factors and its regulation, *Cold Spring Harb. Perspect. Biol.* 1 (4) (2009), a000034.
- [3] T. Liu, et al., NF-kappaB signaling in inflammation, *Signal Transduct. Target Ther.* 2 (2017).
- [4] I.S. Afonina, et al., Limiting inflammation—the negative regulation of NF-kappaB and the NLRP3 inflammasome, *Nat. Immunol.* 18 (8) (2017) 861–869.
- [5] M.S. Hayden, S. Ghosh, Regulation of NF-kappaB by TNF family cytokines, *Semin. Immunol.* 26 (3) (2014) 253–266.
- [6] S.P. Sasi, et al., Breaking the ‘harmony’ of TNF-alpha signaling for cancer treatment, *Oncogene* 31 (37) (2012) 4117–4127.
- [7] M.C. Selemo, et al., Tumor necrosis factor alpha-induced recruitment of inflammatory mononuclear cells leads to inflammation and altered brain development in murine cytomegalovirus-infected newborn mice, *J. Virol.* 91 (8) (2017).
- [8] Q. Lei, et al., TNIP1-mediated TNF-alpha/NF-kappaB signalling cascade sustains glioma cell proliferation, *J. Cell. Mol. Med.* 24 (1) (2020) 530–538.
- [9] G.D. Kalliolias, L.B. Ivashkiv, TNF biology, pathogenic mechanisms and emerging therapeutic strategies, *Nat. Rev. Rheumatol.* 12 (1) (2016) 49–62.
- [10] B. Tian, D.E. Nowak, A.R. Brasier, A TNF-induced gene expression program under oscillatory NF-kappaB control, *BMC Genomics* 6 (2005) 137.
- [11] L. Ashall, et al., Pulsatile stimulation determines timing and specificity of NF-kappaB-dependent transcription, *Science* 324 (5924) (2009) 242–246.
- [12] D.E. Nelson, et al., Oscillations in NF-kappaB signaling control the dynamics of gene expression, *Science* 306 (5696) (2004) 704–708.
- [13] I.E. Wertz, V.M. Dixit, Signaling to NF-kappaB: regulation by ubiquitination, *Cold Spring Harb. Perspect. Biol.* 2 (3) (2010), a003350.
- [14] G. Meroni, G. Diez-Roux, TRIM/RBCC, a novel class of ‘single protein RING finger’ E3 ubiquitin ligases, *Bioessays* 27 (11) (2005) 1147–1157.
- [15] A. Reymond, et al., The tripartite motif family identifies cell compartments, *EMBO J.* 20 (9) (2001) 2140–2151.
- [16] D. Tomar, R. Singh, TRIM family proteins: emerging class of RING E3 ligases as regulator of NF-kappaB pathway, *Biol. Cell.* 107 (1) (2015) 22–40.
- [17] S. Hatakeyama, TRIM family proteins: roles in autophagy, immunity, and carcinogenesis, *Trends Biochem. Sci.* 42 (4) (2017) 297–311.
- [18] M.M. Hu, et al., TRIM38 inhibits TNF-alpha- and IL-1beta-triggered NF-kappaB activation by mediating lysosome-dependent degradation of TAB2/3, *Proc. Natl. Acad. Sci. U. S. A.* 111 (4) (2014) 1509–1514.
- [19] D. Tomar, et al., Nucleo-cytoplasmic trafficking of TRIM8, a novel oncogene, is involved in positive regulation of TNF induced NF-kappaB pathway, *PLoS One* 7 (11) (2012), e48662.
- [20] Q. Li, et al., Tripartite motif 8 (TRIM8) modulates TNF-alpha- and IL-1beta-triggered NF-kappaB activation by targeting TAK1 for K63-linked polyubiquitination, *Proc. Natl. Acad. Sci. U. S. A.* 108 (48) (2011) 19341–19346.
- [21] Y. Cheng, et al., Analysis of DNA methylation patterns associated with the gastric cancer genome, *Oncol. Lett.* 7 (4) (2014) 1021–1026.

- [22] J. Barretina, et al., The cancer cell line encyclopedia enables predictive modelling of anticancer drug sensitivity, *Nature* 483 (7391) (2012) 603–607.
- [23] K. Lotzer, et al., Mouse aorta smooth muscle cells differentiate into lymphoid tissue organizer-like cells on combined tumor necrosis factor receptor-1/lymphotoxin beta-receptor NF-kappaB signaling, *Arterioscler. Thromb. Vasc. Biol.* 30 (3) (2010) 395–402.
- [24] G.A. Versteeg, et al., The E3-ligase TRIM family of proteins regulates signaling pathways triggered by innate immune pattern-recognition receptors, *Immunity* 38 (2) (2013) 384–398.
- [25] Y.T. Kwon, A. Ciechanover, The ubiquitin code in the ubiquitin-proteasome system and autophagy, *Trends Biochem. Sci.* 42 (11) (2017) 873–886.
- [26] P.D. Uchil, et al., TRIM15 is a focal adhesion protein that regulates focal adhesion disassembly, *J. Cell Sci.* 127 (Pt 18) (2014) 3928–3942.
- [27] Y. Fan, et al., Lysine 63-linked polyubiquitination of TAK1 at lysine 158 is required for tumor necrosis factor alpha- and interleukin-1beta-induced IKK/NF-kappaB and JNK/AP-1 activation, *J. Biol. Chem.* 285 (8) (2010) 5347–5360.
- [28] M.G. Koliopoulos, et al., Functional role of TRIM E3 ligase oligomerization and regulation of catalytic activity, *EMBO J.* 35 (11) (2016) 1204–1218.
- [29] Y. Li, et al., Structural insights into the TRIM family of ubiquitin E3 ligases, *Cell Res.* 24 (6) (2014) 762–765.
- [30] J. Woodsmith, R.C. Jenn, C.M. Sanderson, Systematic analysis of dimeric E3-RING interactions reveals increased combinatorial complexity in human ubiquitination networks, *Mol. Cell. Proteomics* 11 (7) (2012) p. M111 016162.
- [31] D. Tomar, et al., TRIM13 regulates ER stress induced autophagy and clonogenic ability of the cells, *Biochim. Biophys. Acta* 1823 (2) (2012) 316–326.
- [32] M. Roy, et al., TRIM8 regulated autophagy modulates the level of cleaved Caspase-3 subunit to inhibit genotoxic stress induced cell death, *Cell. Signal.* 48 (2018) 1–12.
- [33] M.M. Hu, H.B. Shu, Multifaceted roles of TRIM38 in innate immune and inflammatory responses, *Cell Mol. Immunol.* 14 (4) (2017) 331–338.
- [34] F. Okumura, et al., TRIM8 modulates STAT3 activity through negative regulation of PIAS3, *J. Cell Sci.* 123 (Pt 13) (2010) 2238–2245.
- [35] R. Rajsbaum, J.P. Stoye, A. O'Garra, Type I interferon-dependent and -independent expression of tripartite motif proteins in immune cells, *Eur. J. Immunol.* 38 (3) (2008) 619–630.
- [36] W. Zhao, et al., E3 ubiquitin ligase tripartite motif 38 negatively regulates TLR-mediated immune responses by proteasomal degradation of TNF receptor-associated factor 6 in macrophages, *J. Immunol.* 188 (6) (2012) 2567–2574.
- [37] M.X. Jiang, et al., Expression profiling of TRIM protein family in THP1-derived macrophages following TLR stimulation, *Sci. Rep.* 7 (2017) 42781.
- [38] A. Pacis, et al., Gene activation precedes DNA demethylation in response to infection in human dendritic cells, *Proc. Natl. Acad. Sci. U. S. A.* 116 (14) (2019) 6938–6943.
- [39] Z. Zhao, et al., The proinflammatory cytokine TNFalpha induces DNA demethylation-dependent and -independent activation of interleukin-32 expression, *J. Biol. Chem.* 294 (17) (2019) 6785–6795.
- [40] M. Lu, et al., XIAP induces NF-kappaB activation via the BIR1/TAB1 interaction and BIR1 dimerization, *Mol. Cell* 26 (5) (2007) 689–702.
- [41] R. Schwenzler, et al., The human tumor necrosis factor (TNF) receptor-associated factor 1 gene (TRAF1) is up-regulated by cytokines of the TNF ligand family and modulates TNF-induced activation of NF-kappaB and c-Jun N-terminal kinase, *J. Biol. Chem.* 274 (27) (1999) 19368–19374.
- [42] C. Stehlik, et al., Cytokine induced expression of porcine inhibitor of apoptosis protein (iap) family member is regulated by NF-kappa B, *Biochem. Biophys. Res. Commun.* 243 (3) (1998) 827–832.
- [43] Y. Saeki, et al., Lysine 63-linked polyubiquitin chain may serve as a targeting signal for the 26S proteasome, *EMBO J.* 28 (4) (2009) 359–371.
- [44] F. Ohtake, et al., K63 ubiquitylation triggers proteasomal degradation by seeding branched ubiquitin chains, *Proc. Natl. Acad. Sci. U. S. A.* 115 (7) (2018) E1401–E1408.
- [45] F. Ohtake, et al., The K48–K63 branched ubiquitin chain regulates NF-kappaB signaling, *Mol. Cell* 64 (2) (2016) 251–266.
- [46] W.W. Reiley, et al., Deubiquitinating enzyme CYLD negatively regulates the ubiquitin-dependent kinase Tak1 and prevents abnormal T cell responses, *J. Exp. Med.* 204 (6) (2007) 1475–1485.
- [47] G. Maarifi, et al., TRIM8 is required for virus-induced IFN response in human plasmacytoid dendritic cells, *Sci. Adv.* 5 (11) (2019) p. eaax3511.
- [48] Z. Tian, et al., TRIM8 inhibits breast cancer proliferation by regulating estrogen signaling, *Am. J. Cancer Res.* 10 (10) (2020) 3440–3457.
- [49] Y. Tian, et al., RBCK1 negatively regulates tumor necrosis factor- and interleukin-1-triggered NF-kappaB activation by targeting TAB2/3 for degradation, *J. Biol. Chem.* 282 (23) (2007) 16776–16782.
- [50] R.E. Kingston, C.A. Chen, J.K. Rose, Calcium phosphate transfection, *Curr. Protoc. Mol. Biol.* 9 (9) (2003) 1.